Politecnico di Milano

SCHOOL OF INDUSTRIAL AND INFORMATION ENGINEERING
Master of Science – Nuclear Engineering

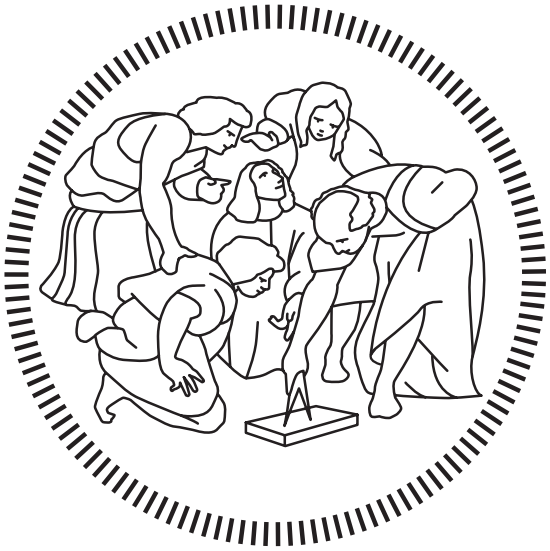

Stability and sensitivity analysis for compressible fluids in MHD problems

Supervisor
Prof. Antonio CAMMI

Co-Supervisors
Dr. Stefano LORENZI
Prof. Matteo PASSONI

Candidate
Francesco PASTORE – 899692

Academic Year 2019 – 2020

Ringraziamenti

Con il termine di questo lavoro di tesi si conclude il mio percorso universitario all'interno delle mura del Politecnico di Milano.
Vorrei ringraziare i miei genitori e la mia famiglia, per il supporto che mi hanno amorevolmente dato in questi anni di studio, comprendendo il percorso impegnativo che ho affrontato e aiutandomi nei momenti di difficoltà con la loro presenza nel quotidiano.
Sono cresciuto molto: ho conosciuto le mie potenzialità ed i miei limiti in ogni sfida universitaria che mi si è parata dinnanzi ed ho scoperto meglio me stesso ed il mondo che mi circonda. L'esempio di docenti e studenti è stato fondamentale in questo senso per la mia formazione a livello professionale ed organizzativo.
Tuttavia, oltre alla sfera puramente scolastica, vorrei ricordare in queste poche righe la famiglia Nucleare con cui ho passato momenti di aggregazione e di festa negli anni di Laurea Magistrale: l'ambiente amichevole ed umano che ho trovato al CESNEF ed al B12 è stato per me importantissimo e stimolante, ha rappresentato una grande opportunità per stringere dei legami che vadano oltre a semplici relazioni tra colleghi e docenti.
Ringrazio il mio relatore Antonio Cammi e correlatore Stefano Lorenzi, per l'esperienza intensa e ricca di stimoli che ha rappresentato questa tesi per me.
Voglio ricordare inoltre i miei compagni di università, in particolare Fabio, Giuseppe e Giovanni, per avermi aiutato e sostenuto nei momenti di difficoltà di questi tre lunghi anni di Magistrale e avermi saputo accettare come loro compagno nella vita quotidiana in università. Inoltre ringrazio Giulio, Giovanni F., Paolo, Andrea, Anna Giulia, Gabriele, Riccardo ed Alessandro per i momenti condivisi assieme in questi anni.
Infine voglio ricordare i miei amici con cui ho condiviso passioni e serate di gioco assieme, tentando di svagarmi tra un esame e l'altro: ringrazio Matteo, Emanuele, Riccardo, Federico, Alessandro, Jacopo, Valentina, Davide ed Angelica.
Questi mesi sono stati intrisi dal dolore e dalla paura di perder tutto ciò che ci è di più caro al mondo. Il mio augurio è che questo periodo giunga al termine grazie allo sforzo dei medici, ricercatori, infermieri, governanti e dell'impegno di ciascuno di noi, contribuendo singolarmente alla collettività ed al nostro prossimo.

Sommario

Questo lavoro di tesi propone diversi strumenti e tecniche numeriche dedicate alla caratterizzazione dinamica di un sistema fluente governato dall'equazione di Navier-Stokes comprimibile in approssimazione unidimensionale, in cui un fluido conduttivo interagisce con un campo magnetico esterno tramite una descrizione MHD (Magneto-hydroynamics).
Nel primo capitolo, viene eseguita una *analisi di stabilità modale*, linearizzando l'insieme delle equazioni di governo di un fluido non conduttivo attorno a un punto di equilibrio e studiando la risposta lineare del sistema a piccole perturbazioni applicate al punto di equilibrio selezionato. Le formule alle differenze finite vengono impiegate per l'approssimazione numerica delle derivate spaziali applicate alla perturbazione delle variabili di stato. Un'analisi di sensitività legata alla discretizzazione della mesh viene eseguita per ogni caso specifico e le mappe di stabilità vengono quindi disegnate per riassumere graficamente i risultati principali. Infine viene adottata una *analisi di sensitività* parametrica ed una riferita ai profili stazionari delle variabili di stato, basata sull'utilizzo della *teoria modale dell'aggiunto* per studiare l'impatto dei parametri principali e dei profili stazionari sulla stabilità del punto di equilibrio.
Il secondo capitolo è dedicato all'applicazione e all'estensione delle tecniche numeriche sviluppate nel primo ad un fluido conduttivo in presenza di un campo magnetico esterno. L'impatto del campo magnetico sulle caratteristiche di stabilità del sistema viene esaminato da vari punti di vista: la modifica delle mappe di stabilità dall'azione del campo magnetico, la dipendenza funzionale della curva di stabilità neutrale per valori incrementali del campo magnetico e una *analisi di sensitività* che coinvolge i termini aggiuntivi inseriti nel sistema di equazioni di governo per la descrizione dell'accoppiamento tra il campo magnetico esterno e il moto del fluido.

Abstract

This thesis work proposes different numerical tools and techniques devoted to the characterization of a hydrodynamic system governed by the compressible Navier-Stokes equation in the unidimensional approximation, in which a conductive fluid interacts with an external magnetic field. The interaction is described within the MHD (Magnetohydroynamics) approximation.
In the first chapter, a *modal stability analysis* is carried out by linearizing the set of governing equations for a non conductive fluid around an equilibrium point and studying the linear stability response of the system for the selected equilibrium point. Finite differences formulas are employed for the numerical approximation of the spatial derivatives applied to the perturbation of the state variables. Mesh sensitivity is performed for each specific case and stability maps are then drawn to sum up graphically the main results. Finally, a *parametric sensitivity analysis* and *base flow sensitivity analysis* based on the adjoint perturbative approach are adopted to study the impact of the main parameters of the system, together with the base flow, on the stability features of the equilibrium point.
The second part of the work is devoted to the application and extension of the numerical techniques developed in the first chapter to a conductive fluid in the presence of an external magnetic field. The impact of the magnetic field on the stability features of the system is examined from various points of view: the modification of the stability maps by the action the magnetic field, the functional dependence of the neutral stability curve for incremental values of the magnetic field and a *sensitivity analysis* involving the additive terms that describe the coupling between the external magnetic field and motion of the fluid.

Estratto

Questo lavoro di tesi propone diversi strumenti e tecniche numeriche dedicate alla caratterizzazione dinamica di un sistema fluente governato dall'equazione di Navier-Stokes comprimibile in approssimazione unidimensionale, in cui un fluido conduttivo interagisce con un campo magnetico esterno tramite una descrizione MHD (Magnetohydroynamics). In particolare, la trattazione si colloca all'interno di un più ampio progetto finalizzato a sviluppare un solver in OpenFOAM che permetta di simulare un plasma per applicazioni fusionistiche in varie configurazioni e geometrie, nell'approssimazione MHD. In questo senso, uno studio preliminare dal punto di vista teorico è stato presentato nel lavoro di tesi di [Trotta et al. 2019], in cui un'analisi di stabilità lineare di un fluido conduttore sotto l'azione di un campo magnetico esterno viene condotta, adattando il modello MHD ad una trattazione monodimensionale e nell'ipotesi che le configurazioni di equilibrio iniziali siano uniformi in spazio.
In questo lavoro è stata messa in discussione la precedente ipotesi di quantità uniformi nello spazio, proponendo un'*analisi modale* del set di equazioni impiegate per il caso monodimensionale non conduttivo. Queste ultime vengono ambientate all'interno di una semplice sistema (un riser) ed i contributi legati alle derivate spaziali delle configurazioni di equilibrio che si instaurano all'interno del sistema vengono aggiunti alla trattazione. Successivamente viene condotta un'*analisi di sensitività* per valutare come piccole fluttuazioni dei principali parametri che caratterizzano il punto di equilibrio, assieme a perturbazioni applicate ai profili di velocità, pressione e densità lungo il riser agiscano sulla stabilità globale del sistema. Infine, le precedenti equazioni vengono accoppiate alla descrizione dinamica del campo magnetico indotto all'interno di un fluido conduttore, sotto l'azione di un campo magnetico esterno. Le principali differenze in termini di stabilità lineare del sistema vengono evidenziate ed l'analisi di sensitività parametrica e di campo viene riproposta per il caso conduttivo.

Analisi modale per il fluido non conduttivo

Il punto di partenza per questa analisi è il lavoro di [Doster and Kendall 1999] dove, sotto l'ipotesi di trattazione monodimensionale, viene studiata la stabilità di un sistema fluente in cui la comprimibilità del fluido evolvente viene considerata. L'articolo si inserisce nel contesto della convezione naturale per sistemi di raffreddamento passivi

di reattori ad acqua leggera. Il set di equazioni impiegate viene qui riportato:

$$\begin{cases} \dfrac{\partial \rho}{\partial t} + \dfrac{\partial \rho v}{\partial z} = 0 \\ \dfrac{\partial \rho u}{\partial t} + \dfrac{\partial \rho u v}{\partial z} = -p\dfrac{\partial v}{\partial z} \\ \rho\dfrac{\partial v}{\partial t} + \rho v\dfrac{\partial v}{\partial z} = -\dfrac{\partial p}{\partial z} - \rho g - k^{'}\dfrac{\rho v^2}{2} \\ \rho = \rho(u,p) \end{cases} \tag{1}$$

I fluidi considerati in questo lavoro di tesi sono acqua sottoraffreddata e sodio liquido. Il primo è stato considerato per riprodurre le condizioni di lavoro tipiche di un reattore ad acqua pressurizzata, il secondo per valutare l'effetto di un campo magnetico esterno sul moto del fluido. Le equazioni di conservazione della massa, dell'energia interna, della quantità di moto e l'equazione di stato governano la dinamica del sistema. Le variabili di stato presenti nel set di equazioni sopra riportato sono la *densità* ρ, la *velocità* v del fluido lungo z, l'*energia interna* u e la *pressione* p. L'equazione di conservazione dell'energia interna è stata adottata in approssimazione inviscida, non essendo gli effetti termici introdotti con la viscosità un punto rilevante della trattazione. Inoltre nell'equazione di conservazione della quantità di moto vi è presente il termine di gravità ρg, positivo se il moto del fluido è in salita, negativo se in discesa, ed un termine dissipativo $k^{'}\frac{\rho v^2}{2}$ che introduce le perdite di carico distribuite nel sistema. Quest'ultimo termine è proporzionale al *coefficiente di attrito per unità di lunghezza*, in m^{-1}, che può essere modellizzato attraverso Eq.(2):

$$k^{'} = k_0 \left(\frac{v_0}{v}\right)^b \tag{2}$$

dove b esprime il regime di moto del flusso (laminare $b = 1.0$, turbolento completamente sviluppato $b \approx 0.2$), v_0 è una velocità di riferimento del sistema e k_0 può essere impiegato come parametro di controllo per aumentare o diminuire l'effetto delle forze viscose sul sistema. Il set di equazioni (1) viene linearizzato attorno ad un punto di equilibrio nell'ipotesi di quantità uniformi lungo z ed un'analisi di stabilità lineare viene condotta sul set di equazioni linearizzate. Applicando la trasformata di Fourier in spazio ed in tempo e ponendo a zero il determinante della matrice della dinamica A, che descrive in formulazione matriciale il sistema di equazioni linearizzato e trasformato mediante Fourier, è possibile ricavare la condizione di stabilità per il sistema nel caso più critico (moto in salita, $\rho g > 0$, supponendo che $v_0 \ll c$, dove c è la velocità del suono del fluido):

$$k_{0,min} = \frac{1}{v_0}\frac{2}{2-b}\frac{|g|}{c} \tag{3}$$

dove c è la velocità del suono del fluido.
La relazione (3) può essere quindi rappresentata all'interno del piano v_0-k_0, ed una prima mappa di stabilità può essere tracciata al variare del coefficiente b :

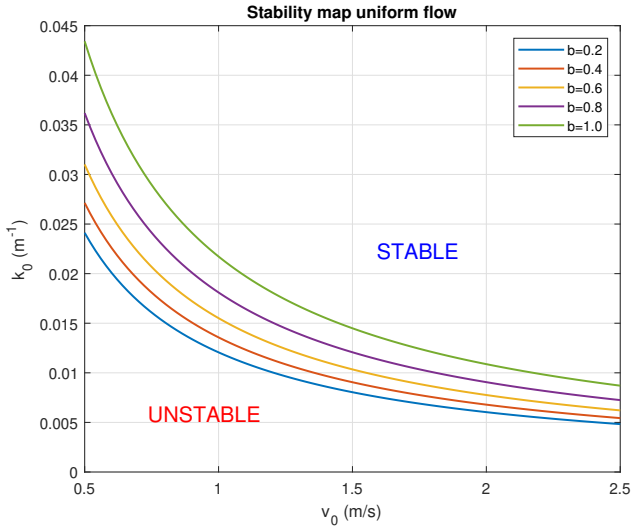

Figure 1: *Mappa di stabilità per flusso monodimensionale comprimibile, profili spaziali uniformi, acqua sottoraffreddata, moto in salita.*

Quindi, l'ipotesi di profili spaziali uniformi viene rilassata: una semplice geometria ed un dominio computazionale vengono introdotti per ambientare le precedenti equazioni ed imporre le condizioni al contorno al problema. Un canale di lunghezza L (Figura 2), le cui dimensioni trasversali sono molto inferiori rispetto alla dimensione longitudinale, viene disposto lungo l'asse z di un sistema di riferimento cartesiano. L'intervallo $[0, L]$ dell'asse z viene quindi suddiviso in N elementi uguali ed una mesh formata da $N + 1$ nodi equispaziati viene a definirsi. Le condizioni al contorno del problema, di tipo Dirichlet, sono riferite alla velocità in ingresso v_{in}, alla densità in ingresso ρ_{in} ed alla pressione in uscita p_{out}.

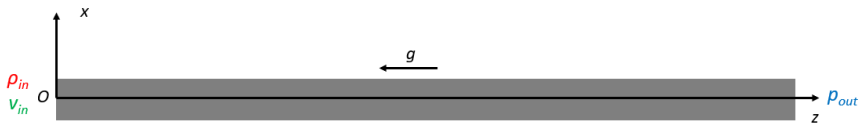

Figure 2: *Geometria, dominio e condizioni al contorno.*

La ricerca del punto di equilibrio viene effettuata tramite la risoluzione del seguente problema non lineare stazionario tramite COMSOL®:

$$\begin{cases} \dfrac{\partial \rho_0 v_0}{\partial z} = 0 \\ \dfrac{\partial \rho_0 u_0 v_0}{\partial z} = -p_0 \dfrac{\partial v_0}{\partial z} \\ \rho_0 v_0 \dfrac{\partial v_0}{\partial z} = -\dfrac{\partial p_0}{\partial z} - \rho_0 g - \dfrac{k' \rho v_0^2}{2} \\ u_0 = \overline{u} + \alpha p_0 + \beta \rho_0 \end{cases} \tag{4}$$

Dove l'ultima equazione in (4) è l'equazione di stato linearizzata, che lega l'energia interna alla densità e pressione. I coefficienti termodinamici α e β sono così definiti:

$$\alpha = \left(\frac{\partial u}{\partial p}\right)_{\rho}, \quad \beta \left(\frac{\partial u}{\partial \rho}\right)_{p}$$

L'informazione nodale dei profili ottenuti e delle corrispettive derivate spaziali è successivamente importata nell'ambiente di MATLAB® per la costruzione della matrice della dinamica discretizzata A.
Il sistema di equazioni (1) viene linearizzato (ogni generica funzione di stato ϕ può essere decomposta nel suo valore stazionario ϕ_0 e nella fluttuazione $\delta\phi$) nuovamente attorno ad un punto di equilibrio, questa volta tuttavia i termini legati alle derivate spaziali dei profili stazionari non vengono trascurati. Sostituendo l'equazione di stato linearizzata, riferita al fluido considerato, e l'equazione di continuità all'interno dell'equazione dell'energia interna, è possibile eliminare la variabile di stato u dal set di equazioni ed ottenere una equazione linearizzata per l'evoluzione della perturbazione della pressione δp nel tempo:

$$\begin{cases} \dfrac{\partial \delta\rho}{\partial t} + v_0\dfrac{\partial \delta\rho}{\partial z} + \dfrac{\partial v_0}{\partial z}\delta\rho + \rho_0\dfrac{\partial \delta v}{\partial z} + \dfrac{\partial \rho_0}{\partial z}\delta v = 0 \\ \dfrac{\partial \delta p}{\partial t} + v_0\dfrac{\partial \delta p}{\partial z} + \delta v\dfrac{\partial p_0}{\partial z} - \dfrac{\beta}{\alpha}\rho_0\dfrac{\partial \delta v}{\partial z} - \dfrac{\beta}{\alpha}\delta\rho\dfrac{\partial v_0}{\partial z} + v_0\left(\dfrac{\beta}{\alpha}\dfrac{\partial \rho_0}{\partial z} + \dfrac{\partial p_0}{\partial z}\right)\dfrac{\delta\rho}{\rho_0} + \\ \qquad + \dfrac{p_0}{\alpha\rho_0}\dfrac{\partial \delta v}{\partial z} + \dfrac{1}{\alpha\rho_0}\dfrac{\partial v_0}{\partial z}\delta p = 0 \\ \dfrac{\partial \delta v}{\partial t} + v_0\dfrac{\partial \delta v}{\partial z} + \delta v\dfrac{\partial v_0}{\partial z} + \left(g + \dfrac{k_0 v_0^2}{2} + v_0\dfrac{\partial v_0}{\partial z}\right)\dfrac{\delta\rho}{\rho_0} = -\dfrac{1}{\rho_0}\dfrac{\partial \delta p}{\partial z} - \left(\dfrac{2-b}{2}\right)k_0 v_0 \delta v \end{cases} \tag{5}$$

Il precedente set di equazioni viene quindi discretizzato in spazio, valutando l'evoluzione in tempo di ciascuna variabile di stato per ogni nodo della mesh. Le derivate spaziali vengono approssimate sfruttando lo schema delle differenze finite centrate per i nodi interni della mesh, mentre per il primo e l'ultimo, rispettivamente, le differenze finite in avanti ed indietro. Il sistema può essere riformulato matricialmente nel seguente modo:

$$\frac{d}{dt}\delta X = A\delta X \tag{6}$$

dove A è la matrice della dinamica del sistema e δX il vettore di stato adottato. Dato che non viene introdotta alcuna perturbazione nelle condizioni al contorno impiegate per il problema stazionario, il vettore di stato può essere espresso trascurando la perturbazione della velocità e densità al primo nodo e della pressione all'ultimo:

$$\delta X = [\delta v_2, \cdot\ \cdot\ \cdot, \delta v_{N+1}, \delta p_1, \cdot\ \cdot\ \cdot, \delta p_N, \delta\rho_2, \cdot\ \cdot\ \cdot, \delta\rho_{N+1}]^T \tag{7}$$

L'*analisi modale* può essere quindi intrapresa. La stabilità lineare è dettata dalla posizione dell'autovalore dominante γ della matrice della dinamica A nel piano complesso ([Lyapunov 1992]): se la parte reale di γ è negativa, il punto di equilibrio è definito stabile, altrimenti è detto instabile. Per prima cosa viene analizzata la

convergenza della parte reale dell'autovalore dominante di A all'aumentare del numero di elementi N dell'intervallo $[0, L]$:

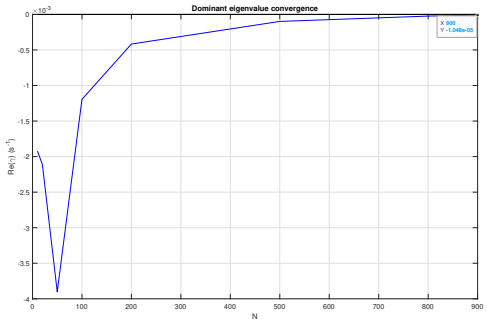

Figure 3: *Grafico di convergenza di $Re(\gamma)$, flusso uniforme, acqua sottoraffreddata.*

La scelta ottimale di N nasce dalla necessità di minimizzare il costo computazionale del calcolo degli autovalori di A, mantenendo un'accuratezza accettabile del metodo numerico. La dipendenza di $Re(\gamma)$ rispetto ad N è legata sia all'ordine di convergenza del metodo numerico adottato per l'approssimazione delle derivate spaziali che agiscono sulle variabili di stato, sia dalla configurazione del sistema presa in oggetto nello studio.
In particolare, tre diverse configurazioni vengono studiate per valutare l'impatto dei gradienti di pressione sul sistema: per prima la configurazione uniforme, utilizzata come benchmark per testare il metodo numerico rispetto al risultato analitico predetto tramite Eq.(3), poi viene considerato un profilo di pressione generato da una perdita di carico distribuita lungo L ed infine un profilo di pressione corrispondente ad una perdita di carico concentrata a metà della lunghezza del canale.
I risultati sotto riportati sono tre diverse mappe di stabilità corrispondenti ai casi sopracitati: in $\times$ viene indicato che il punto di equilibrio individuato dalla coppia $v_{in}(i), k_0(j)$ nel piano v_0-k_0 è instabile, mentre in $\times$ è viceversa segnato il caso stabile:

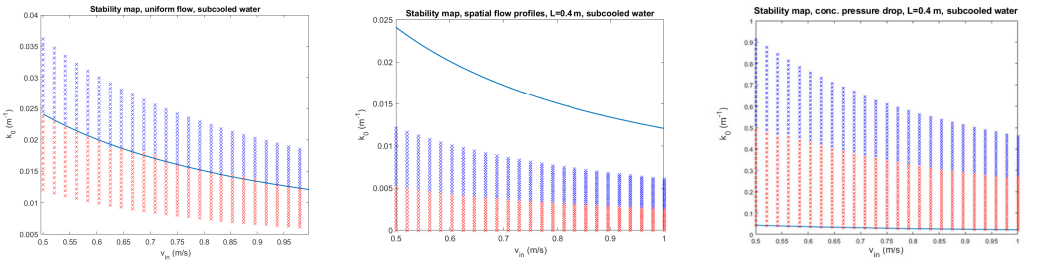

(a) *Profilo uniforme.* **(b)** *Perdita di carico distribuita.* **(c)** *Perdita di carico concentrata.*

Figure 4: *Mappe di stabilità per l'acqua sottoraffreddata*

La linea continua rappresenta il risultato teorico ottenuto con l'Eq.(3): nel primo caso test, si può notare come il metodo numerico sviluppato colga in maniera soddisfacente l'andamento teorico, essendo la linea di demarcazione tra la regione stabile (in blu) ed instabile (in rosso) coincidente con la linea continua. Nella seconda configurazione è invece possibile constatare che l'introduzione di un profilo di pressione legato ad una

perdita di carico distribuita abbia stabilizzato il sistema. Nell'ultima configurazione si può osservare invece come la regione associata alle instabilità modali si estenda al di sopra della linea continua ottenuta per il caso uniforme: la presenza di un profilo di pressione legato ad una perdita di carico concentrata risulta essere fortemente destabilizzante per il sistema. In sintesi, è possibile quindi affermare che l'ipotesi di configurazione uniforme in spazio colga solo in prima approssimazione le caratteristiche di stabilità del sistema e che, per ottenere risultati soddisfacenti ai fini dello studio della stabilità lineare del sistema, uno studio numerico della particolare configurazione presa in oggetto sia quindi necessario.

Analisi di sensitività del fluido non conduttivo

E' interessante valutare come i parametri precedentemente presentati che caratterizzano il fluido studiato, sia a livello termodinamico, riferendosi ad α e β, che a livello idrodinamico, con k_0 e b, influenzino la stabilità di un particolare punto di equilibrio. Inoltre è possibile analizzare come piccole perturbazioni introdotte lungo i profili stazionari delle variabili di stato, assieme alle corrispettive derivate spaziali dei profili lungo il canale, determinino uno shift dell'autovalore dominante rispetto alla configurazione imperturbata. Prendendo come riferimento il lavoro sviluppato da [Schmid and Brandt 2014], un'analisi perturbativa lineare di sensitività è stata adottata nel contesto della *teoria modale dell'aggiunto*, in cui l'oggetto di studio è la valutazione della perturbazione degli autovalori di una matrice a fronte di una piccola perturbazione introdotta all'interno di quest'ultima. In particolare, è possibile dimostrare che, data una piccola perturbazione δA alla matrice della dinamica A, è possibile ottenere il discostamento di ogni autovalore λ_i di A tramite:

$$\delta\lambda_i = \frac{\mathbf{p}_i^\dagger \delta A \mathbf{q}_i}{\mathbf{p}_i^\dagger \mathbf{q}_i} \tag{8}$$

dove $\mathbf{p}_i$ e $\mathbf{q}_i$ sono, rispettivamente, l'autovettore sinistro e destro della matrice A, riferiti all' i-esimo autovalore λ_i e $\mathbf{p}_i^\dagger \mathbf{q}_i$ rappresenta l'operazione di prodotto scalare tra vettori in $\mathbb{C}^n$ (n è la dimensione dei vettori).
L'analisi di sensitività parametrica è stata svolta perturbando fino al 10% del valore di un generico parametro θ la matrice A e mantenendo gli altri parametri costanti (*single-parameter sensitivity analysis* in [Napolitano and Fabbri 1996]). Registrando quindi lo shift della parte reale dell'autovalore dominante $Re(\gamma)$, è possibile verificare se un incremento del parametro ha avuto un impatto stabilizzante o destabilizzante sul sistema. A livello quantitativo, per valutare non solo l'effetto stabilizzante o meno della perturbazione ma anche quanto sia determinante nella stabilità, è stata adottata la definizione di *sensitività relativa* S:

$$S = \frac{Re(\delta\gamma)}{Re(\gamma)} \frac{\theta}{\delta\theta} \tag{9}$$

dove $\delta\theta$ è la massima perturbazione del parametro θ e $Re(\delta\gamma)$ è la corrispondente variazione della parte reale dell'autovalore dominante γ di A. Nella Tabella 1 sono riassunti i principali risultati conseguiti adottando questo approccio:

Parametri	*Sensitività relativa*	*Effetto sul sistema*
α	-0.81	Stabilizzante
β	0.92	Destabilizzante
k_0	-0.79	Stabilizzante
b	0.78	Destabilizzante

Table 1: *Principali parametri che caratterizzano il sistema ed il loro impatto sulla stabilità.*

Lo stesso procedimento viene di seguito adottato per la perturbazione dei profili stazionari calcolati con COMSOL®. L'unica differenza consiste nel modo in cui la perturbazione viene introdotta nel sistema: viene difatti calcolato dapprima il valore medio del profilo selezionato lungo z e poi il 10% di quest'ultimo viene sommato al profilo di partenza per ogni nodo della mesh. La matrice così perturbata viene poi studiata coerentemente con quanto visto in precedenza. In Tabella 2 viene riportato brevemente l'insieme dei risultati ottenuti in questo senso:

Profili stazionari	*Sensitività relativa*	*Effetto sul sistema*
v_0	-0.7392	Stabilizzante
p_0	-0.1220	Stabilizzante
ρ_0	-12.31	Stabilizzante
$\frac{\partial v_0}{\partial z}$	-0.0088	Stabilizzante
$\frac{\partial p_0}{\partial z}$	8.422	Destabilizzante
$\frac{\partial \rho_0}{\partial z}$	$-1.637 \cdot 10^{-15}$	Stabilizzante

Table 2: *Principali profili stazionari che caratterizzano il sistema ed il loro impatto sulla stabilità.*

Analisi modale per il fluido conduttivo

Lo step logico successivo consiste nell'introdurre un campo magnetico esterno ed analizzare come l'interazione tra il campo ed il moto del fluido conduttivo impatti sulla stabilità del sistema. La geometria ed il dominio sono schematizzate in Figura 2.1:

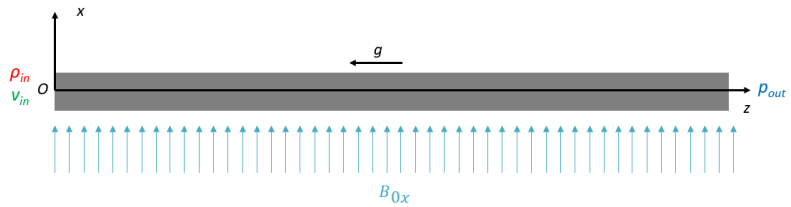

Figure 5: *Geometria, dominio e condizioni al contorno per il caso conduttivo.*

Un campo magnetico uniforme $B_{0,x}$ viene applicato lungo il riser: l'accoppiamento tra il campo ed il moto del fluido genera un campo magnetico indotto $\delta H_{0,x}$, il quale a sua volta da origine ad una forza frenante (forza di Lorentz) che stabilizza il sistema. Il modello MHD viene adattato al caso monodimensionale: di seguito è riportato il sistema di equazioni linearizzate attorno ad un punto di equilibrio:

$$\begin{cases} \dfrac{\partial \delta\rho}{\partial t} = -v_0\dfrac{\partial \delta\rho}{\partial z} - \dfrac{\partial v_0}{\partial z}\delta\rho - \rho_0\dfrac{\partial \delta v}{\partial z} - \dfrac{\partial \rho_0}{\partial z}\delta v \\ \dfrac{\partial \delta p}{\partial t} = -v_0\dfrac{\partial \delta p}{\partial z} - \delta v\dfrac{\partial p_0}{\partial z} + \dfrac{\beta}{\alpha}\rho_0\dfrac{\partial \delta v}{\partial z} + \dfrac{\beta}{\alpha}\delta\rho\dfrac{\partial v_0}{\partial z} - \dfrac{p_0}{\alpha\rho_0}\dfrac{\partial \delta v}{\partial z} + \\ \qquad - v_0\left(\dfrac{\beta}{\alpha}\dfrac{\partial \rho_0}{\partial z} - \dfrac{\partial p_0}{\partial z}\right)\dfrac{\delta\rho}{\rho_0} - \dfrac{1}{\alpha\rho_0}\dfrac{\partial v_0}{\partial z}\delta p \\ \dfrac{\partial \delta v}{\partial t} = -v_0\dfrac{\partial \delta v}{\partial z} - \delta v\dfrac{\partial v_0}{\partial z} - \left(g + \dfrac{k_0 v_0^2}{2} + v_0\dfrac{\partial v_0}{\partial z}\right)\dfrac{\delta\rho}{\rho_0} - \dfrac{1}{\rho_0}\dfrac{\partial \delta p}{\partial z} + \\ \qquad - \left(\dfrac{2-b}{2}\right)k_0 v_0\delta v - B_{0,x}\dfrac{\partial \delta H_x}{\partial z} \\ \dfrac{\partial \delta H_x}{\partial t} = -v_0\dfrac{\partial \delta H_x}{\partial z} - \dfrac{B_{0,x}}{\mu_0}\dfrac{\partial \delta v}{\partial z} + \dfrac{\eta}{\mu_0}\dfrac{\partial^2 \delta H_x}{\partial z^2} \end{cases} \tag{10}$$

Viene sottolineato che, come prima approssimazione, il punto di equilibrio stazionario sia coincidente con il caso non conduttivo. Gli effetti del campo magnetico esterno vengono introdotti per studiare la risposta linearizzata delle perturbazioni delle variabili di stato per $t > 0$. Viene inoltre rimarcato che l'accoppiamento tra campo magnetico indotto ed il moto del fluido avviene tramite il termine $B_{0,x}\frac{\partial \delta H_x}{\partial z}$ presente nell'equazione della quantità di moto e che un nuovo coefficiente, la resistività elettrica η del fluido conduttore (nel caso in esame il sodio liquido) appaia nell'equazione evolutiva della perturbazione del campo magnetico indotto, assieme alla permeabilità magnetica nel vuoto μ_0 (per il sodio liquido, la permeabilità magnetica relativa $\mu_r \approx 1$).
Seguendo la medesima procedura presentata per il caso non conduttivo, viene comparata la risposta del sistema in assenza ed in presenza di un campo magnetico esterno, utilizzando per il raffronto una configurazione di equilibrio uniforme:

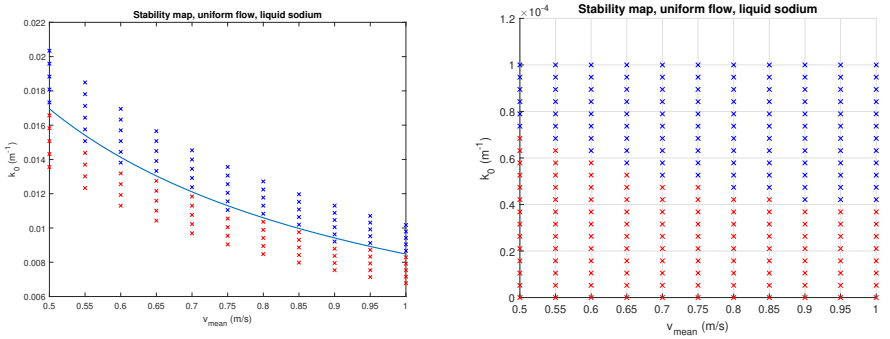

(a) *Profilo uniforme,* $B_0 = 0\ T$. **(b)** *Profilo uniforme,* $B_0 = 1.0\ T$.

Figure 6: *Mappe di stabilità per il sodio liquido.*

L'azione del campo magnetico è evidente: la *curva di stabilità neutrale* che separa la regione stabile da quella instabile ha subito uno shift verso il basso di circa 3 o.d.g.

Infine viene riportata un'analisi parametrica che permette di studiare, posizionandosi su un'isolinea del piano v_0-k_0 a velocità di ingresso costante e pari a $v_{in} = 1.0\ m/s$, come varia il coefficiente di attrito critico $k_{0,min}$ al variare del campo magnetico applicato al sistema:

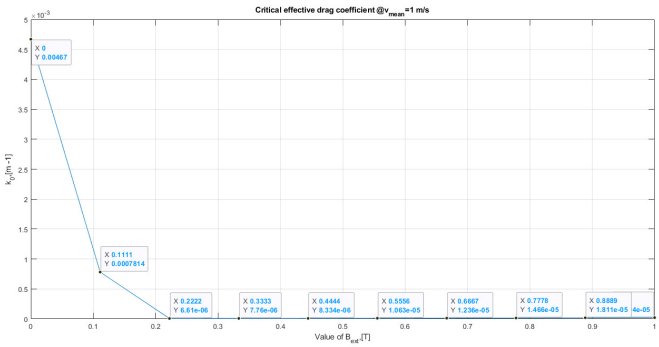

(a) *Da* $B_0 = 0\ T$ *a* $B_0 = 1.0\ T$.

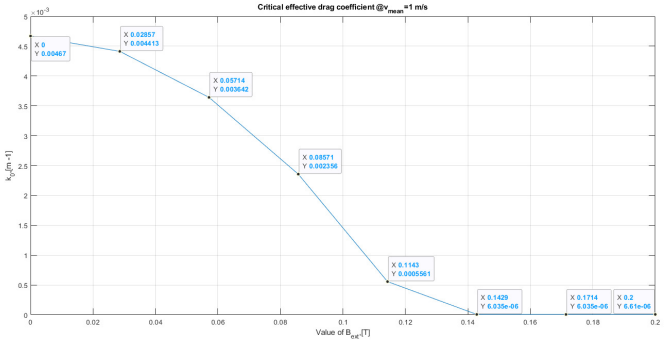

(b) *Da* $B_0 = 0\ T$ *a* $B_0 = 0.2\ T$.

Figure 7: *Variazione del coefficiente di attrito critico all'aumentare dell'intensità del campo magnetico esterno, sodio liquido.*

Analisi di sensitività del fluido conduttivo

In quest'ultima sezione, l'approccio perturbativo applicato per l'analisi di sensitività del fluido non conduttivo viene esteso alla trattazione del fluido conduttivo. Si focalizzerà l'attenzione su come perturbazioni del campo magnetico B_0 e della resistività elettrica η, introdotte per il caso conduttivo, modifichino la stabilità del sistema. Scegliendo un campo magnetico di intensità $B_0 = 0.1\ T$ come profilo imperturbato e andando ad incrementare del 10% il suo valore lungo ciascun nodo, viene riportata la corrispettiva perturbazione della parte reale dell'autovalore dominante (è stato preso in esame un punto di equilibrio instabile):

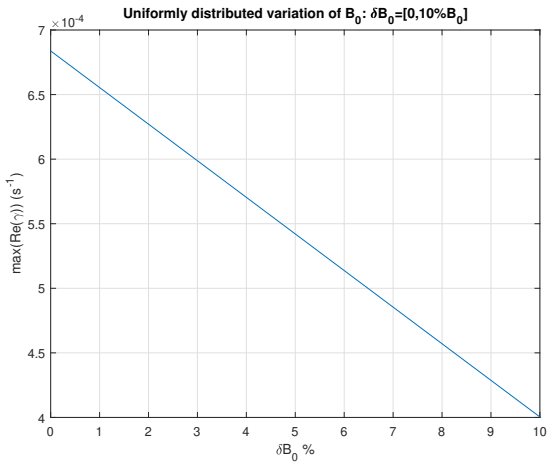

Figure 8: *Shift dell'autovalore dominante dato da un aumento di* B_0 *fino al* 10% *del suo valore imperturbato.*

L'effetto stabilizzante di un incremento del campo magnetico viene ritrovato anche in questo caso. Il corrispettivo valore della sensitività relativa è $S = -4.145$.
Infine, un'analisi di sensitività parametrica viene effettuata su η. I risultati ad essa associati sono i seguenti:

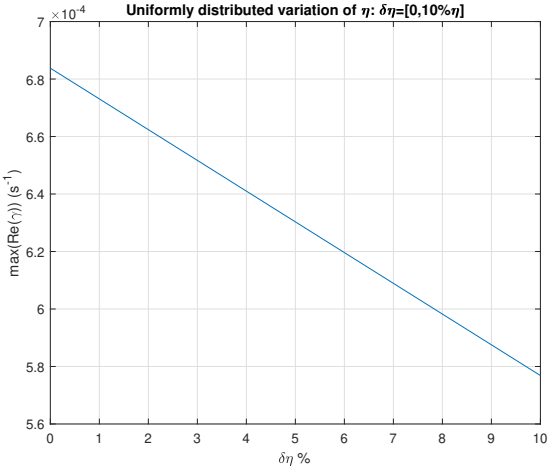

Figure 9: *Shift dell'autovalore dominante dato da un aumento di* η *fino al* 10% *del suo valore imperturbato.*

Si può notare come un incremento di η corrisponda ad una diminuzione della parte reale dell'autovalore dominante, risultando quindi in un'azione stabilizzante per il sistema. Fisicamente questo effetto può essere associato all'introduzione di un fattore dissipativo all'interno dell'equazione evolutiva del campo magnetico indotto. Il corrispettivo valore di sensitività relativa è $S = -1.564$.

Conclusioni

Il lavoro contenuto in questa tesi ha permesso di studiare in maniera dettagliata la stabilità di un sistema governato dalle equazioni della fluidodinamica in ipotesi di flusso comprimibile, introducendo dapprima i termini legati ai gradienti spaziali delle configurazioni di equilibrio studiate, e poi estendendo il modello a fluidi conduttivi, adattando il modello MHD per il caso monodimensionale. Una serie di risultati rappresentati all'interno di mappe di stabilità sono stati presentati, assieme ad un'analisi di sensitività modale per valutare l'impatto che le principali quantità che caratterizzano il sistema hanno sulla stabilità di quest'ultimo.

Contents

Ringraziamenti iii

Sommario v

Abstract vii

Estratto ix

Contents xxi

List of Symbols xxiii

List of Figures xxvii

List of Tables xxxi

Introduction 1

1 Non-conductive fluid 3
1.1 Introduction to the problem . . . 3
1.2 Governing equations for a unidimensional compressible flow . . . 4
1.3 Dynamic stability for uniform flow profiles . . . 6
1.4 Modal analysis: spatial gradients effects . . . 9
1.4.1 Geometry, domain and boundary conditions . . . 9
1.4.2 Stationary solution: unperturbed equilibrium profiles . . . 9
1.4.3 Stationary solution: PWR water . . . 10
1.4.4 Stationary solution: liquid Na . . . 14
1.4.5 Linearization and numerical discretization of unidimensional, compressible NS equations . . . 16
1.4.6 Definition of modal analysis . . . 20
1.4.7 Algorithm to compute the stability maps . . . 21
1.4.8 Results: subcooled water . . . 22
1.5 Sensitivity analysis: non-conductive fluid . . . 29
1.5.1 Introduction to the sensitivity analysis . . . 29
1.5.2 Mathematical derivation . . . 29
1.5.3 Algorithm for parametric sensitivity analysis . . . 31
1.5.4 Base flow sensitivity analysis . . . 32
1.5.5 Algorithm for base flow sensitivity analysis . . . 32
1.5.6 Results: subcooled water . . . 33

1.6 Conclusions 43

2 Conductive fluid **45**
2.1 Introduction to the problem 45
2.2 Governing equations for a conducting fluid 46
2.2.1 MHD governing equations 46
2.2.2 Unidimensional balance equations: conductive fluid 49
2.3 Modal analysis for the conductive fluid 51
2.3.1 Numerical discretization of the unidimensional MHD equations 51
2.3.2 Results: liquid Na 53
2.4 Sensitivity analysis for the conductive fluid 57
2.4.1 Results: liquid Na 57
2.5 Conclusions 60

Conclusions **61**

A Thermodynamic and transport properties of liquid sodium **65**

B Derivation of the coefficients for the state equation of liquid sodium **67**

Bibliography **69**

List of Symbols

The next list describes several symbols that will be later used within the body of the document

Latin

$\bar{s}$	Laplace frequency variable	s^{-1}
$\tilde{c}$	modified speed of sound	$\mathrm{m\,s}^{-1}$
$\tilde{g}$	modified gravitational acceleration	$\mathrm{m\,s}^{-2}$
A	dynamics matrix	
B	magnetic field	T
b	exponent of the drag coefficient model	
c	speed of sound	$\mathrm{m\,s}^{-1}$
C_P	specific heat at constant pressure	$\mathrm{J\,kg}^{-1}\,\mathrm{K}^{-1}$
D	diameter of the channel	m
E	electric field	$\mathrm{V\,m}^{-1}$
f_D	Darcy friction factor	
g	gravitational acceleration	$\mathrm{m\,s}^{-2}$
H	magnetic field intensity	$\mathrm{A\,m}^{-1}$
J	current density	$\mathrm{A\,m}^{-2}$
k	wave-vector	m^{-1}
k_0	stability parameter of the drag coefficient	m^{-1}
k'	effective drag coefficient per unit length	m^{-1}
L	channel's length	m
N	number of subdivisions of the channel's length	

p	pressure	Pa
Re	Reynolds number	
s	massic specific entropy	$\mathrm{J\,kg^{-1}\,K^{-1}}$
T	temperature	K
t	time coordinate	s
u	specific internal energy per unit mass	$\mathrm{J\,m^{-3}}$
v	velocity	$\mathrm{m\,s^{-1}}$
v^*	specific volume	$\mathrm{m^3kg^{-1}}$
w	wave-frequency	$\mathrm{s^{-1}}$
X	state vector	
z	spatial coordinate, longitudinal to the channel	m

Greek

α	state equation linearization coefficient, $u \propto p$	$\mathrm{Jkg^{-1}Pa^{-1}}$
α_p	isobaric thermal expansion coefficient	$\mathrm{K^{-1}}$
$\bar{\gamma}$	polytropic index	
β	state equation linearization coefficient, $u \propto \rho$	$\mathrm{Jm^3kg^{-2}}$
β_T	isothermal compressibility	$\mathrm{Pa^{-1}}$
δ	perturbation of a state variable	
ϵ	roughness	µm
η	electrical resistivity	$\Omega\,\mathrm{m}$
γ	dominant eigenvalue of the dynamics matrix A	$\mathrm{s^{-1}}$
λ	eigenvalues of the dynamics matrix A	$\mathrm{s^{-1}}$
μ	dynamic viscosity	$\mathrm{Pa\,s}$
μ_0	magnetic permeability of vacuum	$\mathrm{H\,m^{-1}}$
μ_r	relative magnetic permeability	
ϕ	general state variable	
ρ	density	$\mathrm{kg\,m^{-3}}$

ρ_e	charge density	$\mathrm{C\,m^{-3}}$
σ	electrical conductivity	$\mathrm{S\,m^{-1}}$
τ	viscous stress tensor	
θ	generic parameter characterizing an equilibrium point	
ς	generic eigenvalue	

Subscripts

0	state variable evaluated at linearization point
i	i-th array element
in	inlet
max	maximum value
min	minimum value
out	outlet
sat	saturation

Superscripts

$*$	complex conjugated
$-$	averaged quantity
$\dagger$	adjoint vector or matrix
$=$	double tensor
$\rightarrow$	vector
$\sim$	perturbed quantity
T	transposed

List of Figures

Figure 1 Mappa di stabilità per flusso monodimensionale comprimibile, profili spaziali uniformi, acqua sottoraffreddata, moto in salita. xi
Figure 2 Geometria, dominio e condizioni al contorno. xi
Figure 3 Grafico di convergenza di $Re(\gamma)$, flusso uniforme, acqua sottoraffreddata. xiii
Figure 4 Mappe di stabilità per l'acqua sottoraffreddata xiii
Figure 5 Geometria, dominio e condizioni al contorno per il caso conduttivo. xv
Figure 6 Mappe di stabilità per il sodio liquido. xvi
Figure 7 Variazione del coefficiente di attrito critico all'aumentare dell'intensità del campo magnetico esterno, sodio liquido. xvii
Figure 8 Shift dell'autovalore dominante dato da un aumento di B_0 fino al 10% del suo valore imperturbato. xviii
Figure 9 Shift dell'autovalore dominante dato da un aumento di η fino al 10% del suo valore imperturbato. xviii

Figure 1.1 Stability map, uniform flow, subcooled water, upflow. 8
Figure 1.2 Geometry, domain and boundary conditions. 9
Figure 1.3 Internal energy as a function of pressure and density. 11
Figure 1.4 Stationary velocity along z, subcooled water. 12
Figure 1.5 Stationary pressure along z, subcooled water. 13
Figure 1.6 Stationary density along z, subcooled water. 13
Figure 1.7 Stationary internal energy along z, subcooled water. 14
Figure 1.8 Stationary velocity along z, liquid sodium. 15
Figure 1.9 Stationary pressure along z, liquid sodium. 15
Figure 1.10 Stationary density along z, liquid sodium. 15
Figure 1.11 Example of mesh for spatial discretization: N=50 elements and length L=0.4 m. 17
Figure 1.12 Sparsity and the diagonal features of A, N=10. 20
Figure 1.13 Convergence plot of $Re(\gamma)$, uniform flow, subcooled water. . . 23
Figure 1.14 Stability map for uniform flow, subcooled water. 24
Figure 1.15 Convergence plot of $Re(\gamma)$, spatial flow profiles, $L = 0.4\ m$, subcooled water. 25
Figure 1.16 Stability map, spatial flow profiles, subcooled water. 26
Figure 1.17 Stationary pressure along z, subcooled water. 27
Figure 1.18 Stationary derivative of pressure along z, subcooled water. . . 27
Figure 1.19 Convergence plot of $Re(\gamma)$, concentrated pressure drop, $L = 0.4\ m$, subcooled water. 27
Figure 1.20 Stability map, concentrated pressure drop, subcooled water. . 28

Figure 1.21 Stability map, concentrated pressure drop, subcooled water. . 28
Figure 1.22 Sensitivity analysis: classical eigenvalue problem vs adjoint eigenvalue problem. 34
Figure 1.23 Sensitivity analysis: a subset of the eigenvalues of A close to imaginary axis of the complex plane: in red the unperturbed eigenvalues, in blue the shift of the eigenvalue for increasing values of α. 35
Figure 1.24 Sensitivity analysis: dominant eigenvalue shift with an increase of α up to the 10% of its unperturbed value. 36
Figure 1.25 Sensitivity analysis: dominant eigenvalue shift with an increase of β up to the 10% of its unperturbed value. 36
Figure 1.26 Sensitivity analysis: dominant eigenvalue shift with an increase of k_0 up to the 10% of its unperturbed value. 37
Figure 1.27 Sensitivity analysis: dominant eigenvalue shift with a decrease of the value of b up to -10% of the value of b. 37
Figure 1.28 Base flow sensitivity analysis: dominant eigenvalue shift with an increase of v_0 up to the 10% of its unperturbed averaged value $\bar{v}_0$. 39
Figure 1.29 Base flow sensitivity analysis: dominant eigenvalue shift with an increase of p_0 up to the 10% of its unperturbed averaged value $\bar{p}_0$. 40
Figure 1.30 Base flow sensitivity analysis: dominant eigenvalue shift with an increase of ρ_0 up to the 10% of its unperturbed averaged value $\bar{\rho}_0$. 40
Figure 1.31 Base flow sensitivity analysis: dominant eigenvalue shift with an increase of the spatial derivative of v_0 up to the 10% of its unperturbed averaged value. 41
Figure 1.32 Base flow sensitivity analysis: dominant eigenvalue shift with a decrease of the spatial derivative of p_0 up to the 10% of its unperturbed averaged value. 41
Figure 1.33 Base flow sensitivity analysis: dominant eigenvalue shift with a decrease of the spatial derivative of ρ_0 up to the 10% of its unperturbed averaged value. 42
Figure 1.34 Stabilizing effect of v_{in} as k_0 is maintained constant. 42

Figure 2.1 Geometry, domain and boundary conditions. 49
Figure 2.2 Convergence plot of $Re(\gamma)$, uniform flow, $B_0 = 0\ T$, liquid sodium. 53
Figure 2.3 Stability map for uniform flow, $B_0 = 0\ T$, liquid sodium. . . . 54
Figure 2.4 Convergence plot of $Re(\gamma)$, uniform flow, $B_0 = 1.0\ T$, liquid sodium. 54
Figure 2.5 Stability map for uniform flow, $B_0 = 1.0\ T$, liquid sodium. . . 55
Figure 2.6 Shift of $k_{0,min}$ with increasing values of B_0, up to $B_0 = 1.0\ T$, liquid sodium. 56
Figure 2.7 Shift of $k_{0,min}$ with increasing values of B_0, up to $B_0 = 0.2\ T$, liquid sodium. 56
Figure 2.8 Base flow sensitivity analysis: dominant eigenvalue shift with an increase of B_0 up to the 10% of its unperturbed value. 58
Figure 2.9 The root locus of A in $\times$ and $\tilde{A}$ in $\cdot$, computed with an increase of B_0 up to the 10% of its unperturbed value. 58
Figure 2.10 Base flow sensitivity analysis: dominant eigenvalue shift with an increase $\delta\eta$ up to the 10% of η. 59

Figure 2.11 Flowchart of this thesis work. 63

Figure A.1 Thermodynamic and transport properties of liquid sodium. . . 66

List of Tables

Table 1 Principali parametri che caratterizzano il sistema ed il loro impatto sulla stabilità. xv
Table 2 Principali profili stazionari che caratterizzano il sistema ed il loro impatto sulla stabilità. xv

Table 1.1 Input parameters for the steady-state simulation of subcooled water. 12
Table 1.2 Input parameters for the steady-state simulation of liquid sodium. 14
Table 1.3 Dominant eigenvalue shift due to a perturbation $\delta\alpha = 10\%\ \alpha$: eigenvalue problem vs adjoint eigenvalue problem. 34
Table 1.4 Single parameter sensitivity analysis results. 38
Table 1.5 Unperturbed averaged values for the state variables and their spatial derivatives. 39
Table 1.6 Summary of the main parameters of the non-conductive problem and their impact over stability. 44
Table 1.7 Summary of the stationary profiles and their spatial derivatives of the non-conductive problem and their impact over stability. 44

Table 2.1 Summary of the main parameters of the non-conductive problem and their impact over stability. 62
Table 2.2 Summary of the stationary profiles and their spatial derivatives of the non-conductive problem and their impact over stability. 62
Table 2.3 Summary of the main physical quantities of the conductive problem and their impact over stability. 62

Introduction

The stability of fluid flows is a problem that has been widely investigated since the nineteenth century, with the fundamental contributes given by Helmholtz, Kelvin, Rayleigh and Reynolds in this sense. A consolidated approach to tackle this kind of problem consists in the research of a equilibrium configuration of the fluid flow studied, the linearization of the governing equations (which, in most cases, are highly nonlinear) describing the motion of the fluid around the equilibrium configuration and the spectral analysis of the dynamics matrix obtained in the linearization process. With this procedure is possible to study the modal amplifications or damping of infinitesimal perturbations of the equilibrium configuration.
This method, referred as *modal stability analysis*, represent a good starting point to access the stability properties of the system studied. However, in a particular kind of problems, the theoretical results don't match with the experimental observations made in laboratory. This discrepancy is related to the *nonnormality* of the dynamics matrix found with the linearization process. Some examples in which the modal stability analysis fails are plane Couette flow and plane Poiseuille flow ([Trefethen and Embree 2005]).
A recent study of [Schmid and Brandt 2014] proposes the employment of the *adjoint theory* to study the nonnormal behaviour of dynamics matrices for different fluid flows problems: *non-modal analysis*, *receptivity analysis* and *sensitivity analysis* represent some application fields of this theory.
In this work, an adjoint-based sensitivity analysis is adopted to study a compressible flow of a conductive fluid under the action of an external magnetic field in the one-dimensional approximation.
The coupling between the motion of the conductive fluid and the external magnetic field is described within the MHD (Magnetohydrodynamics) model.
Magnetohydrodynamics is applied to a wide set of physical problems such as the study of the interaction between the Solar wind and the Earth's magnetosphere, the dynamics of accretion disks around black holes, the dynamo effect present inside the Earth and the physical mechanisms existing inside the stars ([Galtier 2016]).
Technological applications of the MHD model are found in the study of magnetically confined thermonuclear plasmas for fusion research, in the dynamic description of conductive fluids, such as liquid sodium and liquid lithium, employed respectively for fast breeder reactors and in the breeding blanket surrounding Tokamak machines and in the field of space engineering for the electromagnetic propulsion of spacecrafts and orbiting satellites.
The work presented in the following is included inside a wider project devoted to the study and development of a solver in OpenFOAM useful to simulate a magnetically

confined plasma for fusion applications in different configurations and geometries, by employing the MHD model for its description. The project is subdivided in different steps that, together, contribute to the fulfilment of the main task:

- linear stability analysis of conductive fluids within the MHD framework in simple geometries (one-dimensional and two-dimensional configurations).
- sensitivity analysis of the previous problems by means of the adjoint theory.
- implementation of a OpenFOAM solver to study the MHD model in different geometrical configurations and flow regimes.
- development of the adjoint model in OpenFOAM for sensitivity purposes.
- reduction of order of the main and adjoint model developed in OpenFOAM to lower the computational costs of numerical simulations.

A first theoretical and numerical study in this sense is proposed in the work of [Trotta et al. 2019]. The study of a compressible, unidimensional flow of a conductive fluid under the action of an external magnetic field, in the hypothesis of a uniform initial configuration in space, is examined. A series of analytical results regarding the linear stability analysis of the system are obtained via Fourier analysis, with the derivation of dispersion relations for the conductive fluid in the uniform configuration.
Starting from these results, the previous hypothesis of uniform spatial configuration has been questioned as regards the linear stability analysis of the system.
In particular, in the first chapter, a *modal stability analysis* is carried out by setting the equations that describe the motion of a compressible flow in the one-dimensional approximation within a simple geometry (a riser). The linearization of the set of equations around an equilibrium point is performed and the discretization of spatial derivatives acting on the perturbations of the state variables is conducted with the numerical method of finite differences.
The impact of pressure gradients and profiles for different equilibrium configurations is then investigated, highlighting the main differences in terms of linear stability for each specific case.
Subsequently, a *modal sensitivity analysis* is carried out to evaluate the impact on stability of small perturbations on the main parameters of the problem, together with slight increases on the velocity, pressure and density profiles and the their spatial derivatives along the channel.
In the second chapter, the previous equations are coupled with the dynamic description of the magnetic field induced inside a conducting fluid, in the presence of an external magnetic field. The study carried out for the non-conductive case is re-proposed for the conductive case and the differences in terms of linear stability analysis are finally highlighted.

Chapter 1

Non-conductive fluid

Abstract. This chapter proposes different numerical tools and techniques devoted to the dynamical characterization of a hydrodynamic system governed by the compressible Navier-Stokes equation in the unidimensional approximation.
A *modal stability analysis* ([Schmid and Brandt 2014]) is carried out by linearizing the set of governing equations around an equilibrium point and studying the linear stability response of the system for the selected equilibrium point. Finite differences formulas are employed for the numerical approximation of the spatial derivatives applied to the perturbation of the state variables. Mesh sensitivity is performed for each specific case and stability maps are then drawn to resume graphically the main results. Finally, a *parametric sensitivity analysis* and *base flow sensitivity analysis* based on the *adjoint modal perturbative approach* ([Schmid and Brandt 2014]) are adopted to study the impact of the main parameters and the base flow on the stability features of the equilibrium point.

1.1 Introduction to the problem

The aim of this chapter is the dynamic characterization of the unidimensional compressible Navier-Stokes equations ([Doster and Kendall 1999]) in a simple geometry, with different mathematical and numerical tools presented in the work of [Schmid and Brandt 2014], in order to obtain stability results from different points of view and make general considerations about the overall response of the system to infinitesimal perturbations around an equilibrium point.
The first topic to be investigated concerns the *modal analysis* of the system and how spatial derivatives and profiles of the stationary solution affect the dynamic response of the linearized perturbations of the state variables.
The second topic will be a *sensitivity analysis*, in which the main thermo-hydraulic and physical parameters that characterize the flow, together with the base flow profiles and its derivatives, are slightly perturbed, in order to measure how the eigenvalues in the complex plane, describing the dynamics of the system, are affected by this perturbation.
The evolving fluids considered in this study are subcooled water and liquid sodium: the first is chosen because of the complete and accessible characterization of its thermo-hydraulic properties present in literature (no fase transition will be treated,

going beyond the scope of this work), the latter to introduce an external magnetic field in the system and study how the coupling of the induced magnetic field and the flow of the liquid sodium affects the dynamics of the conductive fluid.

1.2 Governing equations for a unidimensional compressible flow

In this section, the equations governing the time behaviour of a compressible, non-conductive fluid flow are presented ([Doster and Kendall 1999]), in the approximation of a unidimensional dependence of the fluid quantities describing the motion of the fluid. The state variables indeed depend only on the spatial coordinate z.
The domain considered in this case study is a simple 1D vertical channel (riser), in which the fluid goes upwards with prescribed inlet velocity v_{in}, inlet density ρ_{in} and outlet pressure p_{out}.
The system of governing equations holding for the description of a compressible fluid in the unidimensional approximation is the following:

- *mass conservation*
$$\frac{\partial \rho}{\partial t} + \frac{\partial \rho v}{\partial z} = 0 \tag{1.1}$$
- *internal energy conservation*
$$\frac{\partial \rho u}{\partial t} + \frac{\partial \rho u v}{\partial z} = -p\frac{\partial v}{\partial z} \tag{1.2}$$
- *momentum conservation*
$$\rho\frac{\partial v}{\partial t} + \rho v\frac{\partial v}{\partial z} = -\frac{\partial p}{\partial z} - \rho g - k^{'}\frac{\rho v^2}{2} \tag{1.3}$$
- *equation of state*
$$\rho = \rho(u, p) \tag{1.4}$$

The state variables describing the fluid motion field and its thermodynamics properties in each local point z are: the fluid velocity v (in m/s), the fluid density ρ (in kg/m^3), the fluid pressure p (in Pa) and its internal energy u (in J/kg).
The volume forces acting in the *momentum equation* (1.3) are the gravitational force term ρg and an effective drag force $k^{'}\frac{\rho v^2}{2}$, which introduces distributed pressure losses inside the system, acting as a dissipative term.
The term $k^{'}$is defined as the *effective drag coefficient per unit length* (measured in m^{-1}) and a possible functional dependence on the flow velocity is:

$$k^{'} = k_0\left(\frac{\tilde{v}}{v}\right)^b \tag{1.5}$$

where $\tilde{v}$ is a reference velocity for the system (in this case it is adopted as reference velocity the inlet velocity v_{in}) and b could be tuned properly to describe different flow

regimes ($b \simeq 0.2$ for a turbolent flow, $b = 1.0$ for a laminar flow).
A physical insight for the effective drag coefficient $k^{'}$ is given: the distributed pressure losses in a uniform channel of diameter D, length L and roughness ϵ can be expressed, in the monodimensional approximation, with the Darcy-Weisbach equation ([Vijayan, Nayak, and N. Kumar 2019]):

$$\frac{\Delta P}{L} = f_D \, \frac{\rho \bar{v}^2}{2D} \tag{1.6}$$

where f_D is the *Darcy friction factor*. The effective drag coefficient per unit length can be restated as a function of the Darcy friction factor:

$$k^{'} = \frac{f_D}{D} \tag{1.7}$$

The Darcy friction factor is determined once the Reynolds number Re, the diameter of the pipe D and the roughness ϵ are set. It can be computed exploiting the *Colebrook-White equation* for $Re > 4000$ ([Shashi Menon 2015]) or by a graphical interpolation on the *Moody diagram*.
For a laminar flow the analytical result, which can be derived from the Poiseuille solution of the NS equation, is recalled:

$$f_D = \frac{64}{Re} \quad Re < 2000 \tag{1.8}$$

Meanwhile, if the flow is in a completely developed turbulent regime, the implicit Colebrook-White equation can be used:

$$\frac{1}{\sqrt{f_D}} = -2log\left(\frac{\epsilon}{3.7D} + \frac{2.51}{Re\sqrt{f_D}}\right) \tag{1.9}$$

If the relative roughness is negligible, the friction losses in the turbulent case results lower then in the laminar case.
The coefficient k_0 in the following study is seen as a stability parameter that can be tuned for each simulation and, eventually, increased to obtain a stabilizing effect for the system.
The *internal energy equation* (1.2) contains the compressibility work term $-p\frac{\partial v}{\partial z}$, in the inviscid approximation. This could be justified by the fact that for liquids like subcooled water or liquid sodium the increase of temperature due to viscous effects is negligible. No external heat sources are present in the following analysis, as thermal effects are not the main issue to be addressed in this work.
The *state equation* (1.4) closes the system of equations, expressing ρ as a function of u and p.
This relationship is one key feature characterizing a compressible flow, i.e. the dependence of the density on pressure, and can be derived analitically by means of the data present in literature for subcooled water and liquid sodium.
The choice of this formulation for the unidimensional compressible Navier-Stokes equations is collocated inside the framework developed by [Doster and Kendall 1999],

in which the main results are presented in the following section.
These results will be the starting point for a wider extension of the study, carried out by exploiting the simulations performed in COMSOL ® Multiphysics inside MATLAB®'s environement, in which the impact of the spatial dependence of the equilibrium points of the system will be investigated.

1.3 Dynamic stability for uniform flow profiles

The main results of the study done by [Doster and Kendall 1999], recalled by [Trotta et al. 2019] in his thesis work, are resumed in this section.
The system of equations (1.1), (1.2), (1.3) and (1.4) is linearized around an unperturbed steady-state initial condition. Each variable of state ϕ can be expressed as the sum of the *equilibrium value* ϕ_0 and the *perturbation* $\delta\phi$:

$$\phi(z,t) = \phi_0(z,0) + \delta\phi(z,t) \tag{1.10}$$

In the following, it is assumed that the steady-state profiles ϕ_0 at the linearization point are homogeneous in space.
This assumption will be then relaxed in the following section, in order to check if it's a conservative approximation in the stability sense.
The analysis is carried out by assuming that the perturbations have a functional form of plane waves:

$$\delta\phi(z,t) = \delta\phi \; exp\left[i\left(kz - wt\right)\right] \tag{1.11}$$

where k is the plane wave's wave-vector, real and positive defined, and w is its wave-frequency, a complex number.
Then, a linear stability analysis is carried out with the hypothesis of homogeneous spatial profiles of the state variables; the linearized system of equations around the linearization point $X_0 = [\rho_0, u_0, v_0, p_0]^T$ is the following:

$$\begin{cases} \dfrac{\partial\delta\rho}{\partial t} + v_0\dfrac{\partial\delta\rho}{\partial z} + \rho_0\dfrac{\partial\delta v}{\partial z} = 0 \\ \dfrac{\partial\delta u}{\partial t} + v_0\dfrac{\partial\delta u}{\partial z} = -\dfrac{p_0}{\rho_0}\dfrac{\partial\delta v}{\partial z} \\ \rho_0\dfrac{\partial\delta v}{\partial t} + \rho_0 v_0\dfrac{\partial\delta v}{\partial z} = -\dfrac{\partial\delta p}{\partial z} - \delta\rho g - \dfrac{k_0\delta\rho v_0^2}{2} - \left(\dfrac{2-b}{2}\right)k_0\rho_0 v_0\delta v \\ \delta\rho - \left(\dfrac{1}{\beta^2}\right)\delta u - \left(\dfrac{1}{c^2}\right)\delta p = 0 \end{cases} \tag{1.12}$$

Substituting (1.11) in the set of equations present in (1.12), a linear system in Fourier space is obtained:

$$\begin{cases} \left[i\left(v_0 k-\omega\right)\right]\delta\rho+\left(i\rho_0 k\right)\delta v=0 \\ \left[i\left(v_0 k-\omega\right)\right]\delta u+\left(i\dfrac{p_0}{\rho_0}k\right)\delta v=0 \\ \left(\dfrac{\tilde{g}}{\rho_0}\right)\delta\rho+\left[\tilde{\xi}+i\left(v_0 k-\omega\right)\right]\delta v+\left(\dfrac{ik}{\rho_0}\right)\delta p=0 \\ \delta\rho-\left(\dfrac{1}{\beta^2}\right)\delta u-\left(\dfrac{1}{c^2}\right)\delta p=0 \end{cases} \tag{1.13}$$

where :

$$\tilde{\xi}\equiv k_0 v_0\frac{2-b}{2}\equiv\tilde{\xi_0}\frac{2-b}{2} \tag{1.14}$$

is the friction term and:

$$\tilde{g}\equiv g+\tilde{\xi}\frac{v_0}{2-b} \tag{1.15}$$

is the modified gravitational acceleration.
The two coefficients in the state equation of (1.13) are defined as:

$$\frac{1}{\beta^2}=\left(\frac{\partial\rho}{\partial u}\right)_p \tag{1.16}$$

$$\frac{1}{c^2}=\left(\frac{\partial\rho}{\partial p}\right)_u \tag{1.17}$$

c could be treated as the sound speed of the fluid[1]. The state vector is the following:

$$\delta X=\left[\delta\rho,\quad \delta u,\quad \delta v,\quad \delta p\right]^T \tag{1.19}$$

The dynamics matrix of system (1.13) is:

$$A=\begin{bmatrix} i\left(v_0 k-\omega\right) & 0 & i\rho_0 k & 0 \\ 0 & i\left(v_0 k-\omega\right) & i\dfrac{p_0}{\rho_0}k & 0 \\ \dfrac{\tilde{g}}{\rho_0} & 0 & \tilde{\xi}+i\left(v_0 k-\omega\right) & \dfrac{ik}{\rho_0} \\ 1 & -\dfrac{1}{\beta^2} & 0 & -\dfrac{1}{c^2} \end{bmatrix} \tag{1.20}$$

[1]The thermodynamic definition of the sound speed is:

$$\frac{1}{c^2}=\left(\frac{\partial\rho}{\partial p}\right)_s \tag{1.18}$$

If thermal effects are neglected, this definition coincides with (1.17) employed in this work.

Solving now $det(A) = 0$, three dispersion relationships $w = w(k)$ are obtained, describing the stability features of the system.
The *stability condition* to be satisfied in order to obtain damped perturbations $\delta\phi$ in time ([Nise et al. 2011]) is:

$$Im(\omega) \leq 0 \qquad \forall\omega \tag{1.21}$$

It can be shown ([Doster and Kendall 1999]) that the most limiting case is given by upflow ($g > 0$): a fundamental result valid for this case, that will be widely employed in the rest of the work, is the stability condition ([Doster and Kendall 1999]):

$$k_0 v_0 \frac{2-b}{2}\left(1 - \frac{v_0}{\tilde{c}}\frac{1}{2-b}\right) > \frac{|g|}{\tilde{c}} \tag{1.22}$$

in which the modified sound speed is introduced:

$$\tilde{c} \equiv c\sqrt{1 - \frac{p_0}{\rho_0^2 \beta^2}} \tag{1.23}$$

In the framework of natural circulation, in which the study of [Doster and Kendall 1999] is collocated, the flow can be considered subsonic ($v_0 << \tilde{c}$), so a simplified condition can be found:

$$k_0 v_0 \frac{2-b}{2} > \frac{|g|}{\tilde{c}} \tag{1.24}$$

Given the velocity v_0 and a flow regime described by b , a minimum value of the control parameter is needed for stabilization:

$$k_{0,min} = \frac{1}{v_0}\frac{2}{2-b}\frac{|g|}{\tilde{c}} \tag{1.25}$$

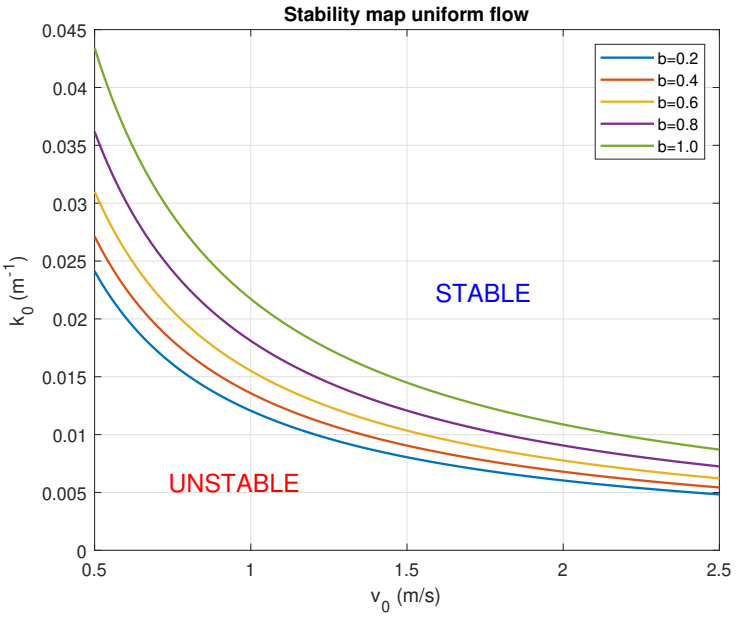

Figure 1.1: *Stability map, uniform flow, subcooled water, upflow.*

In Figure 1.1 the main results of this stability analysis are represented, employing subcooled water at temperature $T_0 = 320°C$ and pressure $p_0 = 15.5MPa$. Different curves at increasing b are reported: the trend is $\propto \frac{1}{v_0}$ and the stability is favored by lower values of b. This is determined by the fact that, in (1.14), for $b < 1$, the friction term is higher than for laminar flows, namely for $b = 1.0$.

1.4 Modal analysis: spatial gradients effects

1.4.1 Geometry, domain and boundary conditions

In this section an extension of the previous model is presented and the main differences will be discussed in detail. The geometry considered is a channel in which the longitudinal dimension is dominant with respect to the transverse ones and the unidimensional approximation is valid.

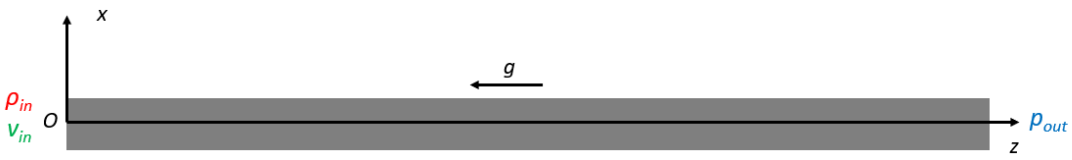

Figure 1.2: *Geometry, domain and boundary conditions.*

The approximation of homogeneous spatial profiles is relaxed and a numerical scheme is employed to approximate the spatial derivatives along the z-axis.
The computational domain is the interval $[0, L]$ on the z-axis, divided in N equal elements, and the selected boundary conditions are chosen to provide a numerically stable benchmark for compressible flows ([Poinsot and Lelef 1992]) which is also physically-reproducible.

Boundary Conditions:

- Inlet density: ρ_{in}
- Inlet velocity: v_{in}
- Outlet pressure: p_{out}

1.4.2 Stationary solution: unperturbed equilibrium profiles

According to the definition of *modal analysis* given by [Schmid and Brandt 2014], an equilibrium point has to be defined first, then the system is perturbed around this point: if the system returns back to the equilibrium point, it's deemed stable; if instead the system diverges from the equilibrium point, it's then unstable. This statement

is collocated inside the definition of Lyapunov stability criterium ([Lyapunov 1992]), in which an infinite time horizon is allowed for the return to equilibrium after a perturbation is introduced in the system (study of the free response of the system). To obtain the equilibrium point above mentioned, the non-linear, steady, compressible Navier-Stokes equations in the unidimensional approximation is to be solved:

$$\begin{cases} \dfrac{\partial \rho_0 v_0}{\partial z} = 0 \\ \dfrac{\partial \rho_0 u_0 v_0}{\partial z} = -p_0 \dfrac{\partial v_0}{\partial z} \\ \rho_0 v_0 \dfrac{\partial v_0}{\partial z} = -\dfrac{\partial p_0}{\partial z} - \rho_0 g - \dfrac{k^{'} \rho v_0^2}{2} \\ u_0 = \overline{\mathrm{u}} + \alpha p_0 + \beta \rho_0 \end{cases} \tag{1.26}$$

The last equation in (1.26) is the state equation for internal energy of the selected evolving fluid, linearized by choosing as thermodynamic coordinates for its evaluation (ρ_{in}, p_{out}) to retrieve the coefficients $(\overline{\mathrm{u}}, \alpha, \beta)$, where:

$$\alpha = -\frac{\beta^2}{c^2}, \quad \beta = \beta^2$$

This procedure is valid if the resulting variation of the pressure and density along the channel is close to the prescribed boundary conditions employed in the numerical simulation. By substituting the state equation inside the internal energy equation of system (1.26), the latter is expressed as a function of ρ and p, leading to:

$$\begin{cases} \dfrac{\partial \rho_0 v_0}{\partial z} = 0 \\ \alpha \rho_0 v_0 \dfrac{\partial p_0}{\partial z} - \beta \rho_0^2 \dfrac{\partial v_0}{\partial z} = -p_0 \dfrac{\partial v_0}{\partial z} \\ \rho_0 v_0 \dfrac{\partial v_0}{\partial z} = -\dfrac{\partial p_0}{\partial z} - \rho_0 g - \dfrac{k^{'} \rho v_0^2}{2} \end{cases} \tag{1.27}$$

This non-linear system is solved by using the "General Form PDE" physics interface of COMSOL® Multiphysics, once the thermophysical properties of evolving fluid are specified and boundary conditions, the flow regime coefficient b and the control parameter k_0 are set for the simulation.

1.4.3 Stationary solution: PWR water

The first fluid studied is subcooled water; the reference temperature [2] and pressure is taken from the operative conditions ([Lamarsh and Baratta 2001]) of a PWR of nominal thermal power of 1GW:

- Inlet Temperature: $T_{in} = 320°C$
- Outlet pressure: $p_{out} = 15.5MPa$

[2]The mean value between the core inlet temperature and the outlet one.

Using the MATLAB® function XSteam [3], the inlet density can be evaluated as a function of the inlet temperature and outlet pressure (with an error given by the variation of the pressure along the length of the channel, from the outlet up to the inlet height):

$$\rho_{in} = \rho_{in}(T_{in}, p_{out}) = 680.20 \ kg/m^3$$

The coefficients α and β are computed by definition:

$$\alpha = \left(\frac{\partial u}{\partial p}\right)_{\rho}, \quad \beta \left(\frac{\partial u}{\partial \rho}\right)_{p} \tag{1.28}$$

The internal energy $u = u(p, \rho)$ is obtained by means of the XSteam function, within the region of the p-T thermodynamic plane confined in:

$$[p_{min}, p_{max}] \times [T_{min}, T_{max}] = [15.0MPa, 20.0MPa] \times [100°C, 330°C] \tag{1.29}$$

In particular, as the saturation temperature evaluated for the lowest pressure considered is $T_{sat}(15MPa) = 342.16°C$, it can be inferred that the chosen region in the p-T plane is referred to subcooled water.
The minimum density computed inside the region (1.29) corresponds to:

$$\rho_{min} = \rho(p_{min}, T_{max}) = \rho(15MPa, 330°C) = 649.62 \ kg/m^3$$

while the maximum is:

$$\rho_{max} = \rho(p_{max}, T_{min}) = \rho(20MPa, 100°C) = 967.43 \ kg/m^3$$

Referring now to the p-ρ thermodynamic plane defined as:

$$[p_{min}, p_{max}] \times [\rho_{min}, \rho_{max}] = [15.0MPa, 20.0MPa] \times [650 \ kg/m^3, 967 \ kg/m^3] \tag{1.30}$$

the internal energy is computed inside the region (1.30).

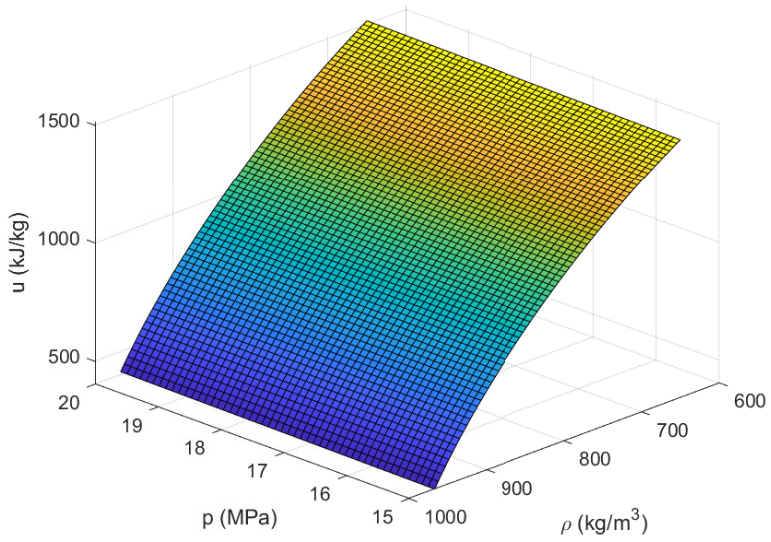

Figure 1.3: *Internal energy as a function of pressure and density.*

[3]Magnus Holmgren (2020). X Steam, Thermodynamic properties of water and steam. MATLAB Central File Exchange.Retrieved August 18, 2020.

The Interpolation Tool CfTool®, embedded in MATLAB®, is then employed to find a polynomial fit of the surface in Figure 1.3, and the coefficients α and β can be finally evaluated (the validity region is confined in (1.30)):

$$\alpha = \left(\frac{\partial u}{\partial p}\right)_{\rho} = 3.297 \cdot 10^{-3}\ J/kgPa$$

$$\beta = \left(\frac{\partial u}{\partial \rho}\right)_{p} = -\frac{1}{6.185 \cdot 10^{-5} + 2.234 \cdot 10^{-10} u_0(\rho_{in}, p_{out})} Jm^3/kg^2$$

where β can be computed once $u_0 = u_0(p_{out}, \rho_{in})$ is found.
The inputs needed to start a steady-state simulation with COMSOL® are:

Simulation parameters:

- Channel length L
- Subdivision of the domain N
- Inlet temperature T_{in}
- Outlet pressure p_{out}
- Inlet velocity v_{in}
- Flow regime b
- Stability parameter of the drag coefficient k_0

For example, given a set of inputs for the model:

L	N	T_{in}	p_{out}	v_{in}	b	k_0
0.6 m	500	320 $°C$	15.5 MPa	1 m/s	1.0	0.0217 m^{-1}

Table 1.1: *Input parameters for the steady-state simulation of subcooled water.*

The corresponding spatial profiles for the state variables at $t = 0\ s$ are the following:

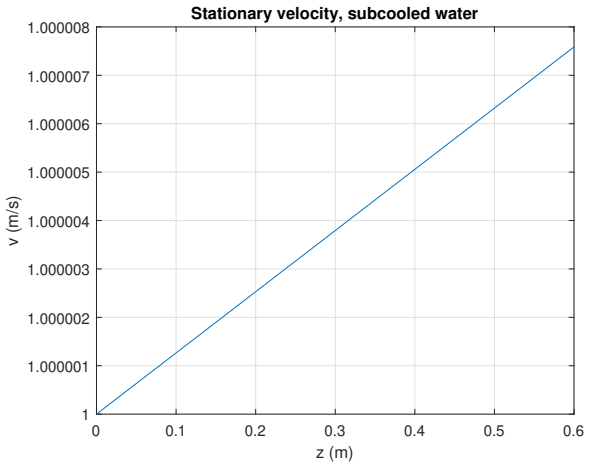

Figure 1.4: *Stationary velocity along z, subcooled water.*

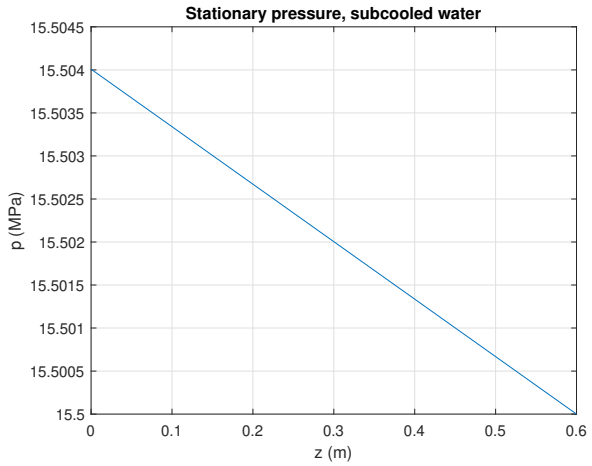

Figure 1.5: *Stationary pressure along z, subcooled water.*

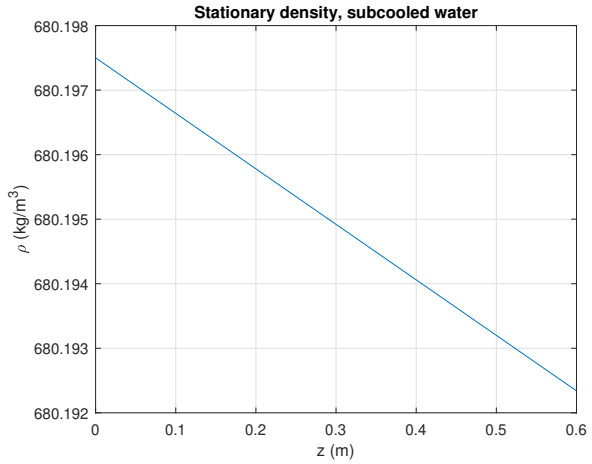

Figure 1.6: *Stationary density along z, subcooled water.*

It can be observed that, apart from the velocity profile in Figure 1.4 and the density profile in Figure 1.6, the main difference between the case studied in Section 1.3 is due to the variation of the pressure along z (Figure 1.5): a pressure drop of about $\Delta p = 0.2$ *bar* is induced by the pressure losses given by the friction term in Eq.(1.14) and by the prevalence needed to overcome the gravitational term ρg present in the momentum equation (1.3), once the outlet pressure is fixed by the boundary condition on the exit of the channel.
As regards the internal energy in Figure 1.7, no thermal effects or heat sources were added to the study, so no appreciable variation of internal energy is expected.

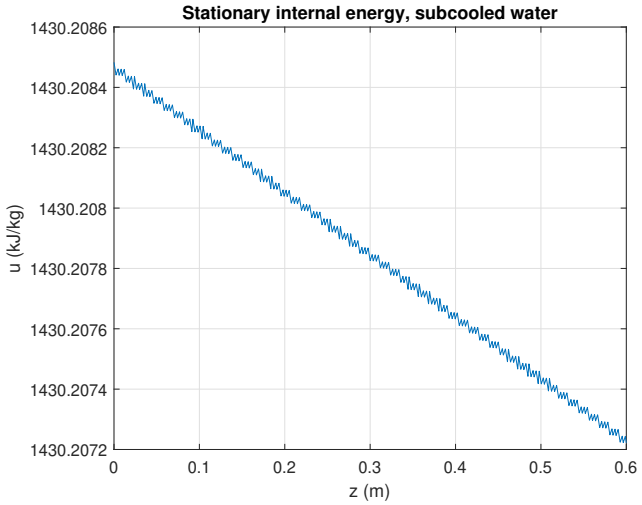

Figure 1.7: *Stationary internal energy along z, subcooled water.*

1.4.4 Stationary solution: liquid Na

The other fluid taken into account is liquid sodium: temperature and pressure used in the simulation are referred to the nominal working conditions of a Fast Breeder Reactor ([IAEA 2013]) supplying 250MWe:

- Inlet Temperature: $T_{in} = 500°C$
- Outlet pressure: $p_{out} = 1\ bar$

Thermophysical properties of liquid sodium are illustrated in detail in the work of [Fink and Leibowitz 1995] and [Li et al. 2017] and are reported in Appendix A.
In Appendix B, an analytical procedure is proposed to derive the thermodynamic coefficients α and β in Eq. (1.28), once the working temperature T_{in} is set.
The same solver used for the steady-state simulation in COMSOL® of subcooled water can be employed in the study of liquid sodium, by changing the thermophysical properties of the state equation in Eq. (1.27). As an example, a steady-state simulation with the following input parameters is reported in the following:

L	N	T_{in}	p_{out}	v_{in}	b	k_0
0.6 m	500	500 $°C$	1 bar	1 m/s	1.0	0.0848 m^{-1}

Table 1.2: *Input parameters for the steady-state simulation of liquid sodium.*

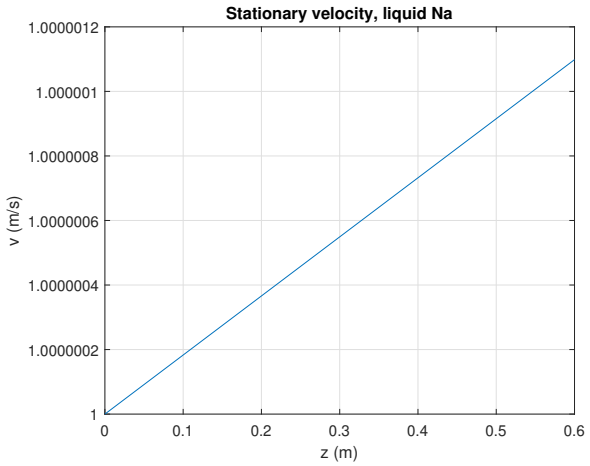

Figure 1.8: *Stationary velocity along z, liquid sodium.*

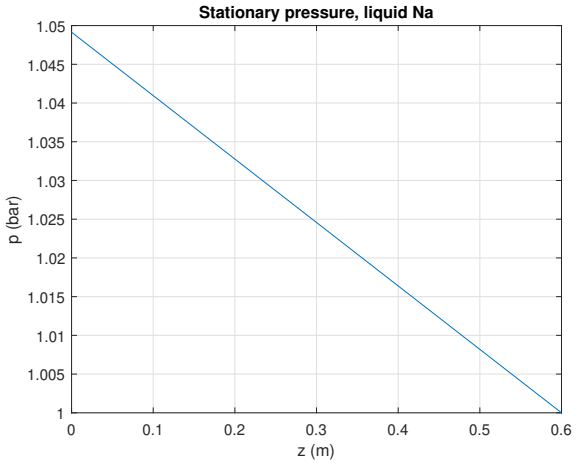

Figure 1.9: *Stationary pressure along z, liquid sodium.*

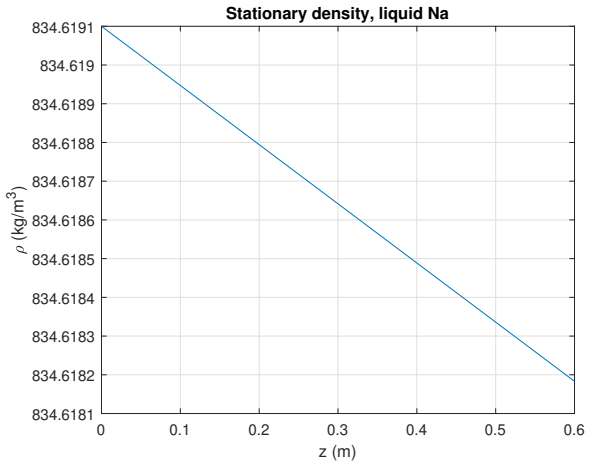

Figure 1.10: *Stationary density along z, liquid sodium.*

1.4.5 Linearization and numerical discretization of unidimensional, compressible NS equations

The results of Sections 1.4.3 and 1.4.4 are employed in the following study to provide physical spatial profiles for the state variables. First, an extension of the linearized set of equation presented in Eq. (1.12) is reported, taking into account also the linear terms associated with the spatial derivatives of the stationary profiles of $X_0 = [\rho_0, u_0, v_0, p_0]^T$:

$$\begin{cases} \dfrac{\partial \delta\rho}{\partial t} + v_0\dfrac{\partial \delta\rho}{\partial z} + \dfrac{\partial v_0}{\partial z}\delta\rho + \rho_0\dfrac{\partial \delta v}{\partial z} + \dfrac{\partial \rho_0}{\partial z}\delta v = 0 \\ \dfrac{\partial \delta u}{\partial t} + v_0\dfrac{\partial \delta u}{\partial z} + \delta v\dfrac{\partial u_0}{\partial z} + v_0\dfrac{\partial u_0}{\partial z}\dfrac{\delta\rho}{\rho_0} = -\dfrac{p_0}{\rho_0}\dfrac{\partial \delta v}{\partial z} - \dfrac{\delta p}{\rho_0}\dfrac{\partial v_0}{\partial z} \\ \dfrac{\partial \delta v}{\partial t} + v_0\dfrac{\partial \delta v}{\partial z} + \delta v\dfrac{\partial v_0}{\partial z} + \left(g + \dfrac{k_0 v_0^2}{2} + v_0\dfrac{\partial v_0}{\partial z}\right)\dfrac{\delta\rho}{\rho_0} = -\dfrac{1}{\rho_0}\dfrac{\partial \delta p}{\partial z} - \left(\dfrac{2-b}{2}\right)k_0 v_0 \delta v \\ \delta u = \alpha\delta p + \beta\delta\rho \end{cases} \tag{1.31}$$

Following the same procedure illustrated in Section 1.4.2, the perturbation of internal energy δu in state equation of the system (1.31) is substituted inside the internal energy equation, leading to an evolutive equation for the perturbation of the pressure δp:

$$\begin{cases} \dfrac{\partial \delta\rho}{\partial t} + v_0\dfrac{\partial \delta\rho}{\partial z} + \dfrac{\partial v_0}{\partial z}\delta\rho + \rho_0\dfrac{\partial \delta v}{\partial z} + \dfrac{\partial \rho_0}{\partial z}\delta v = 0 \\ \dfrac{\partial \delta p}{\partial t} + v_0\dfrac{\partial \delta p}{\partial z} + \delta v\dfrac{\partial p_0}{\partial z} - \dfrac{\beta}{\alpha}\rho_0\dfrac{\partial \delta v}{\partial z} - \dfrac{\beta}{\alpha}\delta\rho\dfrac{\partial v_0}{\partial z} + v_0\left(\dfrac{\beta}{\alpha}\dfrac{\partial \rho_0}{\partial z} + \dfrac{\partial p_0}{\partial z}\right)\dfrac{\delta\rho}{\rho_0} + \\ \qquad + \dfrac{p_0}{\alpha\rho_0}\dfrac{\partial \delta v}{\partial z} + \dfrac{1}{\alpha\rho_0}\dfrac{\partial v_0}{\partial z}\delta p = 0 \\ \dfrac{\partial \delta v}{\partial t} + v_0\dfrac{\partial \delta v}{\partial z} + \delta v\dfrac{\partial v_0}{\partial z} + \left(g + \dfrac{k_0 v_0^2}{2} + v_0\dfrac{\partial v_0}{\partial z}\right)\dfrac{\delta\rho}{\rho_0} = -\dfrac{1}{\rho_0}\dfrac{\partial \delta p}{\partial z} - \left(\dfrac{2-b}{2}\right)k_0 v_0 \delta v \end{cases} \tag{1.32}$$

The set of PDEs (1.32) can be expressed in a matricial form, useful hereafter to make considerations about the *modal analysis* that will be carried out:

$$\frac{\partial}{\partial t}\delta X = A\delta X \tag{1.33}$$

The state vector δX is defined as:

$$\delta X = \begin{bmatrix} \delta v, & \delta p, & \delta\rho \end{bmatrix}^T \tag{1.34}$$

And the dynamics matrix A is defined as:

$$A = \begin{bmatrix} A_{11} & A_{12} & A_{13} \\ A_{21} & A_{22} & A_{23} \\ A_{31} & A_{32} & A_{33} \end{bmatrix} \tag{1.35}$$

where the momentum equation for δv is present in the first row:

$$A_{11} = -v_0 \frac{\partial}{\partial z} - \frac{\partial v_0}{\partial z} - \left(\frac{2-b}{2}\right) k_0 v_0, \quad A_{12} = -\frac{1}{\rho_0}\frac{\partial}{\partial z}, \quad A_{13} = -\frac{g}{\rho_0} - \frac{k_0 v_0^2}{2\rho_0} - \frac{v_0}{\rho_0}\frac{\partial v_0}{\partial z}$$

the internal energy equation for the evolution of δp in time in the second row:

$$A_{21} = \frac{\beta\rho_0^2 - p_0}{\alpha\rho_0}\frac{\partial}{\partial z} - \frac{\partial p_0}{\partial z}, \quad A_{22} = -v_0\frac{\partial}{\partial z} - \frac{1}{\alpha\rho_0}\frac{\partial v_0}{\partial z}, \quad A_{23} = \frac{\beta}{\alpha}\frac{\partial v_0}{\partial z} - \frac{v_0}{\rho_0}\left(\frac{\beta}{\alpha}\frac{\partial \rho_0}{\partial z} + \frac{\partial p_0}{\partial z}\right)$$

and the last row represent the continuity equation referred to $\delta\rho$:

$$A_{31} = -\rho_0\frac{\partial}{\partial z} - \frac{\partial \rho}{\partial z}, \qquad A_{32} = 0, \qquad A_{33} = -v_0\frac{\partial}{\partial z} - \frac{\partial v_0}{\partial z}$$

The matrix (1.35) fully describes the free response of the system to an initial perturbation δX_0, but it cannot be employed yet in this form because the spatial derivatives of the state variables' perturbations δX, as well as the spatial profiles:

$$X_0 = X_0(z) = \begin{bmatrix} v_0, & p_0, & \rho_0 \end{bmatrix}^T$$

and their spatial derivatives:

$$\frac{\partial X_0}{\partial z} = \frac{\partial X_0}{\partial z}(z) = \begin{bmatrix} \frac{\partial v_0}{\partial z}, & \frac{\partial p_0}{\partial z}, & \frac{\partial \rho_0}{\partial z} \end{bmatrix}^T$$

are respectively continuous operators and continuous functions of the spatial coordinate z. To obtain quantitative results a numerical scheme is needed to discretize and approximate the spatial derivatives present in (1.35).
The discretization is performed dividing the pipe's length L in N equal elements of length h. The resulting N+1 nodes are used to evaluate each physical quantity in the domain:

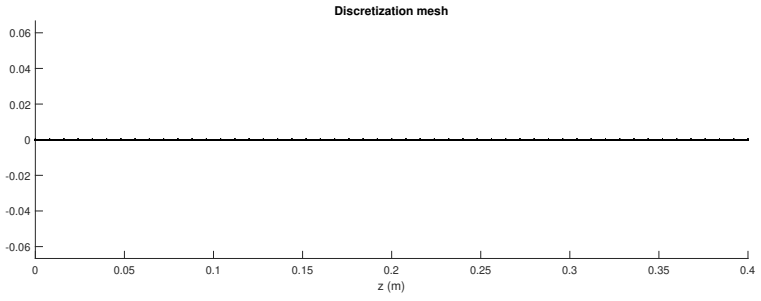

Figure 1.11: *Example of mesh for spatial discretization: N=50 elements and length L=0.4 m.*

The generic state variable $\phi = \phi(z)$ is sampled with the equispaced mesh in Figure 1.11 and it's evaluated in $N+1$ nodes, from node 1 to node $N+1$.

In the following study, no variations of the boundary conditions, imposed in the steady-state problem at time $t = 0^+$, will be considered [4], so homogeneous boundary conditions for the perturbation of the state variables δX are selected, for $t > 0$.

Boundary Conditions for t>0:

- Inlet density perturbation: $\delta\rho_1 = 0$
- Inlet velocity perturbation: $\delta v_1 = 0$
- Outlet pressure perturbation: $\delta p_{N+1} = 0$

This constraints are employed for the composition of the state vector for the perturbation of the state variables δX, in which only non-null entries are present ([Trefethen 2000]):

$$\delta X = [\delta v_2, \cdot\ \cdot\ \cdot, \delta v_{N+1}, \delta p_1, \cdot\ \cdot\ \cdot, \delta p_N, \delta\rho_2, \cdot\ \cdot\ \cdot, \delta\rho_{N+1}]^T \tag{1.36}$$

The data concerning the spatial profiles X_0 and $\frac{\partial X_0}{\partial z}$ are collected by sampling the solution computed in Section 1.4.2 in correspondence to each node composing the numerical mesh. To treat first order spatial derivatives of the perturbated state variables, central finite difference scheme (second order convergence method) is employed:

$$\left.\frac{\partial\delta\phi}{\partial z}\right|_i = \frac{\delta\phi_{i+1} - \delta\phi_{i-1}}{2h} \tag{1.37}$$

This numerical scheme is effective in the interior points of the mesh: to evaluate spatial derivatives of a perturbation $\delta\phi$ in node 1 or $N + 1$, perturbations of the state variable $\delta\phi$ respectively in node 0 and $N + 2$ would be required. As they're not available, spatial derivatives of a perturbation $\delta\phi$ in node 1 are approximated using first order forward finite difference scheme:

$$\left.\frac{\partial\delta\phi}{\partial z}\right|_1 = \frac{\delta\phi_2 - \delta\phi_1}{h} \tag{1.38}$$

and, for node $N + 1$, first order backward finite difference scheme:

$$\left.\frac{\partial\delta\phi}{\partial z}\right|_{N+1} = \frac{\delta\phi_{N+1} - \delta\phi_N}{h} \tag{1.39}$$

Using Eq.(1.37), the discretized form of equations presented in Eq. (1.32), for the i-th generic interior node are reported.
It is stressed that the problem shifted from a system of 3 linear PDEs to a set of 3N linear ODEs.

- *momentum equation*

$$\begin{aligned}\frac{dv_i}{dt} = -v_{0,i}\frac{\delta v_{i+1} - \delta v_{i-1}}{2h} &- \left(\frac{\partial v_{0,i}}{\partial z} + \frac{2-b}{2}\right) k_0 v_{0,i}\delta v_i + \\ &- \frac{1}{\rho_{0,i}}\frac{\delta p_{i+1} - \delta p_{i-1}}{2h} - \left(v_{0,i}\frac{\partial v_{0,i}}{\partial z} + g + \frac{k_0 v_{0,i}^2}{2}\right)\frac{\delta\rho_i}{\rho_{0,i}}\end{aligned} \tag{1.40}$$

[4] This in principle can be handled with the application of the Laplace transform for the time coordinate t: as an example, a stepwise increase δv_{in} in the inlet velocity of the fluid at time $t = 0^+$ is transformed in $\frac{\delta v_{in}}{\bar{s}}$ and inserted in the system as an external input.

- *internal energy equation*

$$\begin{aligned}\frac{dp_i}{dt} = \frac{\beta\rho_{0,i}^2 - p_{0,i}}{\alpha\rho_{0,i}}\frac{\delta v_{i+1} - \delta v_{i-1}}{2h} - \frac{\partial p_{0,i}}{\partial z}\delta v_i - v_{0,i}\frac{\delta p_{i+1} - \delta p_{i-1}}{2h} + \\ - \frac{1}{\alpha\rho_{0,i}}\frac{\partial v_{0,i}}{\partial z}\delta p_i + \frac{\beta}{\alpha}\frac{\partial v_{0,i}}{\partial z}\delta\rho_i - \frac{v_{0,i}}{\rho_{0,i}}\left(\frac{\beta}{\alpha}\frac{\partial\rho_{0,i}}{\partial z} + \frac{\partial p_{0,i}}{\partial z}\right)\delta\rho_i\end{aligned} \tag{1.41}$$

- *continuity equation*

$$\frac{d\rho_i}{dt} = -\rho_{0,i}\frac{\delta v_{i+1} - \delta v_{i-1}}{2h} - \frac{\partial\rho_{0,i}}{\partial z}\delta v_i - v_{0,i}\frac{\delta\rho_{i+1} - \delta\rho_{i-1}}{2h} - \frac{\partial v_{0,i}}{\partial z}\delta\rho_i \tag{1.42}$$

Recalling that the perturbation of velocity δv_1 at $z = 0$ (1.4.5), as well as the perturbation of density $\delta\rho_1$, is null, the evolutive equations for the node 1 for (1.40) and (1.42) will be neglected. The same considerations can be applied at $z = L$ for the perturbation in pressure δp_{N+1} at node $N + 1$.
As a consequence, the momentum equation (1.40), along with the continuity equation (1.42), is evaluated from node 2 to node $N+1$. Internal energy equation (1.41) instead involves nodes from 1 to N.
Formula for forward (1.38) finite differences is applied to the internal energy equation (1.41), while backward (1.39) finite differences for the momentum (1.40) and continuity (1.42) equations. Moreover, the homogeneous boundary conditions for the state variables in Eq.(1.4.5) are adopted for the derivation of the following:

- *momentum equation in node N+1*

$$\begin{aligned}\frac{dv_{N+1}}{dt} = -v_{0,N+1}\frac{\delta v_{N+1} - \delta v_N}{h} - \left(\frac{\partial v_{0,N+1}}{\partial z} + \frac{2-b}{2}\right)k_0 v_{0,N+1}\delta v_{N+1} + \\ + \frac{1}{\rho_{0,N+1}}\frac{\delta p_N}{h} - \left(v_{0,N+1}\frac{\partial v_{0,N+1}}{\partial z} + g + \frac{k_0 v_{0,N+1}^2}{2}\right)\frac{\delta\rho_{N+1}}{\rho_{0,N+1}}\end{aligned} \tag{1.43}$$

- *internal energy equation in node 1*

$$\frac{dp_1}{dt} = \frac{\beta\rho_{0,1}^2 - p_{0,1}}{\alpha\rho_{0,1}}\frac{\delta v_2}{h} - v_{0,1}\frac{\delta p_2 - \delta p_1}{h} - \frac{1}{\alpha\rho_{0,1}}\frac{\partial v_{0,1}}{\partial z}\delta p_1 \tag{1.44}$$

- *continuity equation in node N+1*

$$\begin{aligned}\frac{d\rho_{N+1}}{dt} = -\rho_{0,N+1}\frac{\delta v_{N+1} - \delta v_N}{h} - \frac{\partial\rho_{0,N+1}}{\partial z}\delta v_{N+1} - v_{0,N+1}\frac{\delta\rho_{N+1} - \delta\rho_N}{h} \\ - \frac{\partial v_{0,N+1}}{\partial z}\delta\rho_{N+1}\end{aligned} \tag{1.45}$$

The next step is to compute a discrete version of the dynamics matrix A presented in Eq.(1.35) by means of MATLAB®: the previous discretized momentum equation (1.40) forms the first N rows, internal energy equation (1.41) the second set of N rows and continuity equation (1.42) the last set of N rows; the equations are then reordered in a matricial form, resulting in a $3N \times 3N$ discretization matrix:

$$\frac{d}{dt}\delta X = A\delta X \tag{1.46}$$

using the state vector reported in Eq.(1.36). A sketch of the matrix A is reported to show its sparsity and the diagonal features:

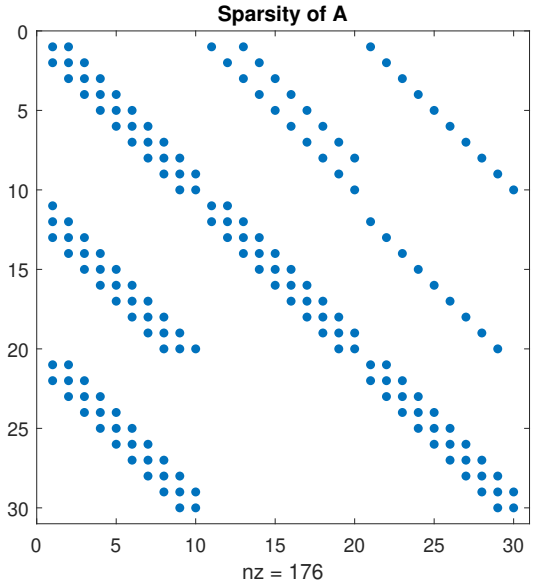

Figure 1.12: *Sparsity and the diagonal features of A, N=10.*

1.4.6 Definition of modal analysis

The *modal analysis* ([Schmid and Brandt 2014], [Trefethen and Embree 2005], [Pini, Cammi, and Luzzi 2016]) consists in the study of the spectral properties of the dynamics matrix A, i.e. its eigenvalues, to extract information about the free response of the system to initial perturbations.
In particular, the examined equilibrium point is considered stable if each eigenvalue λ_i of A, in general contained in $\mathbb{C}$, has $Re(\lambda_i) < 0$. This criterium is one of the main results of the Lyapunov stability theory ([Lyapunov 1992]).
The concept of asymptotic stability is then recalled: if an equilibrium state is slightly perturbed, the time response of the linearized state equations that describe the dynamics of the state variables, is, for a given state variable, a sum of exponential functions of the form:

$$y(t) = \sum_i \alpha_i exp(\lambda_i t) \tag{1.47}$$

The time response is then damped in time if the eigenvalues have $Re(\lambda_i) < 0$: the state of the system will turn back to its equilibrium point.
On the contrary, even if one of the eigenvalues of A has $Re(\lambda_i) > 0$, the system's response is asymptotically unstable and even a small perturbation can be amplified exponentially, distorting and changing irreversibly the equilibrium flow profile chosen in the linearization procedure.
The definition of *dominant eigenvalue* or *dominant pole* is introduced, useful to draw the so-called *stability maps* for the system studied, which is the main result extracted from the *modal anaysis*.
Taking the set of eigenvalues of A, namely λ_i, the one with the maximum real part is

the *dominant eigenvalue* of the system, i.e. the one which fully describe the asymptotic stability of the system to small initial perturbations.
The *dominant eigenvalue* will be referred hereafter as γ:

$$\gamma := \{\gamma \in \lambda_i \mid Re(\gamma) = max(Re(\lambda_i))\} \tag{1.48}$$

1.4.7 Algorithm to compute the stability maps

A definition of *stability map* is reported for sake of completeness.
Stability maps ([Pini, Cammi, and Luzzi 2016]) are diagrams in a plane defined by two parameters that affects directly the stability of the system (in this case k_0 and v_{in}), where a transition curve, namely *neutral stability curve*, separates the asymptotically stable equilibrium points of the system from the unstable ones.
In the following, the stability map presented in Figure 1.1, given by relation the relation in Eq. (1.25), will be used as a starting point for the *modal analysis* in different flow configurations, i.e. with different boundary conditions, flow parameters and lengths of the channel.
The algorithm that will be exploited hereafter for the numerical computation of the stability maps is mainly divided in different steps:

1. Selection of a region in the plane v_{in}-k_0 to be investigated and assembling of two arrays for v_{in} and k_0: each couple $\{v_{in}(i),k_0(j)\}$ in the plane will be marked with a red cross $\times$ if it's deemed unstable, with a blue cross $\times$ if otherwise it's stable.

2. Setting the input parameters for a specific stability map: channel's length L, inlet temperature T_{in}, outlet pressure p_{out} and flow regime b.

3. Plotting of the neutral stability curve found with Eq. (1.25) in the region of interest of the plane v_{in}-k_0, used to compare the numerical results of the *modal analysis* with the results found in the work of [Trotta et al. 2019].

4. Individuation of an optimal discretization number N for the simulation: for a given dynamics matrix A, the convergence of $Re(\gamma)$ is studied by increasing values of N. A particular discretization number N is chosen among all if minimize the dimensions of the matrix[5] A but still satisfying a good convergence of $Re(\gamma)$.

5. Computation, for a given couple $\{v_{in}(i),k_0(j)\}$, of the steady-state solution of system (1.27) with COMSOL®, which represent the equilibrium point to be studied with the *modal analysis*.

6. Assembling of the dynamics matrix A with the data of the steady-state solution, sampled in correspondence to the mesh adopted for the problem, in the MATLAB® environment.

7. Eigenvalue study of matrix A, determination of the sign of the dominant eigenvalue γ: the equilibrium point individuated by $\{v_{in}(i),k_0(j)\}$ is stable if $Re(\gamma) < 0$, otherwise is unstable.

[5] In order to decrease the computational cost in the numerical simulation.

8. Repetition from point 5. to 7. of the algorithm for each couple $\{v_{in}(i),k_0(j)\}$.

This numerical procedure is performed thanks to the useful LiveLink™ *for* MATLAB® environement, which provides access to COMSOL® Multiphysics from MATLAB®'s command prompt.
The access to COMSOL® models is possible through a client/server connection to a COMSOL® Multiphysics local server; then, by changing with a MATLAB ® script the Parameters in the Global Definitions of the COMSOL® model (used to solve the steady-state system (1.27) for each simulation), the sampling of the solutions in correspondence to the nodes of the mesh is possible, along with the assembling of the matrix A for each couple $\{v_{in}(i),k_0(j)\}$.

1.4.8 Results: subcooled water

Firstly, a validation of the numerical method for the modal analysis is carried out by turning off all the spatial derivatives terms, as well as imposing uniform profiles for the equilibrium point by which the linear stability analysis is performed.
In order to do this, the boundary condition selected for the steady-state computation of the equilibrium point are instead extended to the whole length of the channel.
A correspondence between the numerical simulation and the theoretical result depicted in Figure 1.1 is expected. Referring to the numerical algorithm reported in Section 1.4.7, the chosen inlet velocity array in the v_{in}-k_0 plane is included between $v_{in,min} = 0.5\ m/s$ and $v_{in,max} = 1.0\ m/s$.
For each value of the inlet velocity array $v_{in}(i)$, a specific drag coefficient array is assembled, such that it's centred in the $k_{0,min}$ value analytically found with Eq.(1.25).
A set of input parameters for this numerical simulation is chosen:

Simulation parameters:

- Channel's length $L = 0.4\ m$
- Flow regime: $b = 0.2$
- Inlet temperature: $T_{in} = 320\ °C$
- Outlet pressure: $p_{out} = 15.5\ MPa$

Next, choosing for instance the value $v_{in,max} = 1.0\ m/s$, a convergence plot for the real part of the dominant eigenvalue is drawn by taking as $k_0 = k_{0,min}$ the one found with Eq.(1.25):

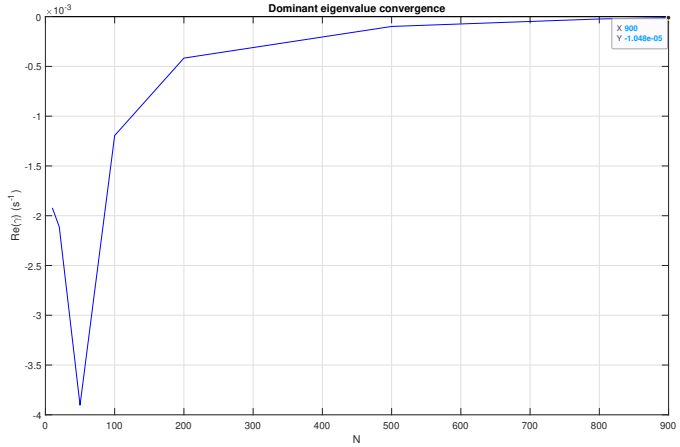

Figure 1.13: *Convergence plot of $Re(\gamma)$, uniform flow, subcooled water.*

Two observations can be done by looking at Figure 1.13: the first one is that, since the chosen drag coefficient k_0 is the one corresponding to the neutral stability curve in Figure 1.1, the real part of the dominant eigenvalue $Re(\gamma)$ should tend to zero in this case, without spatial derivatives or flow profiles. This point finds a correspondence with Figure 1.13: for a discretization number $N = 900$, the real part of the dominant eigenvalue has a value[6] of $Re(\gamma) = -1.048 \cdot 10^{-5}\ s^{-1}$.
The second observation is that the value of $Re(\gamma)$ experience high excursions (up to 2 orders of magnitude) with a non-monotonic trend for low values of N, and then reaches a saturation value for higher values of N up to $N = 900$, so the dominant eigenvalue convergence study is essential to obtain accurate results.
By choosing $N = 900$, an inlet velocity array v_{in} of 25 equispaced points is assembled and, for each $v_{in}(i)$, a correspondent array for the drag coefficient k_0 is made up such that it's centered in $k_{0,min}$, with 30 equispaced elements, spanning from $0.5k_{0,min}$ up to $1.5k_{0,min}$.

[6]The discrepancy between the theoretical prediction and the simulation result is imputable to numerical errors introduced in the approximation of the spatial derivatives of the perturbed state vector δX.

The resulting stability map is reported:

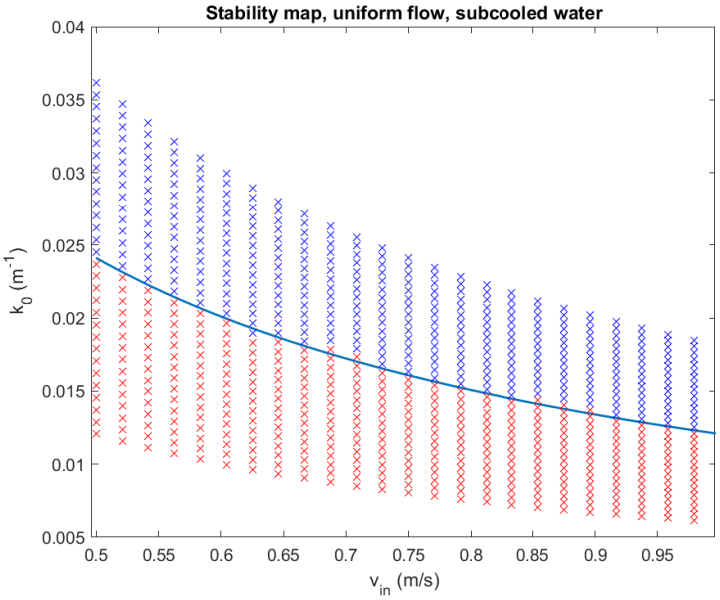

Figure 1.14: *Stability map for uniform flow, subcooled water.*

A good correspondence between the stability result in Eq.(1.25), represented by the solid line in Figure 1.14, and the numerical result can be observed: the transition region from the stable region to the unstable one coincides with good agreement with the theoretical prediction represented by the neutral stability curve.
The introduction of spatial derivatives terms and the flow profiles derived from the steady-state analysis of Eq.(1.27) is now the subject of this section.
A direct comparison between the results reported in Figure 1.14 and the following analysis can be done: the same parameters employed in the uniform flow study are used for the numerical simulation with the spatial derivatives terms, highlighting the differences between the two models.
Regarding the velocity stability parameter in the v_{in}-k_0 plane a clarification needs to be done: while in the uniform flow there is, by definition, a correspondence of $v_{in} = v_0$, in the *modal analysis* that considers instead spatial profiles, the stability parameter for velocity is no more the uniform velocity imposed for the whole length of the channel, but instead the boundary condition for the inlet velocity v_{in}.[7].

Simulation parameters:

- Channel's length $L = 0.4\ m$
- Flow regime: $b = 0.2$
- Inlet temperature: $T_{in} = 320\ °C$

[7]In the cases considered in which the length of the channel L has a order of magnitude of 1 meter, the variation of the velocity along the channel is negligible, so $v_{in} \sim v_0$

- Outlet pressure: $p_{out} = 15.5\ MPa$

The value of $v_{in,max} = 1.0\ m/s$ is chosen again to draw the convergence plot for the real part of the dominant eigenvalue, by setting once more $k_0 = k_{0,min}$:

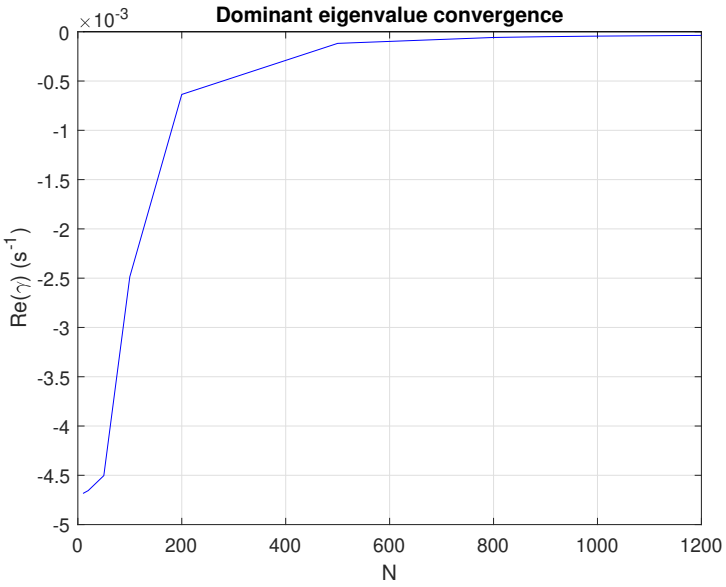

Figure 1.15: *Convergence plot of $Re(\gamma)$, spatial flow profiles, $L = 0.4\ m$, subcooled water.*

The stability map is drawn by selecting $N = 1200$, with the same choice of the velocity intervals as the one used for Figure 1.14. The main difference consists in the choice of the drag coefficient array: the range covered by the elements of the array extends from $k_{0,min} = 0\ m^{-1}$ up to $k_{0,max} = 0.5\ k_{0,min}\ m^{-1}$.

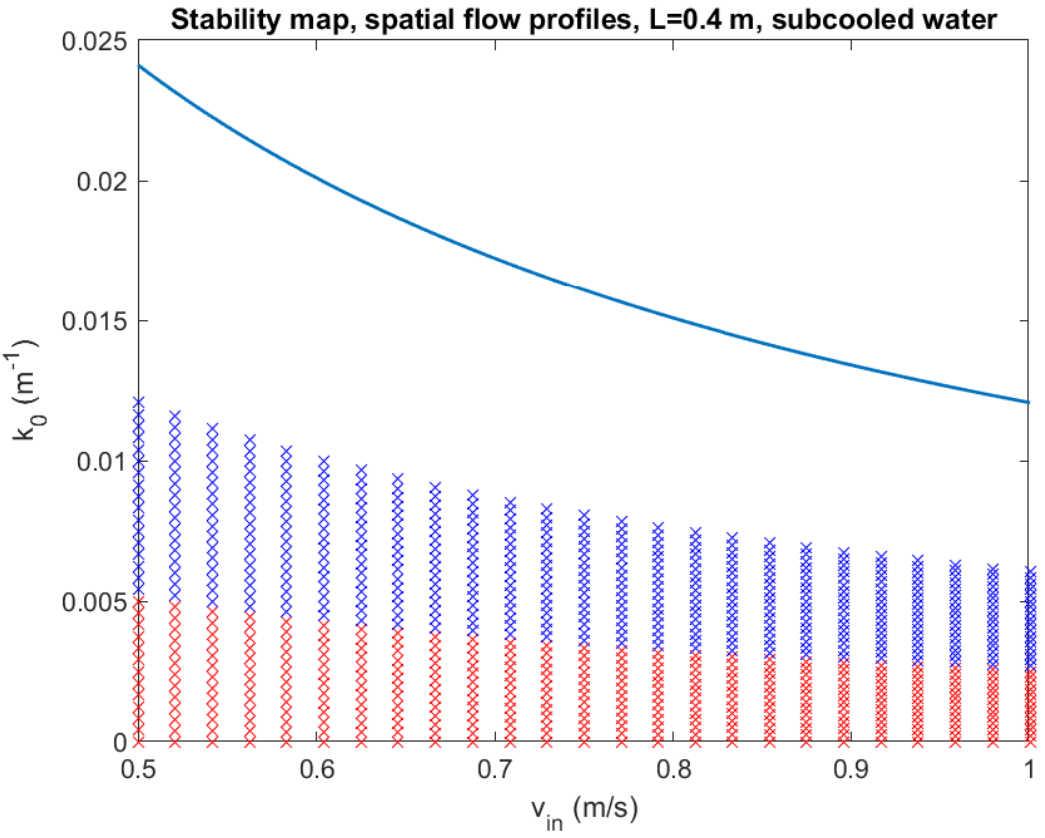

Figure 1.16: *Stability map, spatial flow profiles, subcooled water.*

There is clearly a stabilizing effect on the overall system: the pressure gradient[8] $\frac{\partial p_0}{\partial z}$ acting inside the internal energy equation (1.41), tends to shift the neutral stability curve towards lower values in the v_{in}-k_0 plane. It can be inferred that, for this specific case, the uniform flow approximation is also conservative from the stability point of view.
To further study the action of the pressure gradients on the system, a new flow configuration is examined: a localized pressure drop is introduced at $z = 0.5L$, characterized by a peaked value of the pressure gradient in the correspondence of the pressure drop. The latter is analytically expressed by means of a sigmoid function:

$$\Delta p = 0.001 p_{out} \left[1 + exp\left(\frac{z - 0.5L}{0.001}\right)\right]^{-1} \tag{1.49}$$

where p_{out} is the boundary condition for the steady-state pressure profile. The distributed pressure drop is neglected in this case, to distinguish the action of each profile, taken independently, to the stability of the system. The steady pressure profile is reported, together with its spatial derivative:

[8] Representing the main difference between the uniform flow case in Figure 1.14

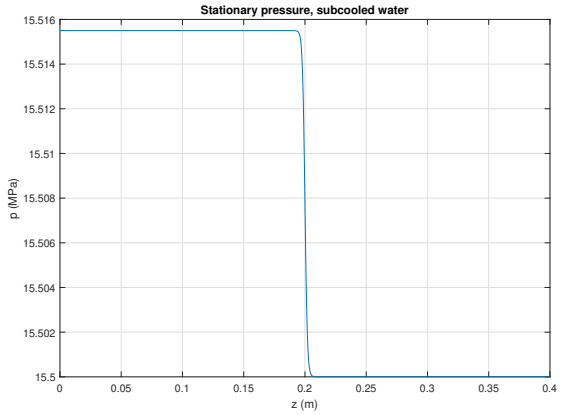

Figure 1.17: *Stationary pressure along z, subcooled water.*

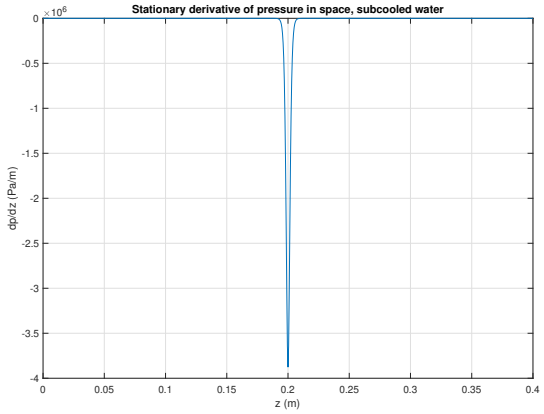

Figure 1.18: *Stationary derivative of pressure along z, subcooled water.*

The simulation parameters employed are equal to the previous cases, in order to appreciate the differences for each spatial profile. The convergence plot is computed with the same inlet velocity and drag coefficient used for Figure 1.15:

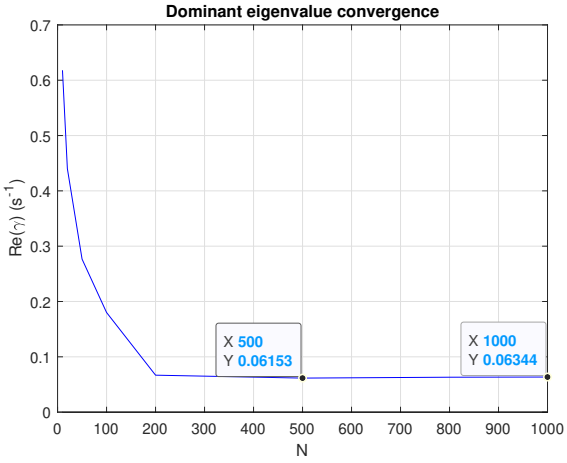

Figure 1.19: *Convergence plot of $Re(\gamma)$, concentrated pressure drop, $L = 0.4$ m, subcooled water.*

In Figure 1.19, differently from the previous convergence plots, the real part of the dominant eigenvalue reaches a saturation value for subdivision numbers of the order of $N = 200$. It can be further observed that the system is widely unstable for $k_0 = k_{0,min}$, in this case the concentrated pressure drop acts on the equilibrium point in a destabilizing way.
The following stability maps are reported, in which the inlet velocity array extends from $v_{in,min} = 0.5\ m/s$ up to $v_{in,max} = 1.5\ m/s$ and the selected discretization number is $N = 300$:

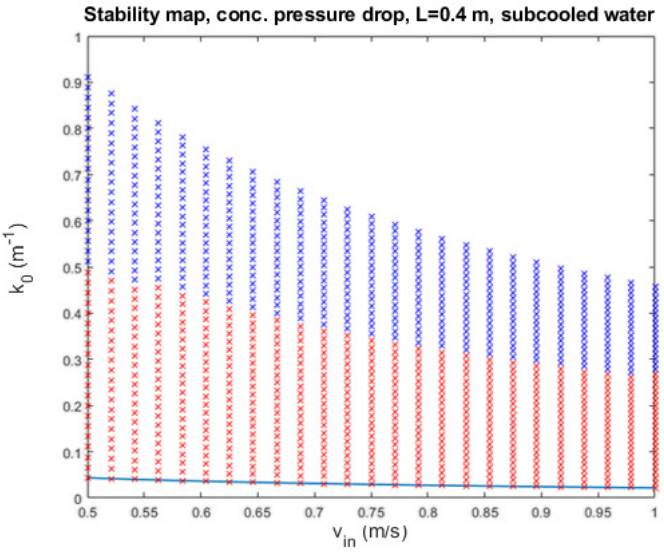

Figure 1.20: *Stability map, concentrated pressure drop, subcooled water.*

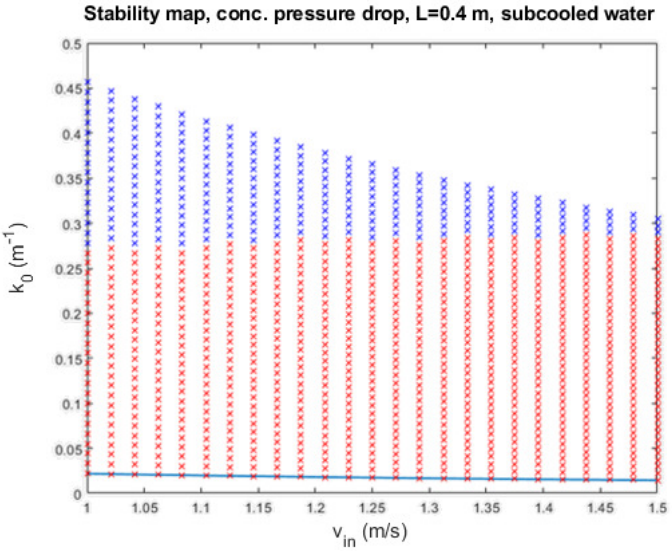

Figure 1.21: *Stability map, concentrated pressure drop, subcooled water.*

In conclusion, the stability maps are widely affected by the shape and magnitude of the pressure gradient expression along z: it is remarked that not only the system is destabilized, but also the functional trend of the neutral stability curve found

numerically (being the transition curve between the stable and unstable region) changes importantly. In fact, observing Figure 1.21, it can be highlighted that the monotonic decrease of $k_{0,min} = k_{0,min}(v_{in})$ found for the previous maps is no longer present here: the system response is linked to the particular equilibrium point selected for the modal analysis, showing how the governing set of equations, even for a simplified monodimensional case, presents high non-linearities embedded inside it.

1.5 Sensitivity analysis: non-conductive fluid

1.5.1 Introduction to the sensitivity analysis

In Section 1.4, different results were presented for subcooled water: the dependence on the linearization point, the boundary conditions for the steady-state solution and the set of parameters that characterizes the equilibrium point has been investigated via linear stability analysis, as well as the impact of the base flow distribution of the state variables along the channel.
As regards the parametric sensitivity of the system, it's interesting to study how these parameters directly affects the stability of the equilibrium point, by slightly perturbing a generic parameter θ from its unperturbed value θ_0 with a small shift $\delta\theta$ and check if the system is sensitive to this perturbation, with a qualitative and quantitative investigation on how much it affects the eigenvalues of A and in particular its dominant eigenvalue γ.
An *eigenvalue sensitivity analysis* is presented, following the outlines reported in [Schmid and Brandt 2014] for the two-dimensional, incompressible benchmarks referred to plane Couette flow and plane Poiseuille flow: a parameter sensitivity analysis and a perturbative study of the base flow characterizing a chosen equilibrium point is conducted in the last part of this chapter.

1.5.2 Mathematical derivation

As the following sections will concern mathematical aspects related to eigenvalue problems referred to the dynamics matrix A and the correspondent set of eigenvectors, the definition of inner product of two column vectors $\mathbf{q}$ and $\mathbf{p}$ in $\mathbb{C}^n$ is given:

$$< \mathbf{p}, \mathbf{q} >= \mathbf{p}^\dagger \mathbf{q} \tag{1.50}$$

where $\mathbf{p}^\dagger$ stands for the transposed, complex conjugated of vector $\mathbf{p}$ and n is the size of the dynamics matrix A, namely $n = 3N$.
Starting with the eigenvalue problem for the i-th eigenvalue λ_i and corresponding eigenvector $\mathbf{q}_i$ of A:

$$A\mathbf{q}_i = \lambda_i \mathbf{q}_i \tag{1.51}$$

the dynamics matrix $A = A(\theta)$ is continuously dependent on the generic parameter θ. A small perturbation[9] $\delta\theta$ is introduced, and as a result the perturbed dynamics matrix $\tilde{A}$ is obtained; all the perturbed terms in Eq.(1.51) are then decomposed in the

[9] In the following mathematical development a linear perturbation analysis is performed, so the perturbation's maximal excursion $\delta\theta$ must have a value not greater than the 10 % of θ

unperturbed quantity (i.e. to Eq.(1.51)) and the correspondent perturbation (denoted with δ):

$$(A + \delta A)(\mathbf{q}_i + \delta\mathbf{q}_i) = (\lambda_i + \delta\lambda_i)(\mathbf{q}_i + \delta\mathbf{q}_i) \tag{1.52}$$

From Eq.(1.52) the second order terms $\delta A\delta\mathbf{q}_i$ and $\delta\lambda\delta\mathbf{q}_i$ could be neglected, provided that the perturbation $\delta\theta$ is small enough. Moreover, with Eq.(1.51), the two terms $A\mathbf{q}_i$ and $\lambda_i\mathbf{q}_i$ cancel out.
The resulting perturbation equation for the eigenvalue problem is:

$$(A - \lambda_i I)\,\delta\mathbf{q}_i = -(\delta A - \delta\lambda_i I)\,\mathbf{q}_i \tag{1.53}$$

with I being the $n \times n$ identity matrix. Then, by taking the inner product with the unknown vector $\mathbf{p}_i$ for both sides of Eq.(1.53):

$$\mathbf{p}_i^\dagger (A - \lambda_i I)\,\delta\mathbf{q}_i = -\mathbf{p}_i^\dagger (\delta A - \delta\lambda_i I)\,\mathbf{q}_i \tag{1.54}$$

it is required that the left hand side of Eq.(1.54) is equal to zero for each value of $\delta\mathbf{q}_i$, namely:

$$\mathbf{p}_i^\dagger (A - \lambda_i I) = 0 \tag{1.55}$$

$$\left(A^\dagger - \lambda_i^* I\right)\mathbf{p}_i = 0 \qquad \forall\delta\mathbf{q}_i \in \mathbb{C}^n \tag{1.56}$$

where λ_i^* is the complex conjugated of λ_i.
By resolving Eq. (1.56), called *adjoint eigenvalue problem*, the solution vector $\mathbf{p}_i$ is the so-called *left eigenvector* of A, or eigenvector of $A^\dagger$.
Some properties of left and right eigenvectors of a matrix A are briefly reported in the following.
For each eigenvalue/eigenvector couple $(\lambda_i, \mathbf{q}_i)$ of A and for each eigenvalue/eigenvector couple $(\varsigma_j, \mathbf{p}_j)$ of $A^\dagger$ it can be proven that $\varsigma_i = \lambda_i^*$ and:

$$< \mathbf{p}_j, \mathbf{q}_i >= 0 \tag{1.57}$$

when $i \neq j$. This means that:

1. Once the set of left and right eigenvectors of A are computed, respectively $\mathbf{p}_j$ and $\mathbf{q}_i$, by means of MATLAB®, the left eigenvector $\mathbf{p}_i$ correspondent to the right one $\mathbf{q}_i$ has an eigenvalue $\varsigma_i = \lambda_i^*$.

2. Exists a bi-orthogonality condition between the basis vectors (i.e. left and right eigenvectors of A) of the finite vectorial spaces Q=*span*$\{\mathbf{q}_i\}$ and P=*span*$\{\mathbf{p}_i\}$.

Finally, rearranging the terms in the right-hand side of Eq.(1.54), an expression for the perturbation of the eigenvalue $\delta\lambda_i$ is available:

$$\delta\lambda_i = \frac{\mathbf{p}_i^\dagger \delta A \mathbf{q}_i}{\mathbf{p}_i^\dagger \mathbf{q}_i} \tag{1.58}$$

This expression is very important for the following study: once the eigenvalue spectrum of A and its left and right eigenvectors are computed, the eigenvalue shift $\delta\lambda_i$, led by $\delta\theta$, can be easily determined via the algebraic expression linking the perturbation

input $\delta A(\delta\theta)$ and the sought output of our problem $\delta\lambda_i$.
In contrast, without the aid of the *adjoint-based perturbative analysis* developed in this section, in order to perform a sensitivity analysis on the dominant eigenvalue, the eigenvalues of $\tilde{A}$ need to be computed for each perturbation $\delta\theta$ considered in the sensitivity study.
The simulations then would require an higher computational cost, since the dimensions of $\tilde{A}$ are linked with the necessity to study the real part of the dominant eigenvalue once the latter has reached a good convergence, like in Figure 1.15.

1.5.3 Algorithm for parametric sensitivity analysis

The main parameters that will be perturbed, the ones referred in Sections 1.5.1 and 1.5.2 with the generic letter θ, are briefly presented:

- Thermodynamic coefficient $\alpha = \left(\frac{\partial u}{\partial p}\right)_\rho$
- Thermodynamic coefficient $\beta = \left(\frac{\partial u}{\partial \rho}\right)_p$
- Drag coefficient stability parameter k_0
- Flow regime coefficient b

Then the algorithm for this *eigenvalue sensitivity analysis*, computed using again the coupling between MATLAB® and COMSOL®, is reported:

1. Selection of an equilibrium point to be investigated: the criteria are the same adopted for the *modal analysis* in Section 1.4.7.
2. Assembling and computation of the eigenvalues λ_i and the set of left and right eigenvectors $\mathbf{p}_i$ and $\mathbf{q}_i$ of the dynamics matrix A.
3. Assembling of a perturbation array for the generic parameter θ named $\delta\theta_i$, whose maximum entry extends up to the 10% of the value of θ employed in the definition of the equilibrium point.
4. Assembling, for each component of $\delta\theta_i$, of the perturbed dynamics matrix $\tilde{A}$ and $\delta A = \tilde{A} - A$.
5. Computation, for each eigenvalue λ_i, of the eigenvalue shift $\delta\lambda_i$ with Eq.(1.58).
6. Visualization of the dominant eigenvalue shift $Re(\delta\gamma)$ for each perturbation $\delta\theta_i$ present in the perturbation array.

1.5.4 Base flow sensitivity analysis

The mathematical tool developed for the adjoint sensitivity theory can be employed also to study the response of the set of eigenvalues of A to perturbations on the base flow. This problem is close to the topic of passive flow control([Schmid and Brandt 2014]): considering a particular configuration of the base flow, a given perturbation on its profile may lead to a correspondent shift of the eigenvalues characterizing the equilibrium point, with a possible modal perturbation growth and consequential trigger of an instability ([Marquet, Sipp, and Jacquin 2008],[Pralits, Brandt, and Giannetti 2010]).
In this specific case, the study concerns a quantitative sensitivity analysis, evaluating the impact of fluctuations on the spatial profiles computed with the steady-state analysis in Section 1.4.2 on the real part of the dominant eigenvalue $Re(\gamma)$.

1.5.5 Algorithm for base flow sensitivity analysis

The spatial profiles involved in this analysis are the following:

- Velocity profile v_0 along z and its spatial derivative $\frac{\partial v_0}{\partial z}$
- Pressure profile p_0 along z and its spatial derivative $\frac{\partial p_0}{\partial z}$
- Density profile ρ_0 along z and its spatial derivative $\frac{\partial \rho_0}{\partial z}$

The algorithm used for this study follows mainly the one presented in Section 1.5.3: the exception is that, instead of perturbing a single parameter, the perturbed matrix $\tilde{A}$ is assembled taking into account a change in the nodal information inserted for $v_{0,i}$, $p_{0,i}$ and $\rho_{0,i}$ and the corresponding spatial derivatives, one at a time.
As the adjoint perturbation method presented in Section 1.5.2 refers to a linear approximation of the eigenvalue study of $\tilde{A}$, the excursion of the perturbation on the base flow needs to be small enough to stay in the linear regime of the response.
It will be considered a shift up to the 10% of the unperturbed *mean value* along z for each state variable listed before, and the correspondent perturbation of the eigenvalue is confronted with its unperturbed value: high excursions lead to a departure from the linear response of the system. Moreover, it is highlighted that this perturbation imposed on the base flow does not affect the boundary conditions of the state variables set in the steady-state computation of the equilibrium point.

The algorithm adopted is the following:

1. Selection of an equilibrium point to be investigated: the criteria are the same adopted for the *modal analysis* in Section 1.4.7.
2. Assembling and computation of the eigenvalues λ_i and the set of left and right eigenvectors $\mathbf{p}_i$ and $\mathbf{q}_i$ of the dynamics matrix A.
3. Assembling of a perturbation array for the generic state variable ϕ (or its spatial derivative) named $\delta\phi_i$, extending up to the 10% of the average value $\bar{\phi}$ computed along z.

4. Assembling, for each component of $\delta\phi_i$, of the perturbed dynamics matrix $\tilde{A}$ and $\delta A = \tilde{A} - A$.

5. Computation, for each eigenvalue λ_i, of the eigenvalue shift $\delta\lambda_i$ with Eq.(1.58).

6. Visualization of the dominant eigenvalue shift $Re(\delta\gamma)$ for each perturbation $\delta\phi_i$ in the perturbation array.

1.5.6 Results: subcooled water

Parametric sensitivity

The algorithm presented in Section 1.5.3 is applied for subcooled water, in the configuration that takes into account also the spatial derivative terms and spatial profiles along z. Differently from the *modal analysis*, in the research of an equilibrium point to be studied, the inlet velocity boundary condition v_{in} and the drag coefficient stability parameter k_0 are fixed (no stability map here is involved).

Simulation parameters:

- Channel's length $L = 0.4\ m$
- Discretization number $N = 800$
- Flow regime: $b = 1.0$
- Inlet temperature: $T_{in} = 320\ °C$
- Outlet pressure: $p_{out} = 15.5\ MPa$
- Inlet velocity: $v_{in} = 2.0\ m/s$
- Drag coefficient: $k_0 = 0.001\ m^{-1}$

The equilibrium point chosen is an unstable one: for $v_{in} = 2.0\ m/s$ the $k_{0,min} = 0.0109\ m^{-1}$, while in this simulation it is set a drag coefficient of $k_0 = 0.001\ m^{-1}$.
It will be seen how the parameters' perturbation affects the position of the dominant eigenvalue for this configuration.
A first validation of the adjoint problem approach is carried out by perturbing the thermodynamic coefficient $\alpha = 0.00330\ J/kgPa$ with a series of increasing perturbations in magnitude, up to the 30% of the unperturbed value of α : the aim is to follow how well the perturbative approach approximate the spectral properties of $\tilde{A}$ with respect to a classical eigenvalue study of $\tilde{A}$.
In this simulation, as well as for the others that will be presented hereafter, only one parameter will be perturbed at a time: the rest is maintained fixed to the unperturbed value chosen for the designation of the equilibrium point. This type of approach is called *single parameter sensitivity analysis* ([Napolitano and Fabbri 1996]).
The real part of the dominant eigenvalue $Re(\gamma)$ is plotted as a function of the percent perturbation of α from its unperturbed value for both the approaches:

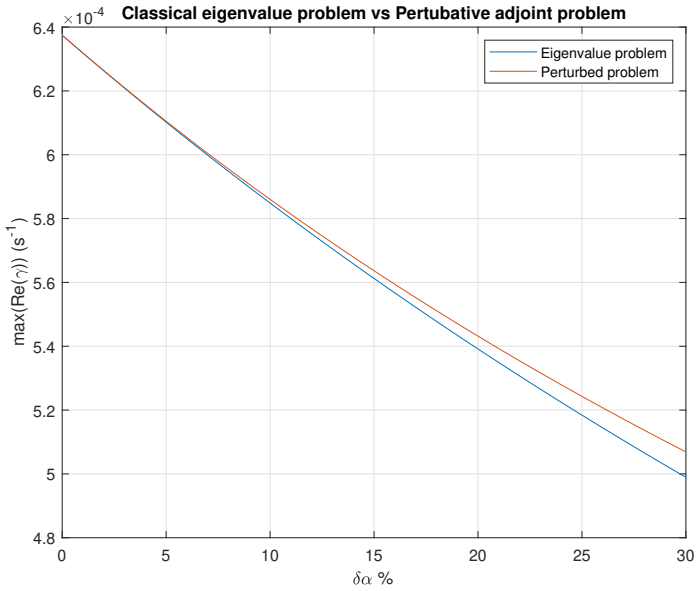

Figure 1.22: *Sensitivity analysis: classical eigenvalue problem vs adjoint eigenvalue problem.*

A perturbation array of 30 elements is employed for the plot in Figure 1.22.
The two curves stem from the unperturbed real part of the dominant eigenvalue and their difference increases as the perturbation increases: an expected result justified by the limited validity of the linear perturbative approach to only small perturbation values in magnitude.
The overall trend is a decreasing one as the value of α increases. It can be also observed that the adjoint approach is more conservative with respect to the classical eigenvalue study of $\tilde{A}$ (the dominant eigenvalue has a greater real part for the former approach). Of course, this considerations are valid only for this particular case, being taken only for an illustrative purpose.
At $\delta\alpha = 10\%\ \alpha$, the perturbative approach reaches a 6-digit accuracy with respect to the reference value of $Re(\gamma)$ given by the eigenvalue problem approach:

$Re(\gamma)$ at $\delta\alpha = 10\%\ \alpha$	
Adjoint problem	$5.844 \cdot 10^{-4}\ \ s^{-1}$
Eigenvalue problem	$5.832 \cdot 10^{-4}\ \ s^{-1}$

Table 1.3: *Dominant eigenvalue shift due to a perturbation $\delta\alpha = 10\%\ \alpha$: eigenvalue problem vs adjoint eigenvalue problem.*

From Table 1.3, it can be inferred that the perturbative approach given by the resolution of Eq.(1.58) has an exhaustive accuracy, compared with the overall precision given by the numerical resolution of the linear modal problem.
As an example, a plot of the eigenvalue spectrum in the complex plane, computed using the same input parameters as the previous simulation, with the exception of the discretization number $N = 50$, and the shifted spectrum by the action of perturbation array $\delta\alpha_i$, is shown:

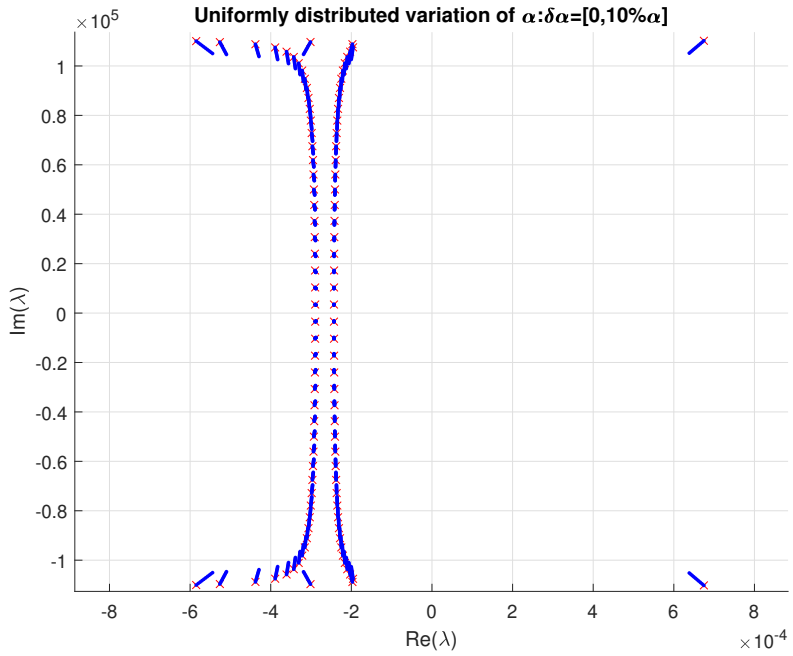

Figure 1.23: *Sensitivity analysis: a subset of the eigenvalues of A close to imaginary axis of the complex plane: in red the unperturbed eigenvalues, in blue the shift of the eigenvalue for increasing values of α.*

A pertubation array $\delta\alpha_i$ of 10 elements, extending up to the 10% of α, was used for Figure 1.23: the red crosses $\times$ represent the unperturbed eigenvalues of A, meanwhile the blue dots $\cdot$ mark the shift of the eigenvalues as the perturbation $\delta\alpha_i$ increases. It can be stated that the dominant eigenvalues (a couple of complex conjugated eigenvalues with $Re(\lambda) \approx 7 \cdot 10^{-3}\ s^{-1}$) tend to move towards the cluster aligned to the vertical line in $Re(\lambda) \approx -3 \cdot 10^{-3}\ s^{-1}$, resulting in a stabilising effect for the equilibrium point studied.
In the following, a series of results derived from the *sensitivity analysis* is presented, obtained with the *single parameter sensitivity analysis* procedure.
The simulation parameters used to individuate the equilibrium point to be studied are the same reported at the beginning of this section.
A series of observations is then reported to comment the sensitivity response of the system to the main parameter characterizing its dynamics.

1. Perturbation of α:
Unperturbed value of $\alpha = 0.00330\ J/kgPa$, dominant eigenvalue shift by an increase of the value of α with a perturbation array of 30 elements, up to the 10% of α:

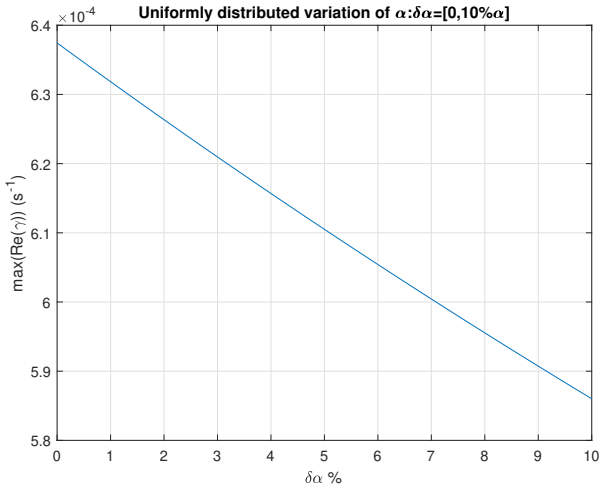

Figure 1.24: *Sensitivity analysis: dominant eigenvalue shift with an increase of* α *up to the* 10% *of its unperturbed value.*

2. Perturbation of β:
Unperturbed value of $\beta = -2527.44\ Jm^2/kg^2$, dominant eigenvalue shift by an increase of the value of β with a perturbation array of 30 elements, up to the 10% of the absolute value of β:

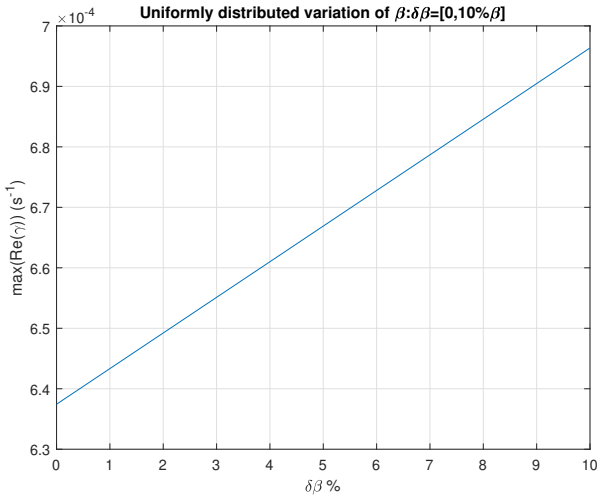

Figure 1.25: *Sensitivity analysis: dominant eigenvalue shift with an increase of* β *up to the* 10% *of its unperturbed value.*

3. Perturbation of k_0:
Unperturbed value of $k_0 = 0.001\ m^{-1}$, dominant eigenvalue shift by an increase of the value of k_0 with a perturbation array of 30 elements, up to the 10% of the value of k_0:

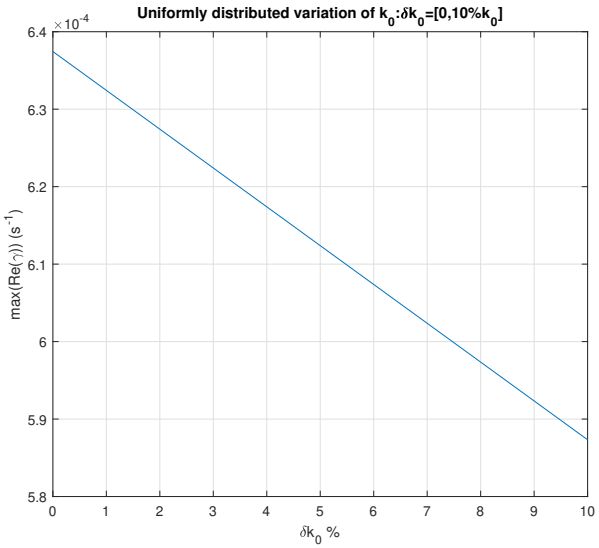

Figure 1.26: *Sensitivity analysis: dominant eigenvalue shift with an increase of k_0 up to the* 10% *of its unperturbed value.*

4. Perturbation of b:
Unperturbed value of $b = 1.0$, dominant eigenvalue shift by a decrease of the value of b with a perturbation array of 30 elements, up to -10% of the value of b:

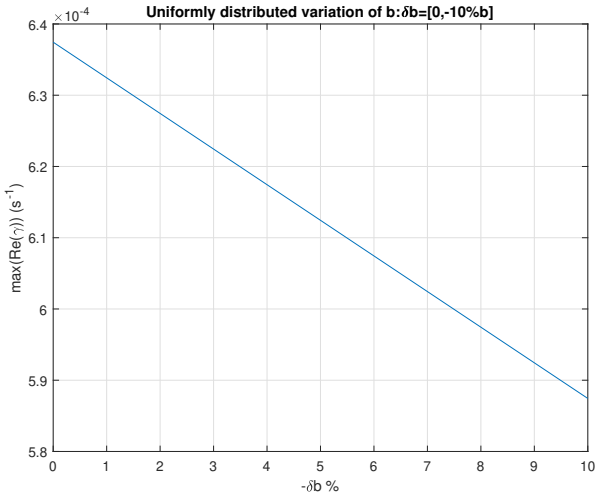

Figure 1.27: *Sensitivity analysis: dominant eigenvalue shift with a decrease of the value of b up to* -10% *of the value of b.*

Some observations can be stated referring to the previous results: first of all, the percent variation of the four parameters α, β, k_0 and b has a similar weight in the shift of the real part of the dominant eigenvalue $Re(\gamma)$.
The system tends to be slightly more sensitive to percent variations of β, but in general the response has the same order of magnitude.

A useful quantity, the *relative sensitivity* S, computed with Eq. (1.59)[10]:

$$S = \frac{Re(\delta\gamma}{)} Re(\gamma) \ \frac{\theta}{\delta\theta} \tag{1.59}$$

is resumed in Table 1.4 for each parameter considered previously:

Parameter	α	β	k_0	b
Relative sensitivity	-0.81	0.92	-0.79	0.78

Table 1.4: *Single parameter sensitivity analysis results.*

The second fundamental observation that can formulated is that, considering an increase in the value of the parameters, some result in a stabilizing effect for the system in that given equilibrium point, others instead in a destabilizing one.
In particular, according to Figures 1.24 and 1.26 and to the sign of S in Table 1.4, α and k_0 have a stabilizing action on the system, while for β and b, in Figure 1.25 and 1.27, a destabilizing impact for the equilibrium point.
This result is reasonable for k_0 and b: according to the stability map computed considering a uniform flow, in Figure 1.1, with increasing values of b the overall system is destabilized (widening of the instability region beneath the neutral stability curves); meanwhile, as k_0 increases, the stability maps reported in Section 1.4 show the corresponding stabilizing effect, with the increment of viscous dissipations in the system.
Less obvious considerations could be predicted a priori for the thermodynamic coefficients ruling the state equation for the internal energy u: this perturbative approach is a simple but powerful tool to perform a linear study of the impact of a set of physical parameters characterizing the properties of the evolving fluid.

Base flow sensitivity

The adjoint-based sensitivity approach is now devoted to the evaluation of the impact of some base flow perturbation to the overall stability of a selected equilibrium point. The equilibrium point (an unstable one) adopted is the same studied in Section 1.5.6:

Simulation parameters:

- Channel's length $L = 0.4\ m$
- Discretization number $N = 800$
- Flow regime: $b = 1.0$
- Inlet temperature: $T_{in} = 320\ °C$
- Outlet pressure: $p_{out} = 15.5\ MPa$
- Inlet velocity: $v_{in} = 2.0\ m/s$

[10] According to the previous plots, a linear trend may be exploited to compute S.

- Drag coefficient: $k_0 = 0.001\ m^{-1}$

A table resumes the averaged values of the state variables for the selected equilibrium point, along with the averaged value of the spatial derivatives, computed on the overall domain.

State variable	$\bar{v}_0$	$\overline{\frac{\partial v_0}{\partial z}}$	$\bar{p}_0$
Average value	2.00 m/s	0.2526e-04 s^{-1}	15.501 Pa
State variable	$\overline{\frac{\partial p_0}{\partial z}}$	$\bar{\rho}_0$	$\overline{\frac{\partial \rho_0}{\partial z}}$
Average value	-6674.12 Pa/m	680.20 kg/m^3	-8.59e-03 kg/m^4

Table 1.5: *Unperturbed averaged values for the state variables and their spatial derivatives.*

Applying the algorithm presented in Section 1.5.5, the set of results computed with MATLAB® is listed below:

1. Perturbation of v_0:
average value of the unperturbed profile $\bar{v}_0 = 2.00\ m/s$, dominant eigenvalue shift by a uniform increase along z of v_0 with a perturbation array of 30 elements, up to 10% of $\bar{v}_0$:

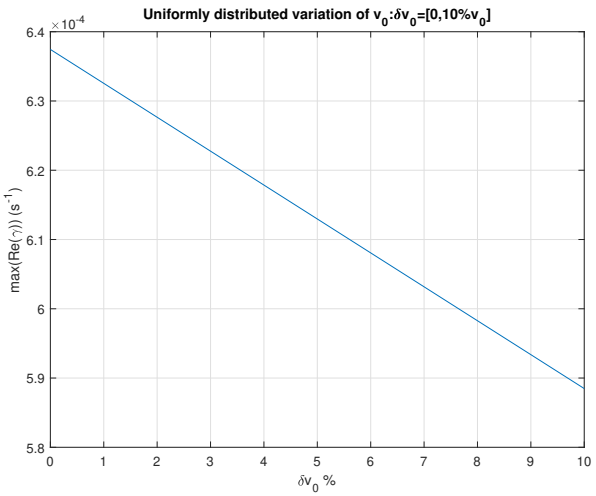

Figure 1.28: *Base flow sensitivity analysis: dominant eigenvalue shift with an increase of v_0 up to the 10% of its unperturbed averaged value $\bar{v}_0$.*

2. Perturbation of p_0:
average value of the unperturbed profile $\bar{p}_0 = 15.501\ MPa$, dominant eigenvalue shift by a uniform increase along z of p_0 with a perturbation array of 30 elements, up to 10% of $\bar{p}_0$:

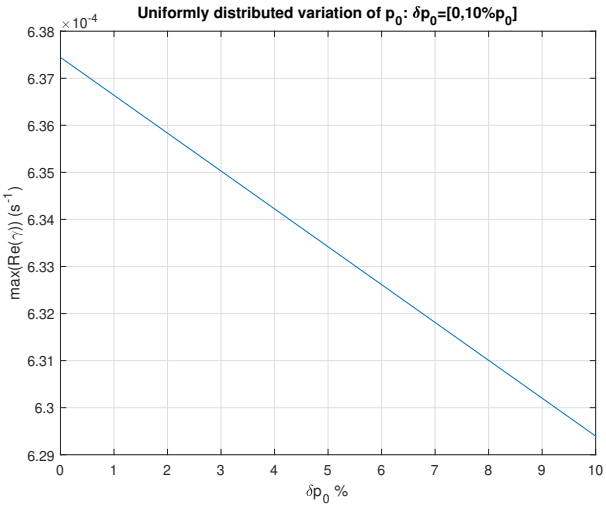

Figure 1.29: *Base flow sensitivity analysis: dominant eigenvalue shift with an increase of p_0 up to the 10% of its unperturbed averaged value $\bar{p}_0$.*

3. Perturbation of ρ_0:

average value of the unperturbed profile $\bar{\rho}_0 = 680.20\ MPa$, dominant eigenvalue shift by a uniform increase along z of ρ_0 with a perturbation array of 30 elements, up to 10% of $\bar{\rho}_0$:

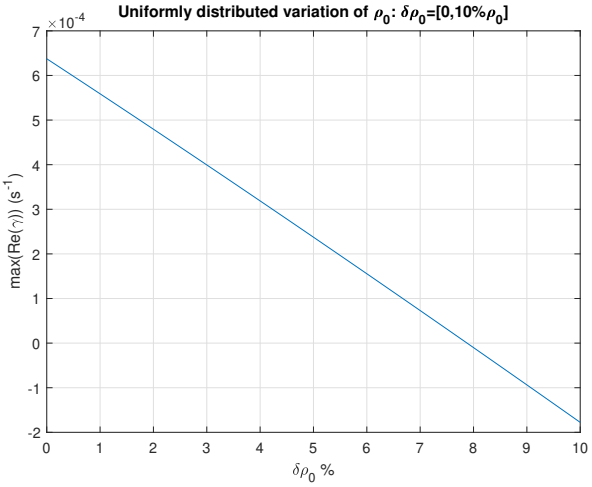

Figure 1.30: *Base flow sensitivity analysis: dominant eigenvalue shift with an increase of ρ_0 up to the 10% of its unperturbed averaged value $\bar{\rho}_0$.*

4. Perturbation of the spatial derivative of v_0:

evaluation of the impact on the equilibrium point of the spatial derivative of velocity, increasing its value up to the 10% of its unperturbed spatial average with an array of 30 elements:

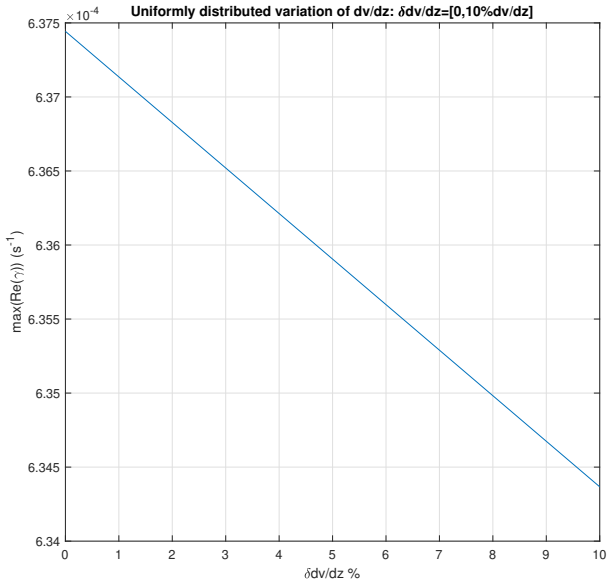

Figure 1.31: *Base flow sensitivity analysis: dominant eigenvalue shift with an increase of the spatial derivative of v_0 up to the 10% of its unperturbed averaged value.*

5. Perturbation of the spatial derivative of p_0:
evaluation of the impact on the equilibrium point of the spatial derivative of pressure, decreasing its value up to the 10% of its unperturbed spatial average with an array of 30 elements:

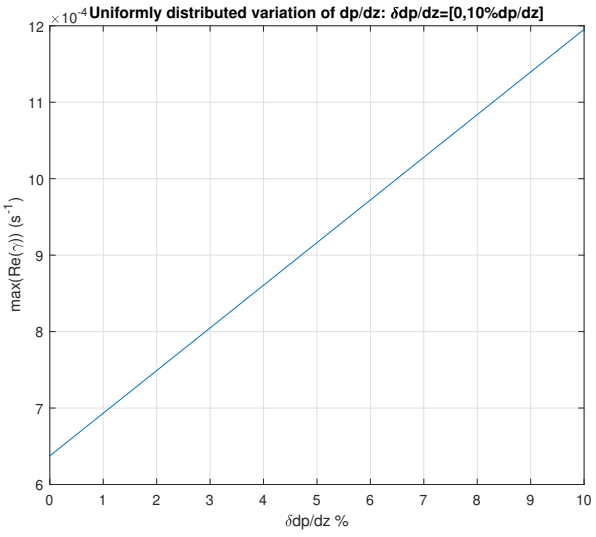

Figure 1.32: *Base flow sensitivity analysis: dominant eigenvalue shift with a decrease of the spatial derivative of p_0 up to the 10% of its unperturbed averaged value.*

6. Perturbation of the spatial derivative of ρ_0:
evaluation of the impact on the equilibrium point of the spatial derivative of density, decreasing its value up to the 10% of its unperturbed spatial average with an array of 30 elements:

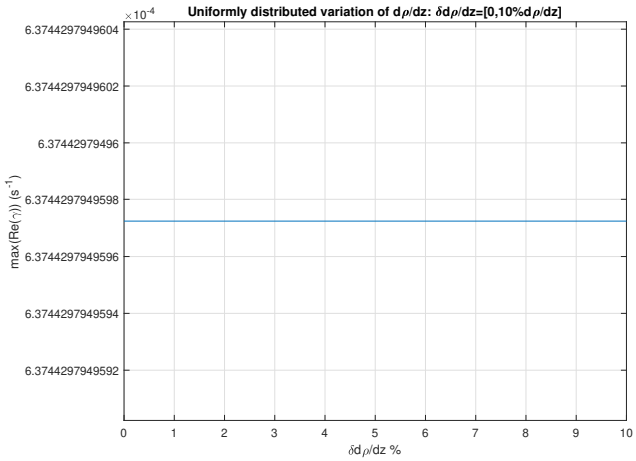

Figure 1.33: *Base flow sensitivity analysis: dominant eigenvalue shift with a decrease of the spatial derivative of ρ_0 up to the 10% of its unperturbed averaged value.*

First of all, it can be noticed that some perturbations on the state variables act on the system with a greater impact with respect to others: in particular, the system is more sensitive to a change of v_0, ρ_0 and $\frac{\partial p_0}{\partial z}$, in contrast to $\frac{\partial v_0}{\partial z}$, p and $\frac{\partial \rho_0}{\partial z}$.
It is recalled that the dominant eigenvalue shift of the real part is well described by the linear approximation only if the correspondent perturbation of the eigenvalue is confined to few percentile points of its unperturbed value: a perturbation of the 10% for ρ_0 and $\frac{\partial p_0}{\partial z}$ leads instead to a change of $\sim 100\%$ for $Re(\gamma)$, the former stabilizing the equilibrium point, the latter destabilizing it.
The validity of this trend for this two particular cases is then well limited, but an information about how much the system is sensitive to these state variables is still very useful.
A physical interpretation can be done to justify the trend of these most sensitive state variables to a perturbation. An increase of velocity (Figure 1.28) is connected to an horizontal shift on the v_{in}-k_0 plane: k_0 is fixed, so if $v_{in} \sim v_0$ is increased, the system moves towards a more stable configuration:

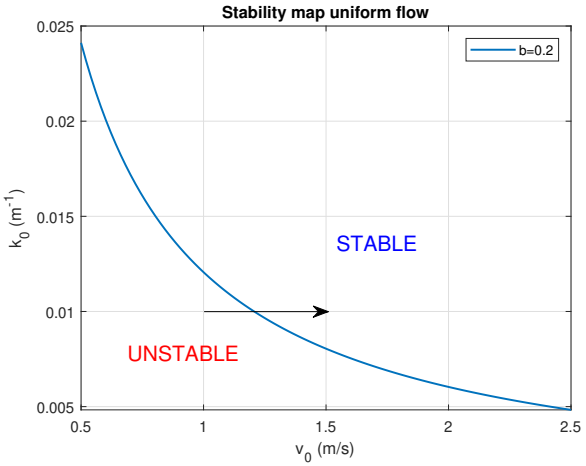

Figure 1.34: *Stabilizing effect of v_{in} as k_0 is maintained constant.*

As regards an increase of the density, in Figure 1.30 can be inferred that the system recognizes an increase of inertia that can be exploited to damp the infinitesimal perturbations that may trigger a modal instability amplification.
Finally, an increase in the steepness of the distributed pressure drop leads to a corresponding decrease of the stability of the equilibrium point: the stationary pressure gradient, appearing in the Internal energy equation, in this case acts as a net driving force that affects and amplifies the perturbations induced in the system by δv and $\delta\rho$.

1.6 Conclusions

The main topics and observations related to this chapter are briefly resumed in the following. The starting point in the development of this work is the [Doster and Kendall 1999] article, in which a uniform, compressible, unidimensional flow is taken into account. The set of equations governing the dynamics of the flow is linearized around an equilibrium point and a linear stability analysis is carried out (Eq.(1.12)). The stability condition for the most unstable case, i.e. when the fluid velocity in opposite to the gravitational acceleration (upflow), is obtained via Fourier analysis and the consequent study of the dispersion relations that characterize the system.
Different stability maps (in Figure 1.1) are drawn in the v_{in}-k_0 plane, each one corresponding to a different flow regime parameter b: as b increases, the instability region confined below the neutral stability curve widens and the system becomes more unstable.
Then, the uniform flow hypothesis is relaxed: a simple geometry and numerical domain are introduced for the problem, and a numerical procedure is undertaken to treat the spatial derivatives of the perturbations of the state variables. A channel of length L, in which the transverse dimensions are small compared to the longitudinal one, is disposed along the z-axis of a Cartesian reference frame. The flow concerns a subcooled fluid that enters the channel with a given inlet velocity and temperature, rises through the channel's length and exits with a prescribed pressure on the outlet. The evolving fluids considered are subcooled water and liquid sodium.
The system of governing equations is linearized around an equilibrium point: differently from the previous analysis, the spatial derivative terms of the steady-state solution are included in the linearized equations (Eq.1.31). The domain is subdivided in N equal elements, forming the numerical mesh of the problem. The steady-state analysis is carried out with COMSOL® and the nodal information is imported in MATLAB®. The approximation of the spatial derivatives is performed using a finite difference method, then a discretized version of the dynamics matrix A is obtained by evaluating the momentum equation, internal energy equation and continuity equation for each node of the mesh. Dirichlet homogeneous boundary conditions for the perturbations of the state variables are applied for the first node of the mesh for δv_i and $\delta\rho_i$ and the last node for δp_i.
The *modal analysis* ([Schmid and Brandt 2014], [Pini, Cammi, and Luzzi 2016]) is performed studying the real part of the dominant eigenvalue $Re(\gamma)$ of the discretized dynamics matrix A. Three different configurations (uniform flow, distributed pressure drop, concentrated pressure drop) are studied with subcooled water by computing

a correspondent stability map for each case (Figures 1.14, 1.16 and 1.20): in the first case, the stability map is analogue to the one found in Figure 1.1, in the second case a stabilizing effect for the system is observed and for the last case a strongly destabilizing one.
Then the system is further examined by means of a *sensitivity analysis* ([Schmid and Brandt 2014]) based on the *adjoint eigenvalues* of the dynamics matrix A: by means of the algebraic link between a perturbation of a parameter or a given base flow and the correspondent eigenvalue shift in Eq.(1.58) a *single parameter sensitivity analysis* ([Napolitano and Fabbri 1996]) and a *base flow sensitivity analysis* are performed on a selected equilibrium point.
The main perturbed parameters are: α, β, k_0 and b;
the main perturbed stationary profiles are: ρ_0, v_0, p_0 and the corresponding spatial derivatives.
A resuming table of the impacts of the perturbation on the system for each quantity listed above is shown, together with the *relative sensitivity* S computed with Eq.(1.59):

Parameters	*Relative sensitivity*	*Stability effect*
α	-0.81	Stabilizing
β	0.92	Destabilizing
k_0	-0.79	Stabilizing
b	0.78	Destabilizing

Table 1.6: *Summary of the main parameters of the non-conductive problem and their impact over stability.*

Stationary profiles	*Relative sensitivity*	*Stability effect*
v_0	-0.7392	Stabilizing
p_0	-0.1220	Stabilizing
ρ_0	-12.31	Stabilizing
$\frac{\partial v_0}{\partial z}$	-0.0088	Stabilizing
$\frac{\partial p_0}{\partial z}$	8.422	Destabilizing
$\frac{\partial \rho_0}{\partial z}$	$-1.637 \cdot 10^{-15}$	Stabilizing

Table 1.7: *Summary of the stationary profiles and their spatial derivatives of the non-conductive problem and their impact over stability.*

Chapter 2

Conductive fluid

Abstract. This chapter is devoted to the application and extension of the numerical techniques developed in Chapter 1 to a conductive fluid in the presence of an external magnetic field. The impact of the magnetic field on the stability features of the system is examined from various points of view: the modification of the stability maps by the action the magnetic field, the functional dependence of the neutral stability curve for incremental values of the magnetic field and a *sensitivity analysis* involving the additive terms inserted in the system of governing equations for the description of the coupling between the external magnetic field and motion of the fluid.

2.1 Introduction to the problem

In this chapter will be studied the action of a magnetic field on the stability features of the system presented in Chapter 1, employing as evolving fluid the liquid sodium. An overview about the general form of the Magnetohydrodynamic model for conductive fluids is presented, with the main assumptions and approximations underlying in the formulation of the model ([Freidberg 2007], [Chen 1984], [Galtier 2016]).
Then, starting with the unidimensional compressible Navier-Stokes equations employed in the study of the non-conductive fluid ([Doster and Kendall 1999]), an extension of the model is reported to include the magnetic induction coupling that characterize the dynamics of a conductive fluid inside an external magnetic field ([Trotta et al. 2019]).
In particular, the *modal analysis* performed in Chapter 1 for liquid sodium is carried out for the conductive model and the stabilizing effect of the external magnetic field is studied, highlighting the main differences for the non-conductive case.
Finally, the mathematical tools developed in Chapter 1 for the *sensitivity analysis*, referred to the main parameters characterizing the system and the stationary base flow, are applied to study how additive perturbations induced in the magnetic field or electrical conductivity impact on the system.

2.2 Governing equations for a conducting fluid

A brief presentation of the main equations that describe the interaction between the hydrodynamic and electromagnetic phenomena in a conductive fluid, in the approximation of *single fluid* ([Freidberg 2007], [Galtier 2016]) and neglecting relativistic effects, is reported. Compressible Navier-Stokes equations and Maxwell equations[1] are coupled together, forming the so-called Magnetohydrodynamic (MHD) model for conducting fluids.

2.2.1 MHD governing equations

The set of equations composing the MHD model is reported, together with the procedure exploited to derive it ([Chen 1984], [Freidberg 2007], [M. Kumar et al. 2016]):

- *Mass balance equation*

$$\frac{\partial \rho}{\partial t} + \nabla \cdot (\rho \vec{v}) = 0 \tag{2.1}$$

- *Momentum balance equation*

$$\rho \frac{\partial \vec{v}}{\partial t} + \rho(\vec{v} \cdot \nabla)\vec{v} = -\nabla p + \nabla \cdot \overline{\overline{\tau}} + \rho \vec{g} + \rho_e \vec{E} + \vec{J} \times \vec{B} \tag{2.2}$$

- *Internal energy balance equation*

$$\rho \frac{\partial u}{\partial t} + \rho(\vec{v} \cdot \nabla)u = -p \nabla \cdot \vec{v} + \overline{\overline{\tau}} : \nabla \vec{v} + \left(\vec{E} + \vec{v} \times \vec{B}\right) \cdot \vec{J} \tag{2.3}$$

- *State equation*

$$u = u(\rho, p) \tag{2.4}$$

- *Rheologic model for the viscous stress tensor*[2]

$$\overline{\overline{\tau}} = \mu \left(\nabla \vec{v} + \nabla \vec{v}^T\right) - \frac{2}{3}\mu \left(\nabla \cdot \vec{v}\, \overline{\overline{I}}\right) \tag{2.5}$$

Where ρ and ρ_e are respectively the mass and charge density, $\vec{v}$ is the velocity field of the fluid, p the thermodynamic pressure, u the internal energy, $\overline{\overline{\tau}}$ the viscous stress tensor,$\vec{J}$ the current density field and $\vec{E}$ and $\vec{B}$ respectively the electric field and magnetic induction field. The units of measurement adopted are reported in the List of Symbols.
Some additive terms, with respect to the non-conductive case, appear in the right-hand side of Eqs.(2.2) and 2.3: the *Lorentz force* term $\rho_e \vec{E} + \vec{J} \times \vec{B}$ in the momentum equation and a source term $\left(\vec{E} + \vec{v} \times \vec{B}\right) \cdot \vec{J}$ for the internal energy equation.
It is also remarked that, in general, the state equation employed in the field of plasma

[1] In the SI unit system.
[2] At first, the assumption of treating the conducting fluid as a *stokesian fluid* is valid.

physics is usually different from Eq.(2.4); a polytropic closure ([Pucella and Segre 2009]) of the form:

$$\frac{d}{dt}\left(p\rho^{-\bar{\gamma}}\right) = 0 \tag{2.6}$$

is often adopted, where $\bar{\gamma}$ is the polytropic index which describes the thermodynamic process followed by the ionized gas (for many applications, an adiabatic closure is chosen, with the hypothesis of no heat exchange between the system and the environment).
Instead, in this work, it's more convenient to maintain the same state equation presented in Chapter 1 for the non-conductive case: the latter is more compatible with the description of a conducting liquid, as liquid sodium.
The set of equations presented this far for the MHD model is not closed yet: the dynamics of the electric and magnetic induction fields, as well as the current density field, is still unknown.
Maxwell's equations, with some simplifying hypothesis holding for the MHD model, are employed to fully close the system.
One important simplification is that the fluid is locally neutral but still conductive, so that ρ_e is null in every point inside the fluid ([Freidberg 2007]).
This approximation, valid when the dynamics of the fluid is mainly dominated by phenomena with characteristic time scales comparable with the ion time scales present inside the conductive fluid, leads to a first simplification in the right-hand side of the momentum balance equation (2.2) of the $\rho_e\vec{E}$ term.
Then, the *generalized Ohm's law*[3], derived from the electron momentum equation in the multi-fluid model ([Freidberg 2007]) and expressed by means of the single-fluid variables, is adopted in the description:

$$\vec{E} + \vec{v} \times \vec{B} = \eta\vec{J} \tag{2.7}$$

where η is the electric resistivity of the conductive fluid, in $\Omega\,\mathrm{m}$.
Eq.(2.7), together with *Faraday's law*, leads to an evolution equation for the magnetic induction field, the *induction equation* for $\vec{B}$:

$$\frac{\partial\vec{B}}{\partial t} = \nabla \times \left(\vec{v} \times \vec{B}\right) + \eta\Delta\vec{B} \tag{2.8}$$

This equation is the starting point to include the electromagnetic effects in a conductive fluid description.
Moreover, Eq.(2.8) contains the solenoidal constraint for the induction field $\vec{B}$:

$$\nabla \cdot \vec{B} = 0 \tag{2.9}$$

In fact, by taking the divergence of (2.8) ([Spruit 2013]), it can be showed that:

$$\frac{\partial}{\partial t}\left(\nabla \cdot \vec{B}\right) = 0 \tag{2.10}$$

[3] As a first approximation, the Hall term and electron diamagnetic term are neglected.

If the initial condition for $\vec{B}$ is divergenceless, Eq.(2.10) guarantees that the solenoidal constraint on $\vec{B}$ remains fulfilled during its evolution.
Hereafter, a useful decomposition of the magnetic induction field $\vec{B}$ is exploited to distinguish the different contributes composing the field:

$$\vec{B} = \vec{B_0} + \mu_0 \mu_R \vec{H} \tag{2.11}$$

where $\vec{B_0}$ is the external induction magnetic field (in T) acting on the system and $\vec{H}$ is the magnetic field intensity, measured in $\mathrm{A\,m^{-1}}$, that is induced inside the conducting fluid.
μ_0 is the magnetic permeability in vacuum ($\mathrm{H\,m^{-1}}$), and μ_r is the relative permeability of the conductive fluid[4].
In this study the external field serves as a time-independent forcing term: the induction equation (2.8) describes the evolution of the magnetic field intensity $\vec{H}$ in time, while the total induction magnetic field acts in both the momentum equation (2.2) and in the generalized Ohm's law (2.7).
The evaluation of the current density field $\vec{J}$ is given by employing the *Ampère's law* in the hypothesis that the displacement current does not affect the dynamics of the fluid[5] In particular, $\vec{J}$ can be computed by simply applying the curl operator on $\vec{H}$:

$$\vec{J} = \nabla \times \vec{H} \tag{2.12}$$

From a phenomenological point of view, the evolutive equation for $\vec{H}$, driven by the coupling between the velocity field and the total magnetic induction field, dictates the time evolution of the current density field $\vec{J}$, by applying Eq.(2.12) to $\vec{H}$ in each instant.
Substituting the generalized Ohm's equation (2.7) in the source term of the internal energy equation (2.3), the final set of equations, in tensorial form, is obtained:

- *Mass balance equation*

$$\frac{\partial \rho}{\partial t} + \nabla \cdot (\rho \vec{v}) = 0 \tag{2.13}$$

- *Momentum balance equation*

$$\rho \frac{\partial \vec{v}}{\partial t} + \rho(\vec{v} \cdot \nabla)\vec{v} = -\nabla p + \nabla \cdot \overline{\overline{\tau}} + \rho \vec{g} + \vec{J} \times \vec{B} \tag{2.14}$$

- *Internal energy balance equation*

$$\rho \frac{\partial u}{\partial t} + \rho(\vec{v} \cdot \nabla)u = -p \nabla \cdot \vec{v} + \overline{\overline{\tau}} : \nabla \vec{v} + \eta J^2 \tag{2.15}$$

- *State equation*

$$u = u(\rho, p) \tag{2.16}$$

[4]For many conductive fluids ([M. Kumar et al. 2016]), its value is ≈ 1

[5]This assumption ([Freidberg 2007]) is associated with the non-relativistic motion regimes of the conducting fluid.

- *Viscous stress tensor*

$$\bar{\bar{\tau}} = \mu \left(\nabla \vec{v} + \nabla \vec{v}^T \right) - \frac{2}{3} \mu \left(\nabla \cdot \vec{v} \, \bar{\bar{I}} \right) \tag{2.17}$$

- *Magnetic induction equation*

$$\frac{\partial \vec{B}}{\partial t} = \nabla \times \left(\vec{v} \times \vec{B} \right) + \eta \Delta \vec{B} \tag{2.18}$$

- *Magnetic field intensity equation*

$$\vec{B} = \vec{B}_0 + \mu_0 \mu_r \vec{H} \tag{2.19}$$

- *Ampère's law*

$$\vec{J} = \nabla \times \vec{H} \tag{2.20}$$

where the source term ηJ^2 in the internal energy equation (2.15) is identified as the Joule effect.

2.2.2 Unidimensional balance equations: conductive fluid

In this section, the governing equations in tensorial form derived in Section 2.2.1 that describe the motion of a conducting fluid under the action of an external magnetic field are now adapted to the one-dimensional case.
In particular, the unidimensional, non-conductive set of equations presented in Section 1.3 are now inserted in the MHD framework and the Lorentz force, together with the magnetic induction equation, is added to the non-conducting model.
Firstly, the geometry adopted, together with the acting forces, fields and boundary conditions, are presented in Figure 2.1:

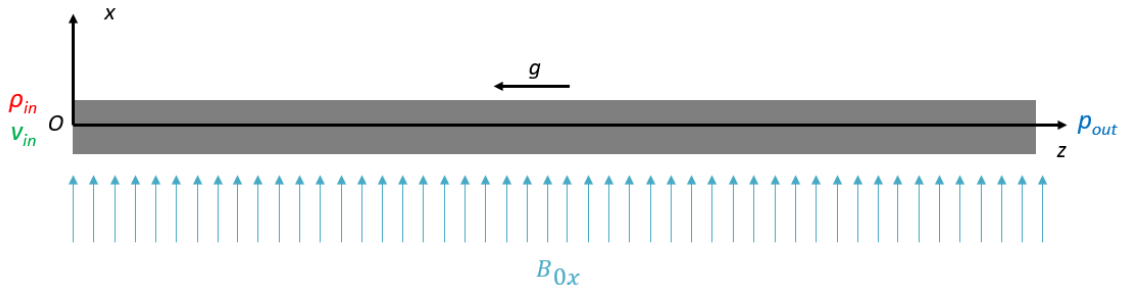

Figure 2.1: *Geometry, domain and boundary conditions.*

The evolving fluid inside the riser is liquid sodium and the main geometrical features, as well as the boundary conditions in the upflow configuration of the channel, are the same adopted for the non-conductive case.
The main difference consists in the presence of an external magnetic field oriented along the x axis of the Cartesian reference frame.
This choice is motivated by the fact that the Lorentz force that arises with a magnetic field applied in this direction acts along the z axis of the reference frame, together

with the gravitational and friction forces along the channel.
This last statement turns into a simplification for the evolution equation of the magnetic field intensity $\vec{H}$. The main component that will be considered in the following is $H_x = H_x(z)$, as the other components don't appear in the monodimensional momentum equation.
Other hypothesis are added as a starting point for this study:

1. The Joule effect present in the internal energy equation (2.15), as well as all thermal effects, will be neglected.

2. The inviscid approximation is applied (as for the non-conductive case) to the internal energy equation.

3. The steady-state equilibrium profiles employed for the linear stability analysis won't take into account any conductive effect: the system will be subjected to an external magnetic field $B_{0,x}$ from $t = 0^+$, acting directly on the perturbations inside the channel, while instead $H_{0,x} = 0\ A/m$.

4. The external magnetic field $B_{0,x}$ is uniform along z.

5. The boundary conditions adopted for the perturbations of the x-component of the magnetic field intensity δH_x are ([M. Kumar et al. 2016], [Jackson 2007]):

$$\delta H_x(0) = 0, \quad \delta H_x(L) = 0 \tag{2.21}$$

The resulting linearized set of equations for the description of the linear stability of an equilibrium configuration in the conductive case is finally presented:

$$\begin{cases} \dfrac{\partial \delta\rho}{\partial t} = -v_0 \dfrac{\partial \delta\rho}{\partial z} - \dfrac{\partial v_0}{\partial z}\delta\rho - \rho_0 \dfrac{\partial \delta v}{\partial z} - \dfrac{\partial \rho_0}{\partial z}\delta v \\ \dfrac{\partial \delta p}{\partial t} = -v_0 \dfrac{\partial \delta p}{\partial z} - \delta v \dfrac{\partial p_0}{\partial z} + \dfrac{\beta}{\alpha}\rho_0 \dfrac{\partial \delta v}{\partial z} + \dfrac{\beta}{\alpha}\delta\rho \dfrac{\partial v_0}{\partial z} - \dfrac{p_0}{\alpha\rho_0}\dfrac{\partial \delta v}{\partial z} + \\ \qquad - v_0 \left(\dfrac{\beta}{\alpha}\dfrac{\partial \rho_0}{\partial z} - \dfrac{\partial p_0}{\partial z} \right) \dfrac{\delta\rho}{\rho_0} - \dfrac{1}{\alpha\rho_0}\dfrac{\partial v_0}{\partial z}\delta p \\ \dfrac{\partial \delta v}{\partial t} = -v_0 \dfrac{\partial \delta v}{\partial z} - \delta v \dfrac{\partial v_0}{\partial z} - \left(g + \dfrac{k_0 v_0^2}{2} + v_0 \dfrac{\partial v_0}{\partial z} \right) \dfrac{\delta\rho}{\rho_0} - \dfrac{1}{\rho_0}\dfrac{\partial \delta p}{\partial z} + \\ \qquad - \left(\dfrac{2-b}{2} \right) k_0 v_0 \delta v - B_{0,x} \dfrac{\partial \delta H_x}{\partial z} \\ \dfrac{\partial \delta H_x}{\partial t} = -v_0 \dfrac{\partial \delta H_x}{\partial z} - \dfrac{B_{0,x}}{\mu_0}\dfrac{\partial \delta v}{\partial z} + \dfrac{\eta}{\mu_0}\dfrac{\partial^2 \delta H_x}{\partial z^2} \end{cases} \tag{2.22}$$

The coupling between the external magnetic field and the hydrodynamic motion of the liquid sodium is given by the term $-B_{0,x}\frac{\partial \delta H_x}{\partial z}$ present in the linearized momentum equation.
The perturbation δH_x is described by the last equation of (2.22): the coupling between the space derivative of the velocity perturbation and the external magnetic field acts as a source term for δH_x, which, in turn, plays a role in the Lorentz force term in the momentum equation.

The induction equation for the x-component of $\delta\vec{H}$ presents the form of an advection-diffusion equation: the magnetic field intensity is transported by the velocity of the fluid v_0 and diffuses with the parabolic term $\frac{\eta}{\mu_0}\frac{\partial^2\delta H_x}{\partial z^2}$ proportional to the electrical resistivity of the liquid sodium.

2.3 Modal analysis for the conductive fluid

2.3.1 Numerical discretization of the unidimensional MHD equations

From now on, δH_x and $B_{0,x}$ are denoted with δH and B_0, to simplify the notation in the equations. The set of PDEs (2.22) is expressed in a matricial form, maintaining the formal setting employed for the *modal analysis* of Eqs.(1.32):

$$\frac{\partial}{\partial t}\delta X = A\delta X \tag{2.23}$$

The state vector δX is now defined as:

$$\delta X = \begin{bmatrix}\delta v, & \delta p, & \delta\rho, & \delta H\end{bmatrix}^T \tag{2.24}$$

And the dynamics matrix A is defined as:

$$A = \begin{bmatrix} A_{11} & A_{12} & A_{13} & A_{14} \\ A_{21} & A_{22} & A_{23} & A_{24} \\ A_{31} & A_{32} & A_{33} & A_{34} \\ A_{41} & A_{42} & A_{43} & A_{44} \end{bmatrix} \tag{2.25}$$

The entries of the internal 3×3 matrix of (2.25) describing the hydrodynamics of the unidimensional, compressible flow are the same as the dynamics matrix A in (1.35). Additive terms arise in the inclusion of conductive effects inside the system: a new column A_{i4} describes the coupling between the perturbations of the state variables and δH (including the coupling with itself in A_{44}) and a new row A_{4i} is introduced to describe the evolution of the perturbation δH in time.

The coupling terms between the hydrodynamics perturbations of the state variables and δH are briefly reported:

$$A_{14} = -B_0\frac{\partial\delta H}{\partial z}, \qquad A_{24} = 0, \qquad A_{34} = 0$$

together with the evolutive equation for δH:

$$A_{41} = -\frac{B_0}{\mu_0}\frac{\partial}{\partial z}, \qquad A_{42} = 0, \qquad A_{43} = 0, \qquad A_{44} = -v_0\frac{\partial}{\partial z} + \frac{\eta}{\mu_0}\frac{\partial^2}{\partial z^2}$$

Then the numerical discretization of the former system of PDEs is performed, using the finite differences schemes presented in Section 1.4.5 and adopting the same mesh for the interval $[0, L]$ along the z axis.
Since the main structure of the discretization matrix A for the momentum equation, internal energy equation and mass continuity equation is the same as for the non-conductive case, only the spatial discretization of the magnetic induction equation will be presented explicitly in the following.
To approximate the first order spatial derivatives, the central finite difference formula is adopted as in Section 1.4.5:

$$\left.\frac{\partial \delta\phi}{\partial z}\right|_i = \frac{\delta\phi_{i+1} - \delta\phi_{i-1}}{2h} \tag{2.26}$$

Differently from the non-conductive case, the induction equation presents also a parabolic term related to the diffusion of the magnetic field δH, so the employment of a formula for the approximation of the second order derivative in space is needed, namely the central finite difference formula for second order derivatives:

$$\left.\frac{\partial^2 \delta\phi}{\partial z^2}\right|_i = \frac{\delta\phi_{i+1} - 2\delta\phi_i + \delta\phi_{i-1}}{h^2} \tag{2.27}$$

Recalling the boundary conditions involving δH (Eq. 2.21), the evaluation of δH_i is limited only on the interior points of the mesh, i.e. from δH_2 to δH_N, being N the number of elements that compose the mesh.
The discrete form of the state vector for the conductive case is then:

$$\delta X = [\delta v_2, \cdot\ \cdot\ \cdot, \delta v_{N+1}, \delta p_1, \cdot\ \cdot\ \cdot, \delta p_N, \delta\rho_2, \cdot\ \cdot\ \cdot, \delta\rho_{N+1}, \delta H_2, \cdot\ \cdot\ \cdot, \delta H_N]^T \tag{2.28}$$

It is stressed that, in this case, the problem shifted from a system of 4 linear PDEs to a set of $4N - 1$ linear ODEs. The discretized form of the induction equation for a generic i-th interior node is:

$$\frac{d\delta H_i}{dt} = -\frac{B_{0,i}}{\mu_0}\frac{\delta v_{i+1} - \delta v_{i-1}}{2h} - v_0\frac{\delta H_{i+1} - \delta H_{i-1}}{2h} + \frac{\eta}{\mu_0}\frac{\delta H_{i+1} - 2\delta H_i + \delta H_{i-1}}{h^2} \tag{2.29}$$

The dynamics matrix A is assembled with the same numerical procedure followed in Section 1.4.7, adopting once again the LiveLink™ connection between COMSOL® Multiphysics and MATLAB®'s command prompt.

2.3.2 Results: liquid Na

A first validation of the new numerical set up developed for the conducting fluid is carried out by imposing $B_0 = 0\ T$ and turning off all the spatial derivatives terms inside A. As for the non-conductive case, a set of input parameters for the simulation needs to be defined, and a convergence analysis of the real part of the dominant eigenvalue $Re(\gamma)$ for increasing values of N is to be performed, to choose the appropriate N for each particular case.

Simulation parameters:

- Channel's length $L = 0.6\ m$
- Flow regime: $b = 1.0$
- Inlet temperature: $T_{in} = 500\ °C$
- Outlet pressure: $p_{out} = 1\ bar$
- External magnetic field: $B_0 = 0\ T$

The inlet velocity chosen for the convergence plot is $v_{in} = 0.5\ m/s$ and the corresponding drag coefficient is $k_0 = k_{0,min}$, computed with the analytical result in Eq. (1.25), in the condition of incipient instability:

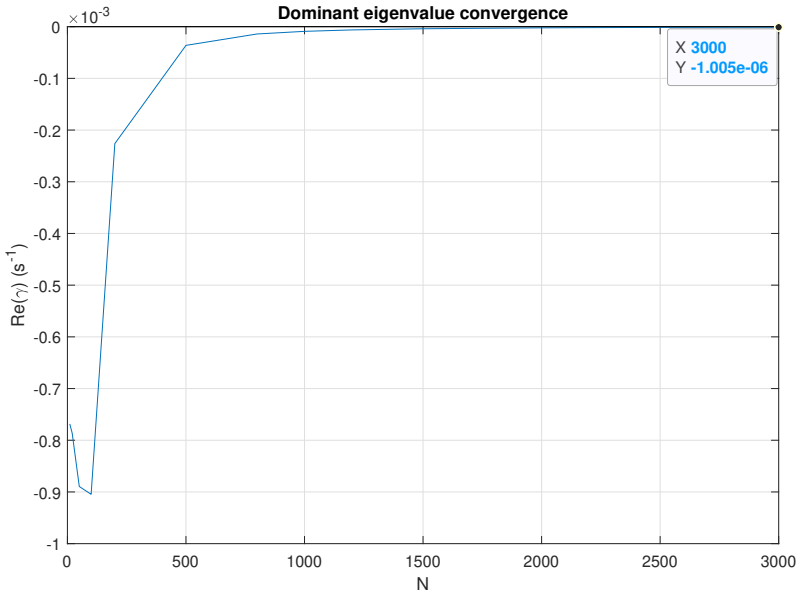

Figure 2.2: *Convergence plot of $Re(\gamma)$, uniform flow, $B_0 = 0\ T$, liquid sodium.*

A compromise between a good accuracy for the numerical method and low computational cost is achieved with $N = 1500$. In the following, a stability map is drawn with an inlet velocity array $v_{in,i}$ of 11 equispaced elements, from 0.5 m/s to 1.0 m/s, and a corresponding $k_{0,i}$ array of 10 elements, for each entry of $v_{in,i}$, is selected, centered on $k_{0,min}$ with a range extension of $0.4k_{0,min}$:

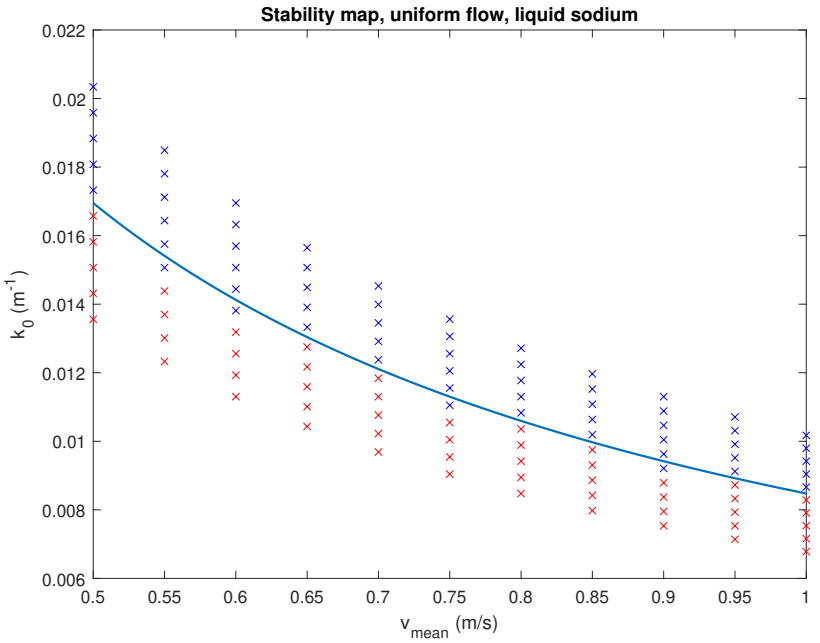

Figure 2.3: *Stability map for uniform flow, $B_0 = 0\ T$, liquid sodium.*

It can be observed that this model fully contains the non-conductive one, with good agreement with the results computed analytically using Eq. (1.25).
Now, the impact of an external magnetic field $B_0 = 1\ T$ is studied, adopting the same parameters of the previous simulation and neglecting the spatial derivatives and profiles along the channel, to make a direct comparison with the non-conductive case found for $B_0 = 0\ T$.
The resulting convergence plot using $v_{in} = 0.5\ m/s$ and the corresponding drag coefficient $k_0 = k_{0,min}$ is:

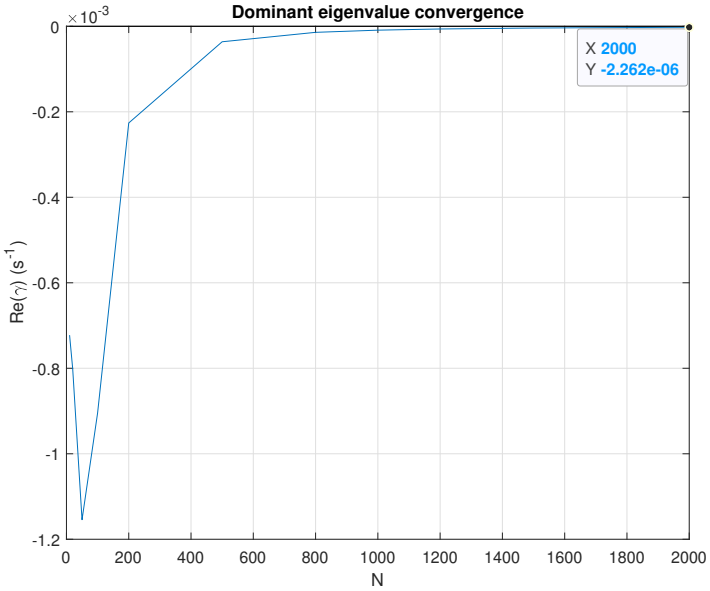

Figure 2.4: *Convergence plot of $Re(\gamma)$, uniform flow, $B_0 = 1.0\ T$, liquid sodium.*

A stability map for $N = 1200$ is drawn, selecting the same inlet velocity interval of Figure 2.3 and employing a fixed drag coefficient array $k_{0,i}$ of 10 elements, equally spaced and ranging from 0 m^{-1} to 10^{-4} m^{-1}:

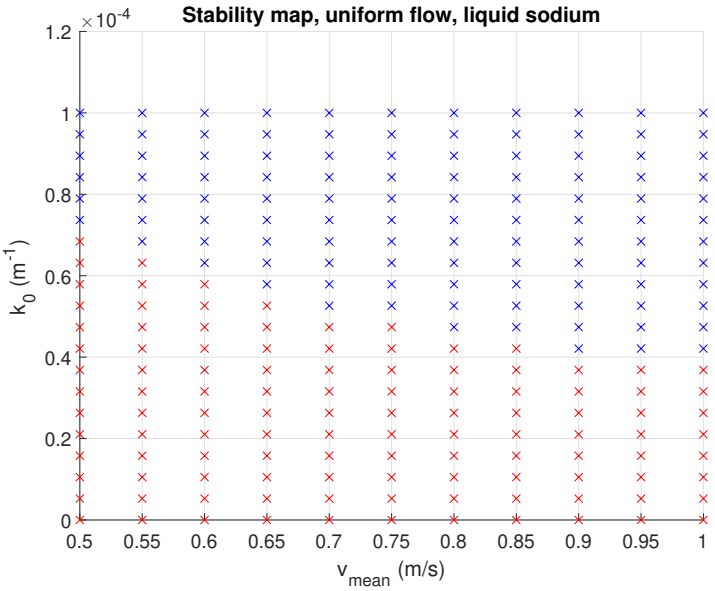

Figure 2.5: *Stability map for uniform flow, $B_0 = 1.0$ T, liquid sodium.*

The action of the external magnetic field B_0 on the neutral stability curve of the system is remarkable: a contraction of the critical drag coefficient of about 3 order of magnitude can be observed.
As an example, by taking the minimum drag coefficient at a velocity $v_{in} = 1.0$ m/s, the case without an external magnetic field signs $k_{0,min} = 8.5 \cdot 10^{-3}$ m^{-1}, meanwhile, for the case of $B_0 = 1.0$ T, the value is $k_{0,min} \approx 4 \cdot 10^{-5}$ m^{-1}.
The effects of spatial derivatives are analogous to those presented in Section 1.4: the pressure gradient of the distributed pressure drop acts as a stabilizing term, meanwhile a localized pressure drop will lead to a marked increase of the instability region in the v_{in}-k_0 plane.
To conclude this section, it's interesting to study how the critical drag coefficient $k_{0,min}$ shifts as the magnetic field B_0 is increased from 0 T to 1.0 T: the study is conducted on the iso-velocity line $v_{in} = 1$ m/s of the v_{in}-k_0 plane with the following input parameters [6]:

Simulation parameters:

- Channel's length $L = 0.6$ m
- Flow regime: $b = 0.2$
- Inlet temperature: $T_{in} = 500$ $°C$
- Outlet pressure: $p_{out} = 1.0$ bar

[6]The spatial derivatives terms are neglected also in this case

- Discretization number: $N = 1200$

An array of 10 uniformly spaced increasing values of B_0 is adopted to study the modal response of the system: for each element of the array, the computation of $k_{0,min}$ is performed with a bisection method[7].
The following trend is obtained:

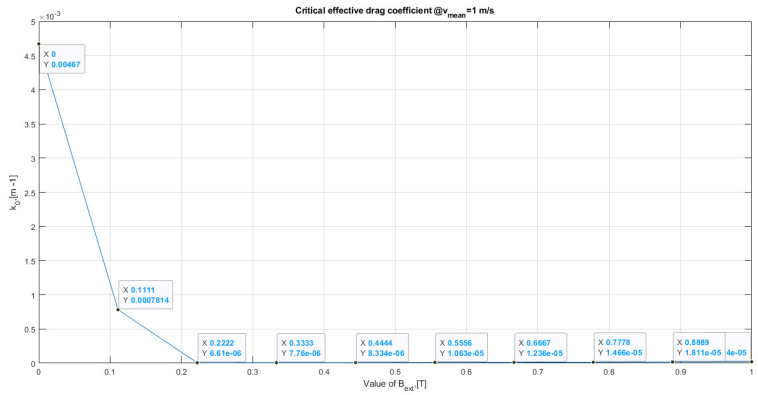

Figure 2.6: *Shift of $k_{0,min}$ with increasing values of B_0, up to $B_0 = 1.0\ T$, liquid sodium.*

Two observations can be made: the first is that the impact of the external magnetic field is important from low values of B_0 and starts to saturate for values situated about at $B_0 = 0.2\ T$, the second is that the values of $k_{0,min}$ present in the saturation point are within the error committed in the eigenvalue analysis[8], so no additional information is available. The study is repeated for lower values of B_0 to better appreciate the trend of $k_{0,min}$ when its excursion is important:

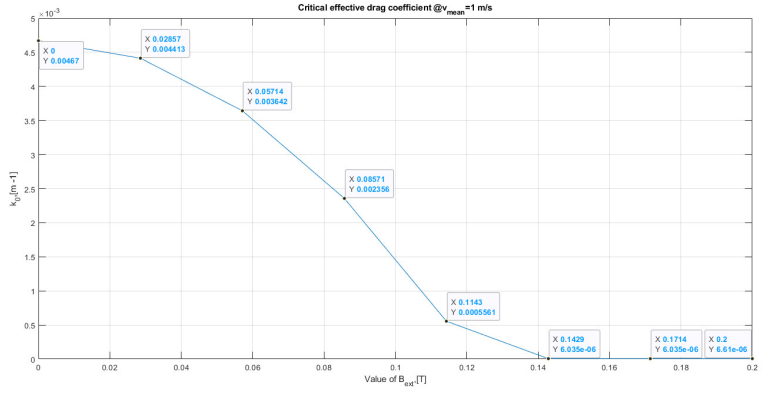

Figure 2.7: *Shift of $k_{0,min}$ with increasing values of B_0, up to $B_0 = 0.2\ T$, liquid sodium.*

[7]The algorithm employs a tolerance of $\Delta k_0 = 10^{-6}\ m^{-1}$

[8]In Figure 2.2, the theoretical result expected using $k_{0,min}$ is $Re(\gamma) = 0\ s^{-1}$, while for $N = 3000$ the value is $Re(\gamma) = -1.005 \cdot 10^{-6}\ s^{-1}$.

2.4 Sensitivity analysis for the conductive fluid

The mathematical development of the perturbative modal analysis performed with the adjoint eigenvectors of the dynamics matrix A in Section 1.5.1 is re-proposed for the conductive case in the following.
Since the perturbative analysis concerning the thermo-hydraulic and flow regime parameters present in A, as well as the perturbations on the base flow for ρ_0, v_0 and p_0 and their spatial derivatives was treated in Section 1.5.1 for the non-conductive case, in this section the central point to be investigated is the impact of perturbations on the external magnetic field B_0 and the electrical resistivity η of the liquid sodium. Thus, coherently to what was done in the previous section, all the spatial derivatives terms will be neglected and uniform spatial profiles of ρ_0, v_0 and p_0 are employed.

2.4.1 Results: liquid Na

First of all, the equilibrium point to be studied is specified. The input parameters are chosen such that the equilibrium point is an unstable one:

Simulation parameters:

- External magnetic field $B_0 = 0.1\ T$
- Channel's length $L = 0.6\ m$
- Flow regime: $b = 1.0$
- Inlet temperature: $T_{in} = 500\ °C$
- Outlet pressure: $p_{out} = 1.0\ bar$
- Discretization number: $N = 1200$
- Inlet velocity: $v_{in} = 1.0\ m/s$
- Drag coefficient: $k_0 = 10^{-6}\ m^{-1}$

A base flow perturbative analysis is then carried out: the external magnetic field B_0 is perturbed with an array of 30 elements; the perturbation δB_0 extends up to the 10% of B_0 and the shift of the real part of the dominant eigenvalue is studied as the perturbation δB_0 increases.

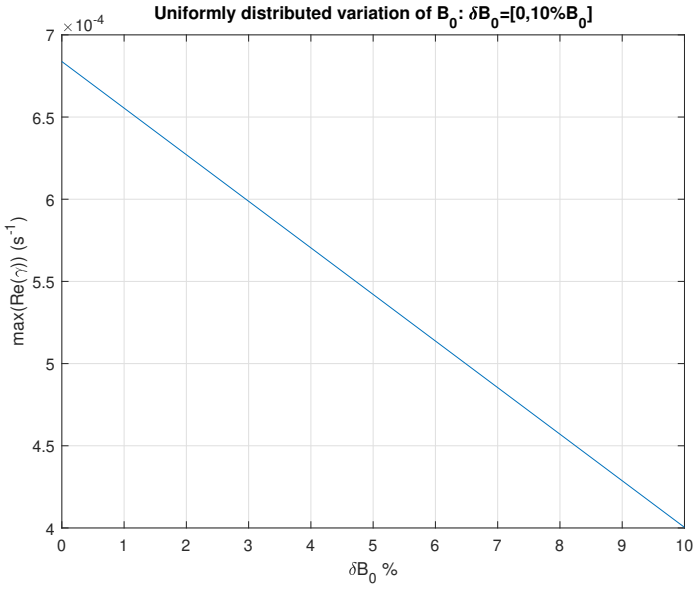

Figure 2.8: *Base flow sensitivity analysis: dominant eigenvalue shift with an increase of B_0 up to the 10% of its unperturbed value.*

The strong stabilizing effect of the magnetic field is once again observed in Figure 2.8: the relative sensitivity, computed with Eq.(1.59), associated to the eigenvalue shift is $S = -4.1446$.
As an illustrative purpose, the root locus for increasing values of B_0 is drawn in the complex plane (as what was done in Figure 1.23):

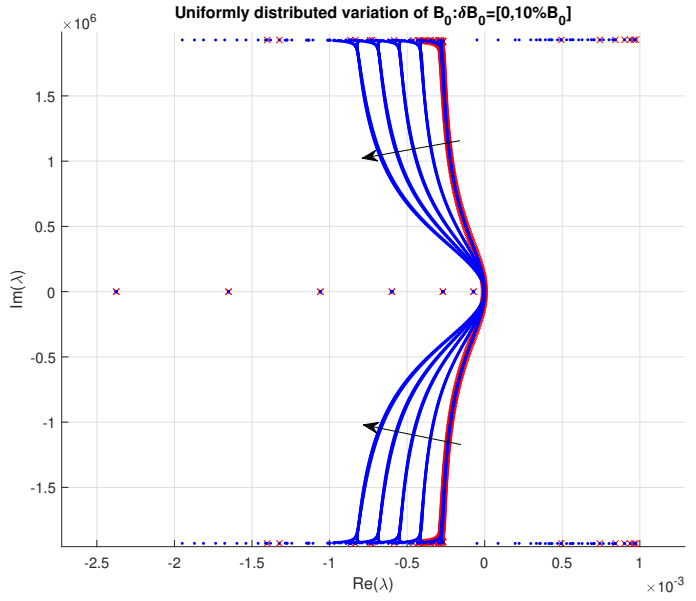

Figure 2.9: *The root locus of A in $\times$ and $\tilde{A}$ in $\cdot$, computed with an increase of B_0 up to the 10% of its unperturbed value.*

Then the *single parameter sensitivity analysis* is applied to study how the electrical resistivity η affects the eigenvalue spectrum of A. The unperturbed value of $\eta =$

$2.7202 \cdot 10^{-7}\ \Omega m$ is set by selecting the inlet temperature $T_{in} = 500°C$ of the liquid sodium. Coherently to what was done in the parametric sensitivity analysis for the non-conductive case, a perturbation array $\delta\eta_i$ of 30 elements, extending up to the 10% of η, is chosen:

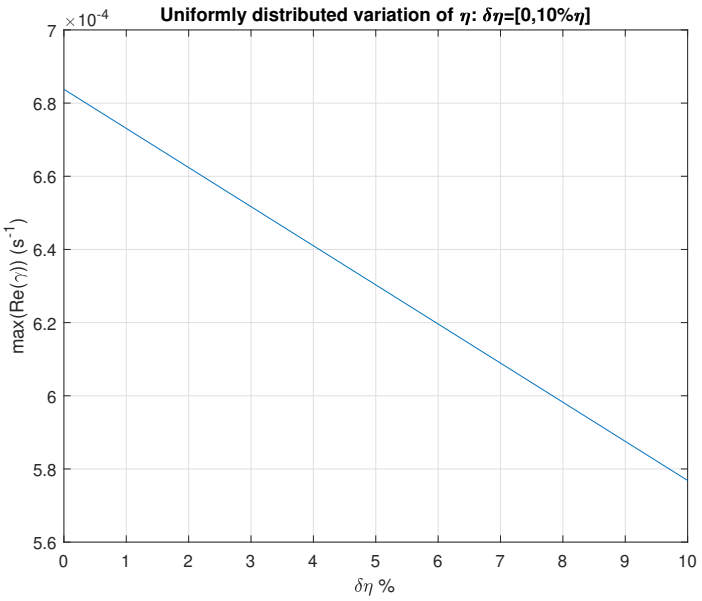

Figure 2.10: *Base flow sensitivity analysis: dominant eigenvalue shift with an increase $\delta\eta$ up to the 10% of η.*

An increase of η leads to a stabilizing effect for the system: the relative sensitivity associated to the eigenvalue shift is $S = -1.5638$. Physically, it can be interpreted as an increase of a dissipative term in the linearized induction equation that tends to damp the perturbations of the magnetic field intensity δH.

2.5 Conclusions

In summary, the logical iter followed in this chapter, together with a collection of the results illustrated in the previous sections, is resumed.
Firstly, the MHD model ([Freidberg 2007], [Chen 1984], [Pucella and Segre 2009]) for a conductive fluid is presented in a general, tensorial form in Section 2.2, and the main hypothesis and assumptions for the validity of the MHD model are remarked.
Then, in Section 2.2.2, the general MHD model is rescaled and adapted to describe the interaction of the external magnetic field $B_{0,x}$ and the motion of the liquid sodium flowing inside the channel. The equations are linearized around an equilibrium point and the numerical discretization procedure adopted for the non-conductive case is applied to this new problem. Another state variable, the magnetic field intensity perturbation δH_x, is introduced, with a corresponding evolutive equation derived from the magnetic induction equation in Eq.(2.18).
The dynamics matrix A is assembled in the MATLAB® environement and the *modal analysis* is carried out: firstly, no external magnetic field is applied, and the stability map obtained is indeed analogous to the non-conductive results presented in Chapter 1, highlighting that the non-conductive model is contained inside the conductive one. Then, an external magnetic field $B_0 = 1\ T$ is imposed, and a corresponding shift of the neutral stability curve of about 3 orders of magnitude can be seen in Figure 2.5.
To further continue the analysis of the impact of an external magnetic field on the system, a parametric study of the critical drag coefficient $k_{0,min}$ on the iso-inlet velocity line in the v_{in}-k_0 plane is conducted and the results are shown in Figures 2.6 and 2.7: the minimum drag coefficient required to reach a stable equilibrium configuration decreases steeply as B_0 increases up to $0.20\ T$, then a saturation value of $k_{0,min} \approx 10^{-6}\ m^{-1}$ is maintained as B_0 further increases, meaning that the stability of the system is no longer ruled by the viscous term in the momentum equation, but instead by the Lorentz force term.
Finally, a *parametric sensitivity analysis* and a *base flow sensitivity analysis* is performed for respectively the electrical resistivity coefficient η and the external magnetic field B_0. For both cases, an increase of the value leads to a stabilizing effect for the equilibrium point: the first is connected with an amplification of the dissipative term present in the magnetic induction equation, the second to a strengthening of the Lorentz force term.

Conclusions

The main topics and results presented in this thesis work are briefly resumed in the following.
In the first chapter the stability of a system governed by the hydrodynamics equations in the hypothesis of compressible flow is investigated. The uniform flow configuration is firstly studied exploiting Fourier analysis for the linear stability response of the system. Then the uniform hypothesis is relaxed, introducing the terms related to the spatial gradients of the equilibrium configurations studied. The impact of the latter is remarkable: some configurations (distributed pressure drop) add stability to the system, other meanwhile (concentrated pressure drop) strongly destabilize it. The stability maps for each configuration are drawn to highlight the differences between each considered case. Then a sensitivity analysis is proposed to study how perturbations on the main parameters and on the equilibrium base flow influence the stability features of the system. Given an increase of the previous quantities, it is evaluated if the dominant eigenvalue of an equilibrium configuration shifts towards a stable regions or not. The quantitative impact for each perturbed quantity is investigated with the definition of *relative sensitivity S*.
Then the solver is extended to the description of conductive fluids, adapting the MHD model for the one-dimensional case. A series of results represented on different stability maps have been illustrated, in the uniform flow configuration, showing the remarkable stabilizing effect of a magnetic field of 1 T with respect to the non-conductive case: the neutral stability curve shifts towards lower values (about 3 orders of magnitude) of the required drag coefficient needed to stabilize the system. A parametric study conducted on the isoline of the v_{in}-k_0 plane at constant inlet velocity shows the functional dependence of the critical drag coefficient for increasing values of the magnetic field intensity. A steep decrease can be observed in the range $0 - 0.2\ T$ and a saturation trend towards zero is reached for higher values of the magnetic field, denoting that the stability of the system is no more dominated by the friction forces present inside the fluid, but instead by the Lorentz force that couples the momentum equation with the magnetic induction equation.
Finally the modal sensitivity analysis is employed to evaluate the impact that the additional physical quantities adopted for the description of the conductive fluid have on the stability of the system: the external magnetic field and the electrical conductivity of the liquid sodium are studied with the adjoint perturbative approach, with the same procedure proposed for the non-conductive case.

A list of tables resumes the main sensitivity results obtained for, respectively, the non-conductive case and the conductive one:

Parameters	*Relative sensitivity*	*Stability effect*
α	-0.81	Stabilizing
β	0.92	Destabilizing
k_0	-0.79	Stabilizing
b	0.78	Destabilizing

Table 2.1: *Summary of the main parameters of the non-conductive problem and their impact over stability.*

Stationary profiles	*Relative sensitivity*	*Stability effect*
v_0	-0.7392	Stabilizing
p_0	-0.1220	Stabilizing
ρ_0	-12.31	Stabilizing
$\frac{\partial v_0}{\partial z}$	-0.0088	Stabilizing
$\frac{\partial p_0}{\partial z}$	8.422	Destabilizing
$\frac{\partial \rho_0}{\partial z}$	$-1.637 \cdot 10^{-15}$	Stabilizing

Table 2.2: *Summary of the stationary profiles and their spatial derivatives of the non-conductive problem and their impact over stability.*

Physical quantity	*Relative sensitivity*	*Stability effect*
B_0	-4.145	Stabilizing
η	-1.564	Destabilizing

Table 2.3: *Summary of the main physical quantities of the conductive problem and their impact over stability.*

In conclusion, a series of considerations are proposed to further extend and enrich this study. First of all, an inclusion of thermal effects in the model and the introduction of the Joule effect and the viscous terms inside the internal energy equation can be adopted to study how these effects alter the neutral stability curves in the stability maps shown in this work.
Then a *non-modal analysis* ([Schmid and Brandt 2014], [Trefethen and Embree 2005]) can be conducted to investigate the amplification over prescribed time-intervals of the perturbations of the state variables: inspecting the stable region of the stability maps obtained in the *modal analysis*, a more detailed stability information is given

with the analysis of the set of eigenvectors of the dynamics matrix A. Indeed, if the set is characterized by *nonnormal* eigenvectors, an amplification in amplitude of the perturbations of the state variables may exceed the linear approximation, leading to a bifurcation of the equilibrium configurations related to a single point in the v_{in}-k_0 plane. Even if the studied equilibrium configuration is asymptotically stable, an instability can be triggered in a finite time span with a non-monotonic trend of the energy associated to the perturbation of the state variables.
Finally, given the generality of the procedure presented in the one-dimensional case study treated in this work, the problem can be extended in two-dimensional and three-dimensional configurations, with the adoption of geometries and boundary conditions useful to model the motion of a magnetically confined thermonuclear plasma in the MHD approximation. The development of an adjoint model of the previous set of equations and a reduction of order via *Dynamic Mode Decomposition* can be useful for a stability and sensitivity characterization of the system and the assessment of the most important parameters from a stability-and-control point of view.

A final diagram is inserted to sum up graphically the main steps of this thesis work:

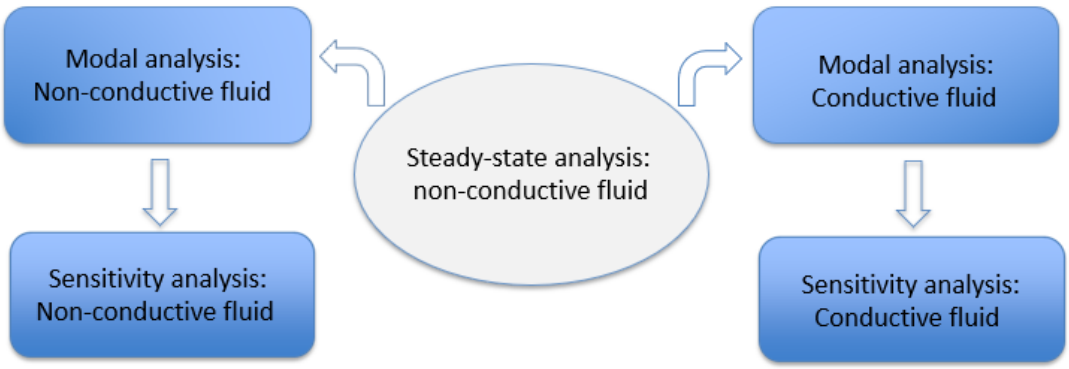

Figure 2.11: *Flowchart of this thesis work.*

Appendix A

Thermodynamic and transport properties of liquid sodium

In this appendix the main relations employed in the previous chapters to express the thermophysical and transport properties of liquid sodium as a function of temperature are reported. The following data refer to liquid sodium at atmospheric pressure. These correlations are present in the work of [Fink and Leibowitz 1995] and [Li et al. 2017]. The temperature dependency of *density*, in $\mathrm{kg\,m^{-3}}$, is:

$$\rho = \rho_c + f\left(1 - \frac{T}{T_c}\right) + g\left(1 - \frac{T}{T_c}\right)^h \tag{A.1}$$

where ρ_c is the critical density of sodium and T_c is the critical temperature of sodium, respectively $\rho_c = 219\,\mathrm{kg\,m^{-3}}$ and $T_c = 2503.7\,\mathrm{K}$. The unit of measure of temperature is in Kelvin. The value of the other coefficients is: $f = 275.32\,\mathrm{kg\,m^{-3}}$, $g = 511.58\,\mathrm{kg\,m^{-3}}$ and $h = 0.5$. The accuracy of this correlation is within the 0.4% if $T < 1100\,\mathrm{K}$.
The *specific heat at constant pressure*, measured in $\mathrm{J\,kg^{-1}\,K^{-1}}$, is expressed by following polynomial approximation:

$$C_P = a_0 + b_0 T + c_0 T^2 + d_0 T^{-2} \tag{A.2}$$

And the corresponding coefficients are: $a_0 = 1658.2\,\mathrm{J\,kg^{-1}\,K^{-1}}$, $b_0 = -0.8479\,\mathrm{J\,kg^{-1}\,K^{-2}}$, $c_0 = 4.451 \times 10^{-4}\,\mathrm{J\,kg^{-1}\,K^{-3}}$ and $d_0 = -2.9926 \times 10^6\,\mathrm{J\,K\,kg^{-1}}$. The relative error associated with this correlation is less than the 0.3%.
The electrical resistivity of liquid sodium, measured in $\Omega\,\mathrm{m}$, has this functional dependence of T:

$$\eta = \begin{pmatrix} -9.9141 + 8.2022 \times 10^{-2}\,T - 1.3215 \times 10^{-4}\,T^2 + 1.7212 \times 10^{-7}\,T^3 \\ -9.0265 \times 10^{-11}\,T^4 + 1.9553 \times 10^{-14}\,T^5 \end{pmatrix} \times 10^{-8} \tag{A.3}$$

This expression deviates from the experimental data obtained in the temperature range of $371\,\mathrm{K} \leq T \leq 1100\,\mathrm{K}$ for the 2%. The isobaric thermal expansion coefficient α_p and the isothermal compressiblity modulus β_T can be estimated with a polynomial interpolation of the experimental data present in literature in the temperature range $371\,\mathrm{K} \leq T \leq 1100\,\mathrm{K}$ with the Interpolation Tool CfTool®, embedded in MATLAB®.

The resulting expression for the *isobaric thermal expansion coefficent*, measured in K^{-1}, is:

$$\alpha_P = 4.882 \times 10^{-14}\, T^3 - 5.029 \times 10^{-11}\, T^2 + 1.09 \times 10^{-7}\, T + 2.022 \times 10^{-4} \quad \text{(A.4)}$$

For the *isothermal compressibility modulus*, measured in Pa^{-1}, the following correlation can be adopted:

$$\beta_T = 1.448 \times 10^{-19}\, T^3 - 9.444 \times 10^{-17}\, T^2 + 1.914 \times 10^{-13}\, T + 1.221 \times 10^{-10} \quad \text{(A.5)}$$

All the previous correlations are resumed in the following plots, where each quantity is expressed as a function of temperature:

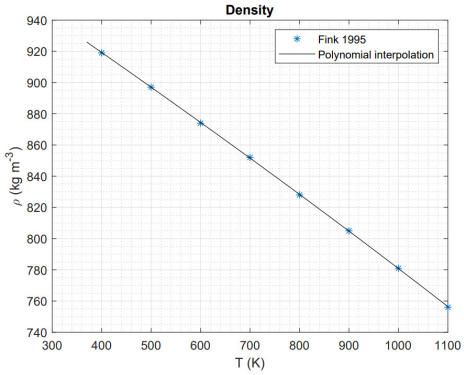

(a) *density*

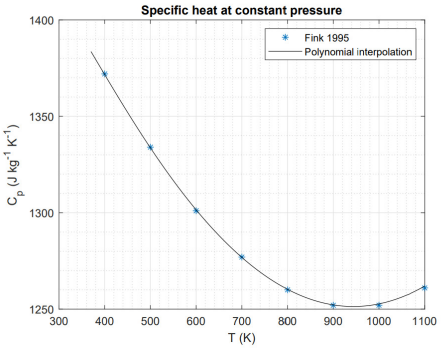

(b) *specific heat at constant pressure*

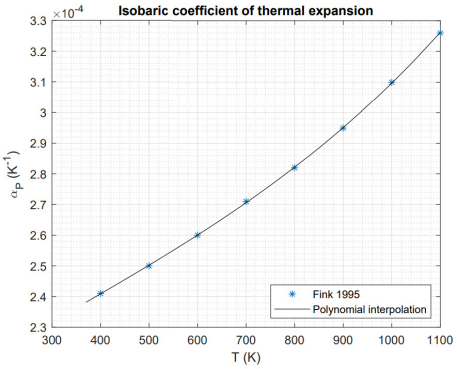

(c) *thermal expansion coefficient*

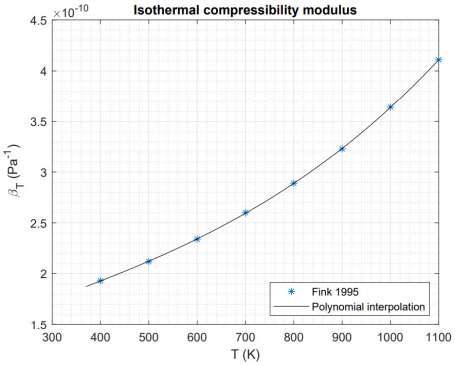

(d) *isothermal compressibility*

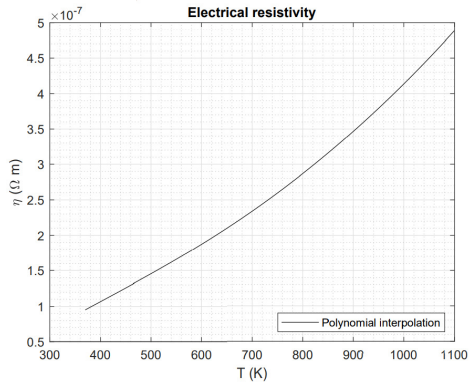

(e) *electrical resistivity*

Figure A.1: *Thermodynamic and transport properties of liquid sodium.*

Appendix B

Derivation of the coefficients for the state equation of liquid sodium

In this appendix, the main steps required to derive the coefficients α and β for the linearized state equation present in Eq.(1.26) are reported.
From Appendix A, the thermodynamic properties of liquid sodium, namely specific heat at constant pressure C_p, isobaric coefficient of thermal expansion α_p, isothermal compressibility modulus β_T and density at $p = 1\ bar$ are defined once the temperature T is set. It is recalled that the isobaric coefficient of thermal expansion α_p is defined as:

$$\alpha_p = \frac{1}{v^*}\left(\frac{\partial v^*}{\partial T}\right)_p \tag{B.1}$$

and the isothermal compressibility modulus β_T as:

$$\beta_T = -\frac{1}{v^*}\left(\frac{\partial v^*}{\partial p}\right)_T \tag{B.2}$$

Starting with the thermodynamic definition of the internal energy per unit mass $u = u(T, p)$, the differential du is expressed by the differentials dT and dp:

$$du = \left(\frac{\partial u}{\partial T}\right)_p dT + \left(\frac{\partial u}{\partial p}\right)_T dp \tag{B.3}$$

The first coefficient can be restated as:

$$\left(\frac{\partial u}{\partial T}\right)_p = \left(\frac{T\partial s - p\partial v^*}{\partial T}\right)_p = \left(\frac{T\partial s}{\partial T}\right)_p - p\left(\frac{\partial v^*}{\partial T}\right)_p = C_p - pv^*\alpha_p \tag{B.4}$$

The second, using Maxwell's relation referred to Gibbs free energy:

$$\left(\frac{\partial s}{\partial p}\right)_T = -\left(\frac{\partial v^*}{\partial T}\right)_p \tag{B.5}$$

is reformulated as follows:

$$\left(\frac{\partial u}{\partial p}\right)_T = \left(\frac{T\partial s - p\partial v^*}{\partial p}\right)_T = T\left(\frac{\partial s}{\partial p}\right)_T - \left(p\frac{\partial v^*}{\partial p}\right)_T = -Tv^*\alpha_p + v^*p\beta_T \tag{B.6}$$

obtaining:

$$du = (C_p - pv^*\alpha_p)\,dT + (v^*p\beta_T - Tv^*\alpha_p)\,dp \tag{B.7}$$

Expressing now $T = T(v^*, p)$ by means of (B.1) and (B.2):

$$dT = \frac{1}{\alpha_p v^*}dv^* + \frac{\beta_T}{\alpha_p}dp \tag{B.8}$$

From $u = u(T, p)$, a new relationship for $u = u(p, v^*)$ is found:

$$du = \left(\frac{\beta_T C_p}{\alpha_p} - Tv^*\alpha_p\right)dp + \left(\frac{C_p - pv^*\alpha_p}{v^*\alpha_p}\right)dv^* \tag{B.9}$$

Finally, reverting from specific volume v^* to density ρ, by definition:

$$v^* = \frac{1}{\rho}, \quad dv^* = -\frac{1}{\rho^2}d\rho \tag{B.10}$$

α can be computed by:

$$\alpha = \left(\frac{\partial u}{\partial p}\right)_\rho = \frac{\beta_T C_p}{\alpha_p} - \frac{T\alpha_p}{\rho} \tag{B.11}$$

and β from:

$$\beta = \left(\frac{\partial u}{\partial \rho}\right)_p = -\frac{\rho C_p - \alpha_p p}{\alpha_p \rho^2} \tag{B.12}$$

In conclusion, α and β can be derived by setting an inlet temperature T_{in} for the liquid sodium and combining properly the previous thermodynamic coefficients, being all a function of temperature.

Bibliography

[Che84] F F Chen. *Introduction to Plasma Physics and Controlled Fusion*. Introduction to Plasma Physics and Controlled Fusion v. 1. Springer, 1984. ISBN: 9780306413322. URL: https://books.google.it/books?id=ToAtqnznr80C.

[Lya92] Aleksandr Mikhailovich Lyapunov. "The general problem of the stability of motion". In: *International journal of control* 55 (1992), pp. 531–534.

[PL92] T. J. Poinsot and S. K. Lelef. "Boundary conditions for direct simulations of compressible viscous flows". In: *Journal of Computational Physics* 101.1 (1992), pp. 104–129. ISSN: 10902716.

[FL95] J.K Fink and L. Leibowitz. "Thermodynamic and Transport Properties of Sodium Liquid and Vapor". In: (1995).

[NF96] P. Napolitano and A. G. Fabbri. "Single parameter sensitivity analysis for aquifer vulnerability assessment using DRASTIC and SINTACS. In: Proceedings of the 2nd HydroGIS conference". In: *IAHS Publication, : Application of Geographic Information Systems in Hydrology and Water Resources Management (Proceedings of the Vienna Conference, April 1996). IAHS Publ. no. 235, 1996* 235 (1996), pp. 559–566.

[DK99] J Michael Doster and Peter K Kendall. *Stability of One-Dimensional Natural-Circulation Flows*. Tech. rep. 1999.

[Tre00] Lloyd N. Trefethen. "Spectral Methods in MATLAB". In: *Spectral Methods in MATLAB* (2000). DOI: 10.1137/1.9780898719598.

[LB01] John R. Lamarsh and Anthony J. Baratta. *Introduction to Nuclear Engineering*. Third edit. Vol. 23. 1. 2001, pp. 74–74. ISBN: 0201824981. DOI: 10.1119/1.1933896.

[TE05] Lloyd N. Trefethen and Mark Embree. "Spectra and Pseudospectra". In: *Spectra and Pseudospectra* (2005). DOI: 10.2307/j.ctvzxx9kj.

[Fre07] Jeffrey P Freidberg. *Plasma Physics and Fusion Energy*. Cambridge: Cambridge University Press, 2007. ISBN: 9780521733175. DOI: DOI:10.1017/CBO9780511755705. URL: https://www.cambridge.org/core/books/plasma-physics-and-fusion-energy/CD7B530D2889F70446F34E14EE0EF703.

[Jac07] J D Jackson. *CLASSICAL ELECTRODYNAMICS, 3RD ED*. Wiley India Pvt. Limited, 2007. ISBN: 9788126510948. URL: https://books.google.it/books?id=2hZ0CgAAQBAJ.

[MSJ08] Olivier Marquet, Denis Sipp, and Laurent Jacquin. "Sensitivity analysis and passive control of cylinder flow". In: *Journal of Fluid Mechanics* 615 (Nov. 2008), pp. 221–252. DOI: 10.1017/S0022112008003662.

[PS09] G Pucella and S E Segre. *Fisica dei plasmi*. Zanichelli, 2009. ISBN: 9788808063830. URL: https://books.google.it/books?id=_wuAQgAACAAJ.

[PBG10] Jan Pralits, Luca Brandt, and Flavio Giannetti. "Instability and sensitivity of the flow around a rotating circular cylinder". In: *Journal of Fluid Mechanics* 650 (May 2010), pp. 513–536. DOI: 10.1017/S0022112009993764.

[Nis+11] Norman Nise et al. *Control Systems Engineering*. Vol. 1. 2011, pp. 1–1002. ISBN: 9783319021348. DOI: 10.1007/978-3-319-02135-5{_}3.

[IAE13] IAEA. "Design Features and Operating Experience of Experimental Fast Reactors". In: (2013).

[Spr13] H. C. Spruit. "Essential Magnetohydrodynamics for Astrophysics". In: August (2013). URL: http://arxiv.org/abs/1301.5572.

[SB14] Peter J Schmid and Luca Brandt. "Analysis of fluid systems: stability, receptivity, sensitivity". In: (2014), p. 26.

[Sha15] E Shashi Menon. "Chapter Five - Fluid Flow in Pipes". In: ed. by E B T - Transmission Pipeline Calculations Shashi Menon and Simulations Manual. Boston: Gulf Professional Publishing, 2015, pp. 149–234. ISBN: 978-1-85617-830-3. DOI: https://doi.org/10.1016/B978-1-85617-830-3.00005-5. URL: http://www.sciencedirect.com/science/article/pii/B9781856178303000055.

[Gal16] Sébastien Galtier. *Introduction to Modern Magnetohydrodynamics*. Cambridge: Cambridge University Press, 2016. ISBN: 9781107158658. DOI: DOI:10.1017/CBO9781316665961. URL: https://www.cambridge.org/core/books/introduction-to-modern-magnetohydrodynamics/E21EBF2FE07ABDD1BDC34C6EB0615EC0.

[Kum+16] M Kumar et al. "Magnetic flux distortion in two-phase liquid metal flow: Model experiment". In: *Journal of Applied Physics* 119.18 (May 2016), p. 185105. ISSN: 0021-8979. DOI: 10.1063/1.4950792. URL: https://doi.org/10.1063/1.4950792.

[PCL16] A Pini, A Cammi, and L Luzzi. "Analytical and numerical investigation of the heat exchange effect on the dynamic behaviour of natural circulation with internally heated fluids". In: *Chemical Engineering Science* 145 (2016), pp. 108–125. ISSN: 0009-2509. DOI: https://doi.org/10.1016/j.ces.2016.01.014. URL: http://www.sciencedirect.com/science/article/pii/S0009250916000233.

[Li+17] Huaming Li et al. "Thermodynamic properties of liquid sodium under high pressure". In: *AIP Advances* 7.4 (2017). ISSN: 21583226. DOI: 10.1063/1.4980023.

[Tro+19] Giuseppe Trotta et al. *An innovative approach for stability analysis of conductive fluids : from incompressible to compressible formulation*. Tech. rep. Politecnico di Milano, 2019.

[VNK19] Pallippattu Krishnan Vijayan, Arun K Nayak, and Naveen Kumar. “Chapter 3 - Governing differential equations for natural circulation systems”. In: ed. by Pallippattu Krishnan Vijayan et al. Woodhead Publishing, 2019, pp. 69–118. ISBN: 978-0-08-102486-7. DOI: https://doi.org/10.1016/B978-0-08-102486-7.00003-2. URL: http://www.sciencedirect.com/science/article/pii/B9780081024867000032.